Coupling between torsional and bending modes of vibration in cantilever beams

G. Armstrong

COUPLING BETWEEN TORSIONAL AND BENDING MODES OF VIBRATION IN CANTILEVER BEAMS.

by

G. ARMSTRONG B.Sc.

A thesis submitted for the degree of Doctor of Philosophy in the Department of Engineering Science, University of Durham.

December 1972.

ACKNOWLEDGEMENTS

The author is extremely grateful to Dr. P.A.T. Gill for his supervision and assistance, and to Professor G.R. Higginson for his continued interest in the project. Thanks are also due to the Technicians in the Department of Engineering Science for their help with the experimental work, and to my wife for her patience in typing a difficult manuscript.

Graeme Armstrong.

ABSTRACT

The work presented is a theoretical and experimental investigation into the effect of coupling between torsional and flexural modes of vibration in cantilever beams.

Two theoretical approaches are made: firstly, a finite element idealisation in which the beam is divided into a number of elements which possess cubic variations of deflection and rotation along their lengths; and, secondly, a more analytical method in which the simultaneous differential equations of motion are solved directly by application of Laplace Transforms.

The investigation is restricted to the simplest cross section which possesses a single axis of symmetry, the isosceles triangle. The exact solutions for the torsion and flexure of such sections of general shape do not as yet exist, but use is made of several approximate techniques which have been developed for this section for the calculation of the torsional stiffness and position of the centre of flexure.

It is shown experimentally and theoretically that torsional oscillations do not take place about the centre of flexure (or centre of torsion), but about a point which may be considered to be coincident with the centroid.

It is shown theoretically and confirmed experimentally that the effect of coupling on either mode is extremely small unless the original frequencies of torsional and flexural motion are almost coincident, in which case the two frequencies are separated into coupled modes which possess both torsional and flexural characteristics. The effect is not, however, as significant as the coupling of flexural modes due to pretwist in sections which approximate to those of turbine blades.

TABLE OF CONTENTS

NOTATION

ENGLISH SYMBOLS

A	Area of cross - section
$[A]$	$[A_1 \quad A_2 \quad A_3 \quad A_4]$ matrix of constants
$[B]$	$[B_1 \quad B_2 \quad B_3 \quad B_4]$ matrix of constants
C	Torsional stiffness per unit length
E	Young's Modulus
$[E]$	$[E_1 \quad E_2 \quad E_3 \quad E_4]$ matrix of constants
$F(z)$, $G(z)$	Functions of z
G	Shear Modulus
I_{xx}, I_{xx}	Second moments of area about XX and xx axes respectively
I_{yy}, I_{yy}	Second moments of area about YY and yy axes respectively
I_{cg}	Polar moment of inertia about centroid per unit length
I_{cf}	Polar moment of inertia about centre of flexure per unit length
i, $i+1$	Node numbers of a typical beam element
k^2_{xx}, k^2_{xx}, k^2_{yy}, k^2_{yy}	Radii of gyration about given axes
k^2_{cg}, k^2_{cf}	Polar radii of gyration about centroid, centre of flexure
l	Length of beam element
L	Length of beam
$\mathcal{L}\, F(z)$	Laplace transform of $F(z) = \int_0^\infty e^{-sz} F(z)\, dz$
M	Bending moment

m	Mass per unit length of beam
p	Circular frequency - radians / second.
r_x , r_y	Coordinates of the centroid from the centre of flexure in x and y directions
T	Kinetic energy
t	Time
T(t)	Function of time
U	Potential energy
V	Shear force
W	A force
xx, yy	Fixed axes through the centre of flexure
x,y	Deflection of centre of flexure in x and y directions
XX , YY	Principal planes
$\hat{x}$, $\hat{y}$	Maximum values
Z	Axes of beam length, through the centres of flexure
z	Distance along the Z axis

GREEK SYMBOLS

α	Angle between the equal sides of the isosceles triangular section.
θ	Angle of elastic twist about the Z axis.
ν	Poisson's ratio
ρ	Density
ϕ	$= \chi_{i+1} - \chi_i = \frac{d\chi}{dz}$
χ	Pretwist about Z axis
ω	Frequency in Hertz

OTHER SYMBOLS

3rd XX	Third mode vibration along XX axis
1st YY	First mode vibration along YY axis
θ', θ''	$\frac{d\theta}{ds}$, $\frac{d^2\theta}{ds^2}$ etc.
$\dot{\theta}$, $\ddot{\theta}$	$\frac{d\theta}{dt}$, $\frac{d^2\theta}{dt^2}$ etc.

Fig. 1 shows the terms used in relation to the beam.(To maintain consistency with familiar usage the above symbols may be redefined in parts of the text. In these cases the redefinition applies only to the section in which it occurs).

FIG 1.: BEAM NOTATION

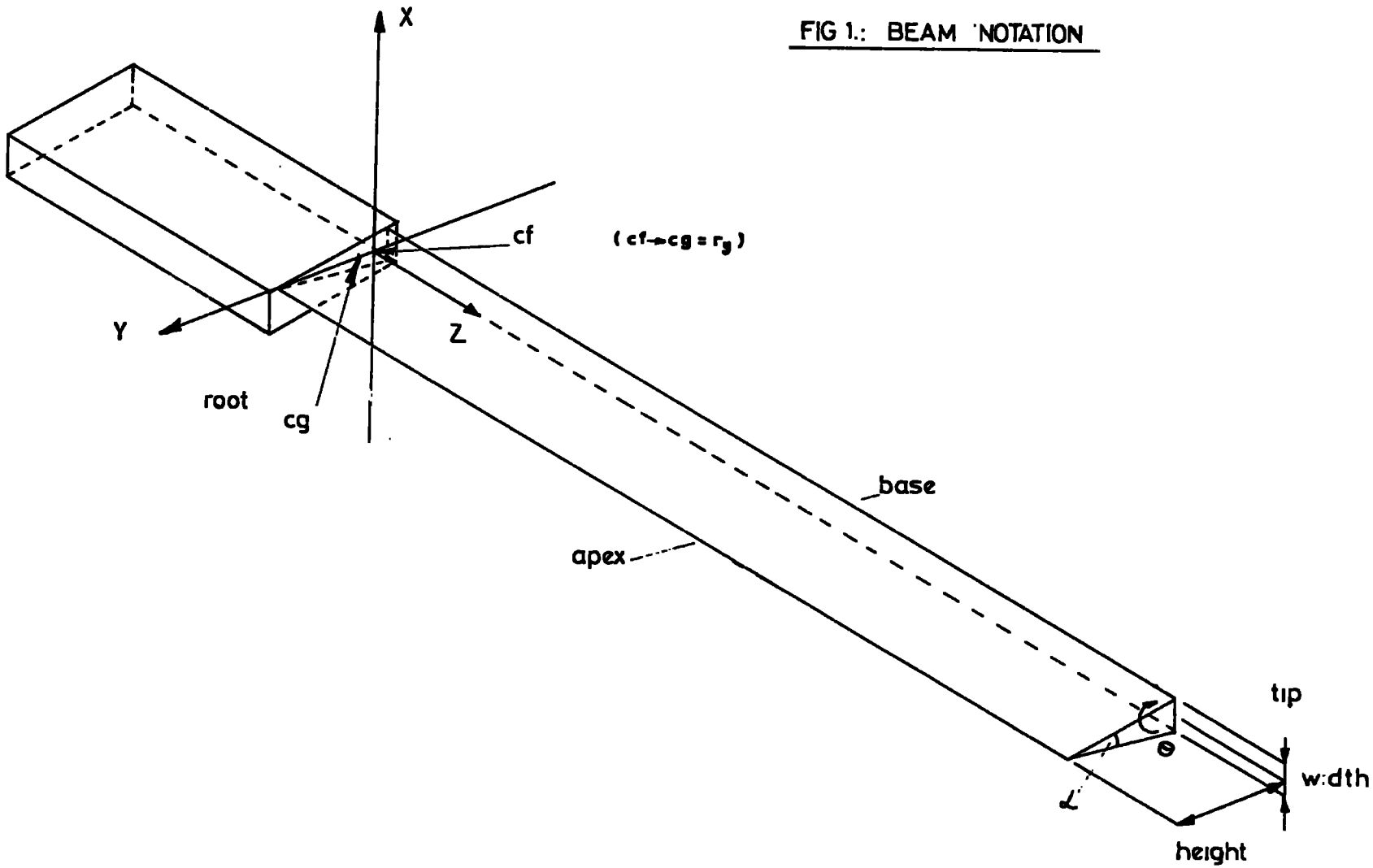

CHAPTER 1

INTRODUCTION

The development of the turbine in the last two decades has produced considerable interest in the study of the vibration of cantilever beams. It is obviously of some importance to the turbine designer to have some indication of the vibration characteristics of the blading, as great damage may be caused by a blade breaking loose due to fatigue failure.

For the untwisted rectangular section (the simplest case) there are three independant types of motion: as the beam is continuous there exist an infinite number of bending modes in both the Yz and Xz planes (Fig.1) and an infinite number of torsional modes about the Z axis. The three types are said to be uncoupled as any mode of a given type has no component of any other type present. Within the limitations of beam theory all the frequencies of each type may be determined analytically by the solution of straightforward differential equations.

Practical turbine blades are usually of aerofoil cross-section, which of course possesses no axes of symmetry, and are pretwisted along their length. They may also be tapered, and, particularly in the low pressure end of the turbine, be braced together by wires to reduce excessive oscillatory movement.

As a first approximation to what is therefore quite a complicated problem, the vibration of pretwisted rectangular sectional cantilevers has been studied by many authors including Carnegie, Rosard and Slyper. Pretwisting couples the two bending modes, producing modes which have both X and Y components. An exact analytical solution of the simultaneous differential equations does not exist but several approximate

techniques have been developed.

Torsional coupling (with either or both of the bending modes) is introduced if the cross section possesses less than two axes of symmetry. In this case the centroid is no longer coincident with the centre of flexure or centre of torsion (Chapter 2, Section 2). Considerations of symmetry show that if the section possesses one axis of symmetry the centre of flexure and centre of torsion will be on that axis.

In studying the vibration of pretwisted rectangular sectioned beams the above investigations have assumed torsional coupling to be negligible, and in general torsional coupling has received little attention. Carnegie however, in an attempt to investigate torsional coupling has studied the flexural vibration of a pretwisted beam of aerofoil section (12, 21).* Although this represents the true turbine blade, it is extremely difficult, if not impossible, to define certain properties of that section - ie. the torsional stiffness and the positions of the centroid and centre of flexure. Whereas Griffith's graphical method (described in Chapter 3, Section 3) may be used to give a fairly accurate value of the torsional stiffness, the centre of flexure can only be found by experiment, and with great difficulty.

The effects of torsional coupling can, however, be studied without encountering the difficulties of the aerofoil and the present work is an investigation of the vibration of the simplest (untwisted) section which possesses a single axis of symmetry: the isosceles triangle. This has several advantages over the aerofoil. Although, to the author's knowledge, no exact analysis of the flexure or torsion of isosceles triangular sectional beams exists, there are several approximate solutions applicable

* References in Appendix 1

to sections of general apex angle, or to ones in which the apex angle is limited to less than about 10°. This means that the torsional stiffness and the coordinates of the centre of flexure may be obtained theoretically to within a reasonable degree of accuracy. It is also much easier to obtain uniform cross-sectional dimensions in the manufacture of the isosceles triangular section.

The author feels, therefore, that in attempting to present a better understanding of the nature of torsional coupling, future work on the vibration of the aerofoil-sectional blade with be facilitated.

CHAPTER 2

HISTORICAL INVESTIGATION

This investigation divides conveniently into three parts. The first deals with the attempts at a solution of the torsional problem for isosceles triangular prisms in the absence of an exact solution for a general triangle, or even a general isosceles triangle. The second section considers the flexural problem of isosceles triangular prisms, from which theoretical estimates of the coordinates of the centre of flexure are obtained ; and the third part deals with different methods of analysing the whole problem of cantilever beam vibration.

2.1 Torsion of isosceles triangular prisms.

St. Venant noted that reasonable accuracy could be obtained by treating the section (not necessarily triangular) as an ellipse having the same cross-sectional area and polar moment of inertia. This method makes use of the exact solution for the ellipse and can give an accuracy of as good as 5% (from torsional frequency experiments) in some cases.

Griffith[1] presented a graphical method which is rather complicated and involves rounding off the corners of the section with a radius dependent upon the angle in the corner and applying a ' torque correction factor '. An approximate formula, applicable to long thin sections of any shape is also given.

The exact solution for the sector of a circle (in terms of infinite series) has been described by Timoshenko[2] and this can be used to give an upper and lower boundary to the torsional stiffness of isosceles triangular sections of small apex angle. Two calculations are made: one in

which the radius of the sector is equal to the length of one of the equal sides of the section; and a second in which the radius equals the perpendicular distance from the apex to the smallest side. The required triangle lies in between these two sections and thus a range of acceptability is obtained by which other methods may be judged. (Fig.3.3.2).

Duncan, Ellis and Scruton [3] presented an approximate stress function solution derived using Ritz's (variational) technique. The expression deduced is exact for an equilateral triangle and the fractional error tends to zero as α tends to zero. A characteristic of this type of approach is that it gives a much better approximation to the stiffness than to the stresses themselves.

Nuttall [4] presented two approximate Rayleigh-Ritz solutions applicable to any isosceles triangle. These are derived from the exact solutions for an equilateral triangle and a right angled isosceles triangle, both of which are series solutions. He concluded that the formula derived from the equilateral triangle is more accurate for $\alpha < 60^\circ$ and the formula derived from the right angled isosceles triangle should be used for $\alpha > 90^\circ$. In the range $60^\circ \leq \alpha \leq 90^\circ$ the formulae serve as a check on each other.

Scholes and Slater [5] presented an empirical formula similar to Griffith's, and it was claimed that the formula is an improvement on Griffith's at small values of the ratio maximum thickness to chord, as Griffith's correction is not sufficiently effective at these values.

A comparison of these methods is presented in Chapter 5 for varying apex angle in the range 2° to 60°, and the cross sectional area is constant.

2.2. The centre of flexure.

The centre of flexure, or shear centre, is defined as that point through which the resultant of a system of transverse loads acts so that the section deflects without rotating. By symmetry it is seen that if a section possesses an axis of symmetry, then the centre of flexure lies on that axis. However, in the case of the isosceles triangular sections considered in this work, it is required to know the displacement of the centre of flexure from the centroid along the axis of symmetry, as it is this displacement which causes coupling between torsional and flexural modes of vibration.

There is another point associated with a cross-section, called the centre of twist, which is the point of zero deflection (in the plane of the section) under the action of a pure couple acting in the plane of the section. The relationship between these two points has been considered by Duncan, Ellis and Scruton [3] and Timoshenko [2] who concluded that by the reciprocal theorem for a rigid encastré support the centres are coincident, and that for practical fixing conditions they are almost coincident. Experimental evidence presented by the former authors confirmed this, and in this work the centres of flexure and twist are assumed to be coincident.

Once the bending stress function for a section is known the calculation of the coordinates of the centre of flexure is trivial, but an exact stress function for a general isosceles triangle does not exist and therefore approximate methods must be considered.

Griffith and Taylor[6] presented a method of calculating the shear stresses in bending using soap films and stated that a simplification inspired by the soap film experiments and valid for sections whose boundaries consist of nearly parallel curves or straight lines, permits a mathematical solution leading to the formula for the centroid-centre of flexure distance r_y (Fig. 1) as

$$r_y = \frac{\int y t^3 dy}{\int t^3 dy}$$

where t is the half-thickness of the section.

This formula was refuted by Duncan[8] who derived an approximate stress function and, for thin sectioned bars, arrived at the formula

$$r_y = \frac{1+3\nu}{1+\nu} \frac{\int y t^3 dy}{\int t^3 dy}$$

It is seen that Duncan's formula reduces to Griffiths when $\nu = 0$.

Both Griffith and Duncan presented experimental evidence in support of their formulae, but Scholes and Slater[5] in applying them to a bar of thin trapezoidal section indicated that their own experimental results agree more closely with Griffith's formula than with Duncan's.

Both formulae are applied to the sections considered in this work.

Young, Elderton and Pearson[9] considered the torsion produced when a section of a cantilever, possessing one axis of symmetry, is deflected by a concentrated load applied at the centroid at right angles to the axis of symmetry. The work is restricted to the sectors of a circle and, as

with the torsional stiffness, approximations may be obtained by considering the sectors of equal apex angle to the isosceles triangle, (Fig.3.3.2). However, no mention is made of the centre of flexure or any similar concept, but its position may be calculated from the results presented in the paper.

2.3. Methods of analysis of beam vibrations.

An analytical solution governing the vibration of uniform pre-twisted rectangular sectioned beams has been obtained by Troesch, Anliker and Ziegler[10] with the assumption that the flexural rigidity in one direction is infinite. However, the method is very involved and lacks extension to more general cases, and therefore the problem is approached using approximate methods and numerical procedures.

Rayleigh's method, involving the equating of the maximum potential and kinetic energies is useful in that the final equations are fairly simple. Usually it is only possible to obtain the fundamental mode, but by assuming an appropriate higher mode shape which is orthogonal to the lower modes an approximation to the mode frequency is possible.

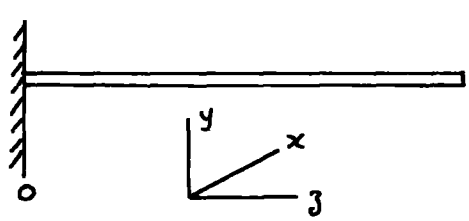

Fig.(2.3.1)

Assuming a mode shape Y(z) it can be shown[11] that the circular frequency p is given by

$$p^2 = \frac{\int_0^L E I_{xx} \left(\frac{d^2 y}{dz^2}\right)^2 dz}{\int_0^L \rho A y^2 dz}$$

The closer the assumed shape Y(z) is to the exact mode shape, the closer the approximate frequency is to the exact value.

Although the method is severely limited by the required assumption of a mode shape, it has been successfully applied by Carnegie[12] in the determination of fundamental modes of vibration of uniform pretwisted rectangular sectioned cantilevers. In this, Carnegie obtained the mode shapes from the results of a previous paper[13] dealing with the static bending of the cantilevers.

Rayleigh's method may be extended, and its usefulness considerably improved, by assuming for Y(z) a series in the form

$$Y(z) = \sum_{r=1}^{n} A_r Y_r(z)$$

where each Yr(z) satisfies the boundary conditions. This is the basis of the Rayleigh-Ritz or Ritz procedure. A characteristic of the Rayleigh method is that it gives values of p which are higher than the true value. This is due to the fact that the inaccuracy of the assumed mode shape is equivalent to applying additional constraints to the system. To minimise this the coefficients are chosen to give a minimum value of p.

The equations

$$\frac{\partial p^2}{\partial A_r} = 0 \qquad r = 1, 2, 3 \ldots n$$

are found, giving an n th order equation in p^2, the roots of which are the first n frequencies of the system.

The method may be iterated as more terms of the series are employed, hence giving an assessment of the accuracy.

The method of matrix iteration is an iterative procedure in which a mode shape is assumed and iteration performed until the mode shapes stabilise.

In matrix form the equations of motion may be written

$$\{y\} = \lambda[A]\{y\} \qquad 2.3.1$$

Where $\lambda = 1/p$ for stiffness formulation and p^2 for flexibility formulation (the Stodola method).

A deflected shape is assumed for $\{y\}$ on the right hand side of 2.3.1 which may be very rough indeed. The operation of 2.3.1 is performed resulting in $\{y\}$ on the left hand side. This is normalised by making a chosen amplitude unity, giving a new starting shape for the right hand side. It can be shown that after successive iterations the deflected shape stabilises to the dominant root of the equation, i.e. the lowest value of λ .

Higher modes (or lower, depending on the formulation) are possible but are rather difficult and convergence becomes slower. The lowest mode $\{y\}_1$ must be accurately determined before it is " purified out " of the second mode $\{y\}_2$, using the condition of orthogonality, otherwise an attempt to converge to $\{y\}_2$ will amplify the component of $\{y\}_1$ yielding eventually the original $\{y\}_1$.

Good agreement was obtained by Slyper[14] for the first seven modes of vibration of uniform rectangular beams of pretwist 0°, 90.9° and 877° using this method programmed for digital computation, but there is a risk of instability inherent in the method and it is felt to have been superceded by more modern techniques.

The Holzer method for torsional oscillations has been adapted by Myklestad to analyse beam vibrations. The beam is divided into a finite number of stations with the distributed mass of the beam replaced by concentrated masses at the stations.

By working from one end of the system to the other, the deflection, slope, moment and shear are computed at each station for an assumed value of p. The values of p which satisfy the boundary conditions of the problem are the natural frequencies.

In the case of simple flexure in the Yz plane, the matrix equation

$$\begin{Bmatrix} y \\ \frac{dy}{dz} \\ M \\ V \end{Bmatrix}_n = \begin{bmatrix} & A & \end{bmatrix} \begin{Bmatrix} y \\ \frac{dy}{dz} \\ M \\ V \end{Bmatrix}_0$$

M = moment

V = shear

is formed, where $A_{i,j} = f(p^2)$

Application of the boundary conditions

$$y_0 = \frac{dy}{dz}_0 = M_n = V_n = 0$$

gives a determinant whose value may be plotted against p^2:

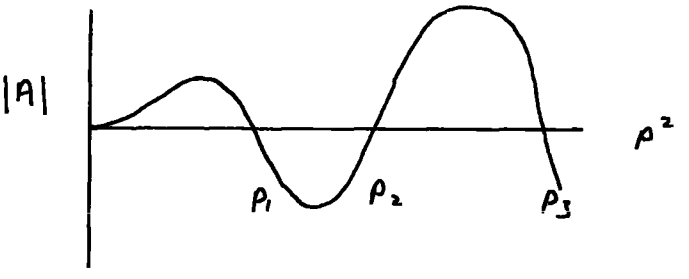

The boundary conditions are then satisfied when the determinant is zero.

The method was employed by Rosard and Lester[15] to analyse the vibration of uniform pretwisted rectangular sectioned cantilevers of various width/thickness ratios and by Isakson and Eisley[16] who further extended the method to cover rotations (about an axis parallel to the x axis in Fig. 2.3.1) pretwisted rectangles, but the latter did not obtain sufficient results to enable general conclusions to be drawn.

It is thought that this approach is superior to that of Stodola as first and higher modes are obtained with equal ease without any need of " purification ". It has been criticised as a trial and error method, but a reasonable estimate of the required frequency is usually available and a swiftly converging iteration procedure easily programmed. It also has the advantage that individual frequencies may be investigated without the need of obtaining all frequencies.

Gendler and Mendelsohn[17] claimed an improvement on the Myklestad method by introducing the concept of station functions. It is stated that the Myklestad method involves the assumptions that the inertial loads in an interval can be replaced by a resultant concentrated mass and that this load produces the same deflection as the distributed load.

Station functions eliminate these assumptions by assuming that the inertial loads are continuous functions along the beam; ie. the beam is approximated to the sum of a set of continuous station functions each of which satisfies the boundary conditions and vanishes at all stations other than the one with which it is associated.

With modern computing techniques it is doubtful whether this offers any real advantage over the original Myklestad.

Although the above methods may be used for the solution of relatively simple problems without the use of a computer, its arrival naturally permits their extension to more general problems, as has been indicated. Use of a computer also enables the equations of motion to be solved directly by various numerical integration routines, and the advent of finite element theory means that such complex problems as car body vibration can be solved.

Dawson, Ghosh and Carnegie used the direct numerical solution of the equations of motion to determine the effect of slenderness ratio on the natural frequencies of uniform pretwisted rectangular sections, allowing for shear deformation and rotary inertia (18). By suitable substitution the equations of motion are reduced to a set of eight first order linear differential equations which are solved as follows:

1). A trial frequency is assumed, and the four known boundary values at the root set to their respective values.

2). The four unknown values at the root are assigned arbitrary values and the eight equations solved by a Runge-Kutta process yielding a set of solutions at the tip.

3). This procedure (with the same frequency) is repeated three times with the unknowns at the root set to other arbitrary values.

4). There are now four sets of independent solutions and since the differential equations are linear, the complete solution is a linear combination of the four sets of independent solutions.:

If $Y_i(L)$ $_{i=1 \to 8}$ is the complete solution at the tip,

$$\therefore Y_i(L) = \sum_{\nu=1}^{4} a_\nu \, Y_{i,\nu}(L)$$

where $Y_{i,\nu}(L)$ is the "νth" independent solution.

Application of the boundary values at the tip yields the matrix equation:

$$[Y_{i,\nu}]\{a\} = \{0\}$$

and the condition that the differential equations have a solution satisfying the boundary conditions is that

$$|Y_{i,\nu}| = 0$$

In the finite element method, the structure is assumed to be divided into elements to which are ascribed a finite number of degrees of freedom. The stiffness and distributed mass matrices for each element are calculated, which are then assembled to form the stiffness and mass matrices of the overall structure. After application of the boundary conditions, the problem reduces to an eigenvalue problem of the form

$$[[K] - \rho^2 [M]]\{\delta\} = \{0\}$$

where $[K]$ is the structural stiffness matrix

$[M]$ is the structural mass matrix

and $\{\delta\}$ is the structural nodal displacements.

The term " node " in this context refers to the extremities of an element, not to the nodes of the elastic curve of the structure.

It is difficult to draw comparisons between these methods as much depends on the efficiency of the programming. It can be said, though, that numerical integration probably requires less storage than a finite element solution of the same problem, but finite element theory does not require foreknowledge of the equations of motion and is therefore more general.

Dokumaci, Thomas and Carnegie[19] illustrated the use of finite element theory applied to the vibration of uniform pretwisted rectangular sectional beams, and good agreement was obtained with other methods. This theory is extended by the present author to cover uniform pretwisted beams of any cross sectional shape, details of which appear later in this thesis.

A more sophisticated application is shown by Ahmad, Anderson and Zienkiewicz[20] using thick curved shell elements to analyse the vibration of turbine and compressor blading. The agreement between theory and experiment is not very good, but may possibly be explained by the difficulty of true experimental modelling.

CHAPTER 3

THEORETICAL ANALYSIS

Introduction.

The equations of motion governing the most general case of uniform beam vibration, that of pretwisted asymmetric section are given by Carnegie[12].

$$\left.\begin{aligned} EI_{xx}\frac{\partial^4 y}{\partial z^4} + EI_{xy}\frac{\partial^4 x}{\partial z^4} + m\frac{\partial^2 y}{\partial t^2} + mr_x\frac{\partial^2 \theta}{\partial t^2} &= 0 \\ EI_{yy}\frac{\partial^4 x}{\partial z^4} + EI_{xy}\frac{\partial^4 y}{\partial z^4} + m\frac{\partial^2 x}{\partial t^2} + mr_y\frac{\partial^2 \theta}{\partial t^2} &= 0 \\ C\frac{\partial^2 \theta}{\partial z^2} - I^{*}_{cg}\frac{\partial^2 \theta}{\partial t^2} + mr_y\frac{\partial^2 x}{\partial t^2} + mr_x\frac{\partial^2 y}{\partial t^2} &= 0 \end{aligned}\right\} \quad 3.1$$

(* Carnegie assumes that torsional oscillations take place about the centre of flexure and therefore replaces I_{cg} with I_{cf}. This is incorrect, for reasons which are presented in section 5 of this chapter).

In the particular case of a rectangular section, $r_y = r_x = o$ and the equations 3.1 reduce to

$$\left.\begin{aligned} EI_{xx}\frac{d^4 y}{dz^4} + EI_{xy}\frac{d^4 x}{dz^4} - m\rho^2 y &= 0 \\ EI_{yy}\frac{d^4 x}{dz^4} + EI_{xy}\frac{d^4 y}{dz^4} - m\rho^2 x &= 0 \\ C\frac{d^2 \theta}{dz^2} + I_{cg}\rho^2\theta &= 0 \end{aligned}\right\} \quad 3.2$$

(assuming harmonic motion $x = \hat{x} \sin pt$ etc.) - in which the first two equations are simultaneous and the third represents the uncoupled torsional motion.

For a straight beam, symmetrical about one axis only (say the Y, hence $r_x = o$) vibration takes place in the principal planes YZ and XZ, and $I_{xy} = o$.

Hence

$$\left.\begin{aligned} EI_{yy}\frac{d^4x}{dz^4} - m\rho^2 x &= m r_y \rho^2 \theta \\ C\frac{d^2\theta}{dz^2} + I_{cg}\rho^2\theta &= -m r_y \rho^2 x \\ EI_{xx}\frac{d^4y}{dz^4} - m\rho^2 y &= 0 \end{aligned}\right\} \quad 3.3$$

- in which the first two are simultaneous governing the coupled torsion/bending in the XX direction, and the third represents the uncoupled YY direction movement.

Boundary conditions and secondary effects.

The above equations do not take into account the secondary effects of rotary inertia and shear deformation. However, Dawson, Ghosh and Carnegie indicated[18] that for the beams considered in this work the effects of these will be negligible.

Carnegie[12] included the effect of the bending of longitudinal fibres in torsion and derived the fourth order equation

$$C_1\theta'''' - C\theta - Ak^2_{cg}\rho^2\theta = 0 \qquad 3.4$$

(where C_1 is a constant for the section) for torsional motion.

By the calculus of variations the boundary conditions

$$\theta = \theta'' = 0 \quad \text{at } z = 0$$

$$\theta' = \theta''' = 0 \quad \text{at } z = L$$

were derived, amongst other possible sets of conditions. Carnegie then stated that for an encastré support it would probably be more realistic to let $\theta' = 0$ at $z = 0$, but the above conditions are defended on the grounds that higher modes would be little affected by a change in root condition and lower modes are little affected by the bending of longitudinal fibres. The condition $\theta' = 0$ at $z = 0$ is only adopted when fibre bending is considered, as in this case the torque T_θ is given by

$$T_\theta = C\theta' - C\theta'''$$

otherwise

$$T_\theta = C\theta'$$

and therefore $\theta' = 0$ at $z = L$

The warping displacement w is defined [7] by a function

$$w = \theta' \psi(x, y)$$

from which the same equation for torsional motion (3.4) was derived by Barr (communications to 22) who stated that the conditions for a cantilever are: at $z = 0$, twist and warping displacement zero.

ie. $\theta = \theta' = 0$

and at $z = L$, torque and warping stress zero

ie. $$C\theta' - C_1\theta''' = 0$$

and $$\theta'' = 0$$

Both agree however, that for a long thin beam there would be close

agreement in frequency between the two sets of results.

As the same equation may be deduced from the two apparently independent concepts of fibre-bending and section warping, it may be deduced that these concepts are in fact inter-related; the one causing the other.

The effect of fibre bending on torsional modes has been studied by Carnegie[12] who concluded that the frequencies are raised by a factor which increases with mode number. For the first torsional mode (which is the only one considered in this work) the beam frequencies are raised by approximately 0.3% (Appendix 2), which may be neglected when compared with the accuracy with which the torsional stiffness can be determined. The effect of fibre bending (or section warping) is therefore not considered, and the torsional boundary conditions assumed are

$$\text{at } z = 0 \qquad \theta = 0$$

$$\text{and at } z = L \quad \text{Torque} = 0 \quad \text{ie.} \quad \theta' = 0$$

Solution of the equations

Dokumaci, Thomas and Carnegie presented a matrix displacement analysis [19] of the pretwisted rectangular sectioned beam, and for the purpose of investigating torsional coupling the author adapted this method to include sections possessing one or no axes of symmetry, with or without pretwist. Additionally, a very much faster program, based on the solution of the first two equations of 3.3 by Laplace Transforms is presented, and is used when initial estimates of the frequencies are readily available. Although the computer operation of this method

employs certain numerical procedures, it is basicly an analytical solution, as it solves the equations directly, without recourse to a mathematical idealisation or numerical integration.

3.1. Matrix displacement analysis.

The beam is assumed to be divided into a number of elements, the extremities of which are termed nodes. Each element has only a finite number of degrees of freedom, in this case the deflections of the nodes in the x and y planes, the slopes $\frac{dx}{dz}$, $\frac{dy}{dz}$, the rotation θ about the z axis, and the torque $\frac{d\theta}{dz}$. A cubic variation along the element for x, y and θ is assumed and the energy expressions for a typical beam element are derived in terms of the nodal displacements. Application of Lagrange's equations gives the element dynamic stiffness matrix, and the complete matrix for the whole beam is formed by assembling the element matrices and applying the boundary conditions. The eigenvalue problem can then be solved for the frequencies and mode shapes of vibration.

The equations for strain energy and kinetic energy of a pretwisted uniform beam of asymmetric section are

$$U = \frac{1}{2}\int_0^\ell \begin{bmatrix} y'' & x'' & \theta' \end{bmatrix} \begin{bmatrix} \cos\chi & \sin\chi & 0 \\ -\sin\chi & \cos\chi & 0 \\ 0 & 0 & 1 \end{bmatrix} \begin{bmatrix} EI_{xx} & 0 & 0 \\ 0 & EI_{yy} & 0 \\ 0 & 0 & C \end{bmatrix} \begin{bmatrix} \cos\chi & -\sin\chi & 0 \\ \sin\chi & \cos\chi & 0 \\ 0 & 0 & 1 \end{bmatrix} \begin{Bmatrix} y'' \\ x'' \\ \theta' \end{Bmatrix} dz \qquad \text{— 3.1.1}$$

$$T = \frac{m}{2}\int_0^\ell \begin{bmatrix} \dot{y} + r_x\dot{\theta} \end{bmatrix} \begin{bmatrix} \dot{x} + r_y\dot{\theta} \end{bmatrix} \begin{bmatrix} k_g\dot{\theta} \end{bmatrix} \begin{bmatrix} \dot{y} + r_x\dot{\theta} \\ \dot{x} + r_y\dot{\theta} \\ k_g\dot{\theta} \end{bmatrix} dz \qquad 3.1.2$$

which may be written

$$U = \frac{1}{2}\int_0^{\ell} [E_1^T] \begin{bmatrix} EI_{xx} & 0 & 0 \\ 0 & EI_{yy} & 0 \\ 0 & 0 & C \end{bmatrix} [E_1]\, dz \qquad 3.1.3$$

$$T = \frac{m}{2}\int_0^{\ell} [E_2^T][E_2]\, dz \qquad 3.1.4$$

where $$[E_1] = \begin{bmatrix} y'' \cos\chi - x'' \sin\chi \\ y'' \sin\chi + x'' \cos\chi \\ \theta' \end{bmatrix}$$

and $$[E_2] = \begin{bmatrix} \dot{y} + r_x \dot{\theta} \\ \dot{x} + r_y \dot{\theta} \\ k_{cg}\dot{\theta} \end{bmatrix}$$

Assume a cubic variation along the element for x y and θ of the form

$$y = [1 \quad z \quad z^2 \quad z^3][A]$$

$$x = [1 \quad z \quad z^2 \quad z^3][B]$$

$$\theta = [1 \quad z \quad z^2 \quad z^3][E]$$

then the continuity of displacements along an element on a fixed frame as in Fig. 3.1.1 is given by

$$y = \left\{[1 \; z \; z^2 \; z^3]\sin\chi, [1 \; z \; z^2 \; z^3]\cos\chi, 0 \; 0 \; 0 \; 0\right\}\begin{bmatrix}[B] \\ [A] \\ [E]\end{bmatrix} \qquad 3.1.5$$

$$x = \left\{[1 \; z \; z^2 \; z^3]\cos\chi, -[1 \; z \; z^2 \; z^3]\sin\chi, 0 \; 0 \; 0 \; 0\right\}\begin{bmatrix}[B] \\ [A] \\ [E]\end{bmatrix} \qquad 3.1.6$$

$$\theta = \left\{0 \; 0 \; 0 \; 0 \; 0 \; 0 \; 0 \; 0 \; 1 \; z \; z^2 \; z^3\right\}\begin{bmatrix}[B] \\ [A] \\ [E]\end{bmatrix} \qquad 3.1.7$$

Nodal displacements of the element (i, i+1) are represented as a vector

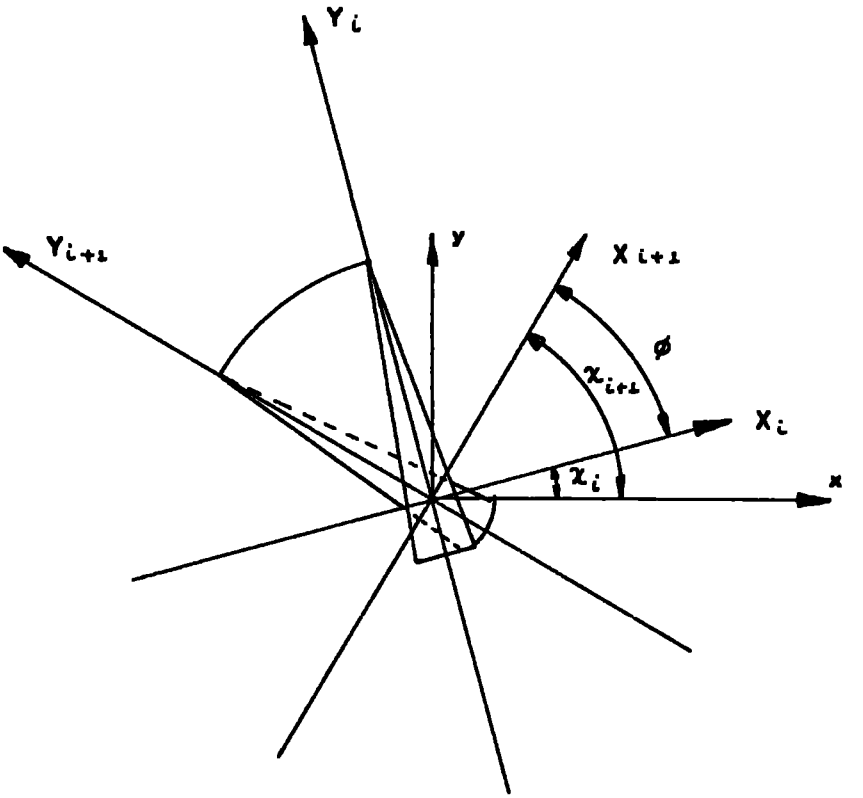

FIG 3.1.1. COORDINATE AXES
PRETWISTED BEAM

$$\{\vartheta\} = \left\{ y_i, x_i, \frac{dy}{d_3} i, \frac{dx}{d_3} i, \theta_i, \frac{d\theta}{d_3} i, y_{i+1}, x_{i+1}, \frac{dy}{d_3} i+1, \frac{dx}{d_3} i+1, \theta_{i+1}, \frac{d\theta}{d_3} i+1 \right\}$$

which may be written

$$\{\vartheta\} = [D][C]$$

where

$$[C] = [B_1 \ A_1 \ B_2 \ A_2 \ E_1 \ E_2 \ B_3 \ A_3 \ B_4 \ A_4 \ E_3 \ E_4]$$

and $[D]$ is given in Appendix 3.

Thus

$$[C] = [D^{-1}]\{\vartheta\} \qquad \text{——} \quad 3.1.8$$

From equations 3.1.5, 6, 7 and 8

$$[E_1] = [\epsilon_1][C] = [\epsilon_1][D^{-1}]\{\vartheta\}$$

and

$$[E_2] = [\epsilon_2][\dot{C}] = [\epsilon_2][D^{-1}]\{\dot{\vartheta}\}$$

where

$$[\epsilon_1] =$$

$$\begin{bmatrix} 0, -\phi^2, 2\phi, -\phi^2 3, 0, 0, 4\phi 3, -\phi^2 3^2 + 2, 6\phi 3^2, -\phi^2 3^3 + 6 3, 0, 0 \\ -\phi^2, 0, -\phi^2 3, -2\phi, 0, 0, -\phi^2 3^2 + 2, -4\phi 3, -\phi^2 3^3 + 6 3, -6\phi 3^2, 0, 0 \\ 0, 0, 0, 0, 0, 1, 0, 0, 0, 0, 2_3, 3_3^2 \end{bmatrix}$$

and $[\epsilon_2] =$

$$\begin{bmatrix} 0, 1, 0, 3, r_x, 3 r_x, 0, 3^2, 0, 3^3, r_x 3^2, r_x 3^3 \\ 1, 0, 3, 0, r_y, 3 r_y, 3^2, 0, 3^3, 0, r_y 3^2, r_y 3^3 \\ 0, 0, 0, 0, k_{cg}, 3 k_{cg}, 0, 0, 0, 0, 3^2 k_{cg}, 3^3 k_{cg} \end{bmatrix}$$

Hence 3.1.3 and 3.1.4 become

$$U = \frac{1}{2}[\vartheta^T][D^{-1}]^T[k][D^{-1}]\{\vartheta\}$$

$$\text{or} \quad \frac{1}{2}[\vartheta^T][N]\{\vartheta\} \qquad \text{——} \quad 3.1.9$$

$$\text{and} \quad T = \frac{m}{2}[\dot{\vartheta}^T][D^{-1}][m][D^{-1}]\{\dot{\vartheta}\}$$

$$\text{or} \quad \frac{m}{2}[\dot{\vartheta}^T][M]\{\dot{\vartheta}\} \qquad \text{——} \quad 3.1.10$$

$$\text{where} \quad [m] = \int_0^{\ell} [\epsilon_2^T][\epsilon_2] \, d_3$$

and $$[k] = \int_0^{\ell} [\epsilon_1^T] \begin{bmatrix} EI_{xx} & 0 & 0 \\ 0 & EI_{yy} & 0 \\ 0 & 0 & C \end{bmatrix} [\epsilon_1] \, dx$$

as shown in Appendix 3.

Applying Lagrange's equations to 3.1.9 and 3.1.10 for a conservative system

$$\left[\frac{\partial U}{\partial D}\right] + \frac{d}{dt}\left[\frac{\partial T}{\partial \dot{D}}\right] = 0 \qquad 3.1.11$$

and since $[N]$ and $[M]$ are symmetric

$$\left[\frac{\partial U}{\partial D}\right] = [N]\{D\} \quad \text{and} \quad \frac{d}{dt}\left[\frac{\partial T}{\partial \dot{D}}\right] = m[M]\{\ddot{D}\}$$

Hence 3.1.11 becomes

$$[N]\{D\} + m[M]\{\ddot{D}\} = 0$$

Assuming harmonic motion of circular frequency p,

$$\{D\} = \{\hat{D}\} e^{ipt} \qquad \text{where } i = \sqrt{-1}$$

$$\text{i.e.} \quad [[N] - p^2[M]]\{\hat{D}\} = 0$$

$[N]$ and $[M]$ may be summed for the whole beam to give

$$[[\Sigma N] - p^2 m [\Sigma M]]\{\hat{D}\} = 0$$

which may be solved as an eigenvalue problem.

3.2. Solution by Laplace Transforms

For an untwisted beam whose cross-section is symmetrical about the Y axis, the equations of coupled bending and torsional vibration 3.1 reduce to

$$x'''' = -\frac{m}{EI_{yy}} \ddot{x} - \frac{m r_y}{EI_{yy}} \ddot{\theta}$$

$$\theta'' = \frac{m r_y}{c} \ddot{x} + \frac{m (r_y^2 + k^2_{cg})}{c} \ddot{\theta}$$

and the third equation is independent of x and θ and governs the uncoupled motion in the YY direction.

The above equations further reduce to

$$x'''' = a\ddot{x} + b\ddot{\theta} \qquad 3.2.1$$

$$\theta'' = c\ddot{x} + d\ddot{\theta} \qquad 3.2.2.$$

where $a = \frac{-m}{EI_{yy}}$; $b = \frac{-m r_y}{EI_{yy}}$; $c = \frac{m r_y}{c}$; $d = \frac{m(r_y^2 + k^2_{cg})}{c}$

Consider that the solutions are separable, and of the form

$$x = F(\xi) \cdot T(t)$$

$$\theta = G(\xi) \cdot T(t)$$

where both time functions are equal for a given normal mode.

Substituting in 3.2.1 and 3.2.2

$$F'''' = (aF + bG)\ddot{T}/T$$

$$\therefore \frac{F''''}{aF+bG} = \frac{\ddot{T}}{T} = -p^2$$

ie. $$\ddot{T} + p^2 T = 0$$

hence p represents the circular frequency of vibration,

$$F'''' = -p^2 (aF + bG) \quad \text{——} \quad 3.2.3$$

and

$$G'' = -p^2 (cF + dG) \quad \text{——} \quad 3.2.4$$

The boundary conditions are that at z = 0, deflection, slope and rotation are zero; and at z = L, bending moment, shear force and torque are zero, ie.

$$F(0) = F'(0) = G(0) = 0$$

$$F''(L) = F'''(L) = G'(L) = 0$$

Taking Laplace Transforms of 3.2.3

$$\mathcal{L}(F'''') = -\rho^2 a\, \mathcal{L}(F) - \rho^2 b\, \mathcal{L}(G)$$

$$\therefore\ s^4 \mathcal{L}(F) - s^3 F(0) - s^2 F'(0) - s F''(0) - F'''(0) = -\rho^2 a \mathcal{L}(F) - \rho^2 b\, \mathcal{L}(G)$$

$F''(o)$ and $F'''(o)$ are unknown, therefore they are replaced by Q and R (which are functions of t alone) hence

$$s^4 \mathcal{L}(F) - sQ - R = -\rho^2 a\, \mathcal{L}(F) - \rho^2 b\, \mathcal{L}(G) \quad \text{— 3.2.5}$$

Similarly, taking Laplace Transforms of 3.2.4, and replacing the unknown $G^1(o)$ with W (a function of t alone):

$$s^2 \mathcal{L}(G) - W = -\rho^2 c\, \mathcal{L}(F) - \rho^2 d\, \mathcal{L}(G) \quad \text{—— 3.2.6}$$

Solving 3.2.5 and 3.2.6 simultaneously for $\mathcal{L}(F)$ and $\mathcal{L}(G)$ it is found that

$$\mathcal{L}(G) = \frac{s^4 W - s\rho^2 c Q - R\rho^2 c + W\rho^2 a}{s^6 + s^4\rho^2 d + s^2\rho^2 a + \rho^4(ad - bc)} \qquad 3.2.7$$

and

$$\mathcal{L}F = \frac{s^3 Q + s^2 R - W\rho^2 b + s\rho^2 dQ + R\rho^2 d}{s^6 + s^4\rho^2 d + s^2\rho^2 a + \rho^4(ad - bc)} \qquad 3.2.8$$

Assume now that $\mathcal{L}$ (F) may be reprsented as

$$\mathcal{L}(F) = \frac{As + B}{s^2 - \alpha} + \frac{Cs + D}{s^2 - \beta} + \frac{Es + H}{s^2 - \gamma}$$

where α, β, γ are the roots of the denominator of 3.2.8 and A,B,C,D,E and H are constants which are determined by equating coefficients of s^n, n = 0 to 5.

Hence $\mathcal{L}(F)$ is given by $\mathcal{L}(F) =$

$$\frac{G(\rho^2\alpha+\alpha)}{(\beta-\alpha)(\gamma-\alpha)}\left\{\frac{s}{s^2-\alpha}\right\}+\frac{G(\rho^2\alpha+\beta)}{(\alpha-\beta)(\gamma-\beta)}\left\{\frac{s}{s^2-\beta}\right\}+\frac{G(\rho^2\alpha+\gamma)}{(\alpha-\gamma)(\beta-\gamma)}\left\{\frac{s}{s^2-\gamma}\right\}$$

$$+\frac{R(\rho^2\alpha+\alpha)}{(\beta-\alpha)(\gamma-\alpha)}\left\{\frac{1}{s^2-\alpha}\right\}+\frac{R(\rho^2\alpha+\beta)}{(\alpha-\beta)(\gamma-\beta)}\left\{\frac{1}{s^2-\beta}\right\}+\frac{R(\rho^2\alpha+\gamma)}{(\alpha-\gamma)(\beta-\gamma)}\left\{\frac{1}{s^2-\gamma}\right\}$$

$$+\frac{W(-\rho^2\alpha)}{(\beta-\alpha)(\gamma-\alpha)}\left\{\frac{1}{s^2-\alpha}\right\}+\frac{W(-\rho^2\alpha)}{(\alpha-\beta)(\gamma-\beta)}\left\{\frac{1}{s^2-\beta}\right\}+\frac{W(-\rho^2\alpha)}{(\alpha-\gamma)(\beta-\gamma)}\left\{\frac{1}{s^2-\gamma}\right\}$$ ——3.2.9

Similarly, as the denominators of 3.2.7 and 3.2.8 are identical, (G) is given by $\mathcal{L}(G) =$

$$\frac{Q(-\rho^2c)}{(\beta-\alpha)(\gamma-\alpha)}\left\{\frac{s}{s^2-\alpha}\right\}+\frac{Q(-\rho^2c)}{(\alpha-\beta)(\gamma-\beta)}\left\{\frac{s}{s^2-\beta}\right\}+\frac{Q(-\rho^2c)}{(\alpha-\gamma)(\beta-\gamma)}\left\{\frac{1}{s^2-\gamma}\right\}$$

$$\frac{R(-\rho^2c)}{(\beta-\alpha)(\gamma-\alpha)}\left\{\frac{1}{s^2-\alpha}\right\}+\frac{R(-\rho^2c)}{(\alpha-\beta)(\gamma-\beta)}\left\{\frac{1}{s^2-\beta}\right\}+\frac{R(-\rho^2c)}{(\alpha-\gamma)(\beta-\gamma)}\left\{\frac{1}{s^2-\gamma}\right\}$$

$$\frac{W(\rho^2a+\alpha^2)}{(\beta-\alpha)(\gamma-\alpha)}\left\{\frac{1}{s^2-\alpha}\right\}+\frac{W(\rho^2a+\beta^2)}{(\alpha-\beta)(\gamma-\beta)}\left\{\frac{1}{s^2-\beta}\right\}+\frac{W(\rho^2a+\gamma^2)}{(\alpha-\gamma)(\beta-\gamma)}\left\{\frac{1}{s^2-\gamma}\right\}$$

——— 3.2.10

Taking inverse Laplace Transforms of 3.2.9 and 3.2.10 and letting

$$[A(3)] = \frac{\rho^2\alpha+\alpha}{(\beta-\alpha)(\gamma-\alpha)}\begin{Bmatrix}\cosh\alpha^{1/2}3\\ \cos\alpha^{1/2}3\end{Bmatrix} + \frac{\rho^2\alpha+\beta}{(\alpha-\beta)(\gamma-\beta)}\begin{Bmatrix}\cosh\beta^{1/2}3\\ \cos\beta^{1/2}3\end{Bmatrix} + \frac{\rho^2\alpha+\gamma}{(\alpha-\beta)(\beta-\gamma)}\begin{Bmatrix}\cosh\gamma^{1/2}3\\ \cos\gamma^{1/2}3\end{Bmatrix},$$

$$[B(3)] = \frac{\rho^2\alpha+\alpha}{(\beta-\alpha)(\gamma-\alpha)}\begin{Bmatrix}\alpha^{-1/2}\sinh\alpha^{1/2}3\\ \alpha^{-1/2}\sin\alpha^{1/2}3\end{Bmatrix} + \frac{\rho^2\alpha+\beta}{(\alpha-\beta)(\gamma-\beta)}\begin{Bmatrix}\beta^{-1/2}\sinh\beta^{1/2}3\\ \beta^{-1/2}\sin\beta^{1/2}3\end{Bmatrix} + \frac{\rho^2\alpha+\gamma}{(\alpha-\gamma)(\beta-\gamma)}\begin{Bmatrix}\gamma^{-1/2}\sinh\gamma^{1/2}3\\ \gamma^{-1/2}\sin\gamma^{1/2}3\end{Bmatrix},$$

$$[C(3)] = \frac{(-\rho^2\alpha)}{(\beta-\alpha)(\gamma-\alpha)}\begin{Bmatrix}\alpha^{-1/2}\sinh\alpha^{1/2}3\\ \alpha^{-1/2}\sin\alpha^{1/2}3\end{Bmatrix} + \frac{(-\rho^2\alpha)}{(\alpha-\beta)(\gamma-\beta)}\begin{Bmatrix}\beta^{-1/2}\sinh\beta^{1/2}3\\ \beta^{-1/2}\sin\beta^{1/2}3\end{Bmatrix} + \frac{(-\rho^2\alpha)}{(\alpha-\gamma)(\beta-\gamma)}\begin{Bmatrix}\gamma^{-1/2}\sinh\gamma^{1/2}3\\ \gamma^{-1/2}\sin\gamma^{1/2}3\end{Bmatrix},$$

$$[D(3)] = \frac{-\rho^2 c}{(\beta-\alpha)(\gamma-\alpha)}\begin{Bmatrix}\cosh\alpha^{1/2}3\\ \cos\alpha^{1/2}3\end{Bmatrix} + \frac{-\rho^2 c}{(\alpha-\beta)(\gamma-\beta)}\begin{Bmatrix}\cosh\beta^{1/2}3\\ \cos\beta^{1/2}3\end{Bmatrix} + \frac{-\rho^2 c}{(\alpha-\gamma)(\beta-\gamma)}\begin{Bmatrix}\cosh\gamma^{1/2}3\\ \cos\gamma^{1/2}3\end{Bmatrix},$$

$$[E(3)] = \frac{-\rho^2 c}{(\beta-\alpha)(\gamma-\alpha)}\begin{Bmatrix}\alpha^{-1/2}\sinh\alpha^{1/2}3\\ \alpha^{-1/2}\sin\alpha^{1/2}3\end{Bmatrix} + \frac{-\rho^2 c}{(\alpha-\beta)(\gamma-\beta)}\begin{Bmatrix}\beta^{-1/2}\sinh\beta^{1/2}3\\ \beta^{-1/2}\sin\beta^{1/2}3\end{Bmatrix} + \frac{-\rho^2 c}{(\alpha-\gamma)(\beta-\gamma)}\begin{Bmatrix}\gamma^{-1/2}\sinh\gamma^{1/2}3\\ \gamma^{-1/2}\sin\gamma^{1/2}3\end{Bmatrix},$$

$$[H(3)] = \frac{(\rho^2\alpha+\alpha^2)}{(\beta-\alpha)(\gamma-\alpha)}\begin{Bmatrix}\alpha^{-1/2}\sinh\alpha^{1/2}3\\ \alpha^{-1/2}\sin\alpha^{1/2}3\end{Bmatrix} + \frac{(\rho^2\alpha+\beta^2)}{(\alpha-\beta)(\gamma-\beta)}\begin{Bmatrix}\beta^{-1/2}\sinh\beta^{1/2}3\\ \beta^{-1/2}\sin\beta^{1/2}3\end{Bmatrix} + \frac{(\rho^2\alpha+\gamma^2)}{(\alpha-\gamma)(\beta-\gamma)}\begin{Bmatrix}\gamma^{-1/2}\sinh\gamma^{1/2}3\\ \gamma^{-1/2}\sin\gamma^{1/2}3\end{Bmatrix},$$

(Where the hyperbolic functions in the chain brackets are chosen if the root is positive, and the trigonometric functions if the root is negative) then

$$F = Q[A(3)] + R[B(3)] + W[C(3)] \quad \text{— 3.2.11}$$

$$\text{and} \quad G = Q[D(3)] + R[E(3)] + W[H(3)] \quad \text{— 3.2.12}$$

Applying the boundary conditions at z = L, the matrix equation

$$\begin{bmatrix} [A'(L)] & [B''(L)] & [C''(L)] \\ [A'''(L)] & [B'''(L)] & [C'''(L)] \\ [D'(L)] & [E'(L)] & [H'(L)] \end{bmatrix} \begin{Bmatrix} Q \\ R \\ W \end{Bmatrix} = \begin{Bmatrix} 0 \\ 0 \\ 0 \end{Bmatrix} \qquad 3.2.13$$

is formed, and the condition that p is a natural frequency of the system is that the determinant of the coefficients of Q,R and W on the left hand side of 3.2.13 is zero.

3.3 Torsional stiffness: methods of calculation

1. Elliptical approximation

The exact stress function solution for the ellipse yields

$$C = \frac{A^3 G}{4\pi^2 k_{cg}^2}$$

and can be applied to certain non elliptical sections with reasonable accuracy.

2. Griffith's methods[1]

a). Graphical method

This is rather complicated and can be difficult to apply but nevertheless good agreement is obtained with other more sophisticated methods.

It is deduced that a first approximation may be obtained from the formula

$$C = \tfrac{1}{2}\, G.A.\left(\frac{2A}{P}\right)^2$$

where p is the section perimeter.

However, there are two important cases in which this formula requires modification; the presence of sharp outwardly projecting corners (as in the triangle) causes the formula to give a low value to C. This problem is overcome by rounding off the corner with a radius r which is a certain fraction of the radius of the inscribed circle. The fraction depends on the angle in the corner in question (λ) and a graph, obtained partly from known results and partly from soap film measurements was presented in the paper. After the rounding off process, a new figure is obtained, with Area A_1 and perimeter P_1 and thus a corrected value of C is obtained from

$$C_1 = \frac{1}{2} G.A.\left(\frac{2A_1}{P_1}\right)^2$$

The second case requiring modification occurs when the ratio

$$a/\frac{2A}{P}$$ (a = radius of inscribed circle)

is appreciably less than unity. This makes the value C_1 too large by an amount which is nearly the same for all sections having the same value of the above ratio and hence a correction factor (k) is included which is obtained from a graph of $a/\frac{2A}{P}$ against K.

The modified formula is now

$$C_2 = \frac{1}{2} . G.K.A \cdot \left(\frac{2A_1}{P_1}\right)^2$$

As has been stated, this method is tedious in its practical application, but by employing curve-fit procedures for determining r and K it may be programmed for digital computation. The graphs from

which the rounding off radius r and correction factor K are obtained are included for reference in Appendix 5.

b). Direct formula

Griffith presented a formula applicable only to extremely thin sections, which is exact for an infinitely long rectangular section. It is deduced by considering that the longitudinal curvature of a soap film on a long narrow slit may be neglected, giving the formula

$$C = \frac{G}{3}\int \xi y^3 dx = \frac{G}{3} I$$

c = length of section.

y = half width at distance x along the section.

(Fig. 3.3.1)

It is further stated that the case of ellipses suggests the modification

$$C = \frac{G \frac{1}{3} I}{1 + \frac{4}{3}\frac{I}{Ac^2}}$$

A = sectional area

which allows for longitudinal curvature of the soap film.

3. Approximation to the sector of a circle[2]

There exists an exact stress function solution (in the form of a series) for the torsion of a sector of a circle, which may be applied to the thin isosceles triangle:

From figure (3.3.2) it can be seen that the isosceles triangle OCD is greater in area than the sector OAB but less than the sector OCD, and therefore the torsional stiffness of the triangle should lie in between the known values of the two sectors. Obviously, the difference between the torsional stiffness of the two decreases as tends to zero.

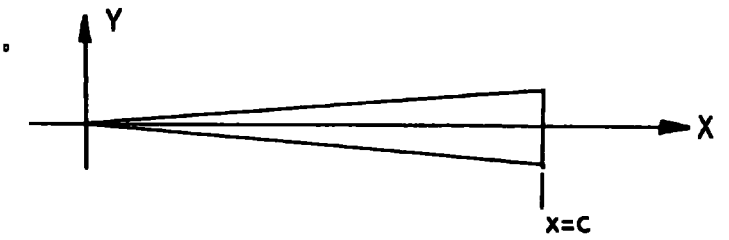

FIG. 3.3.1

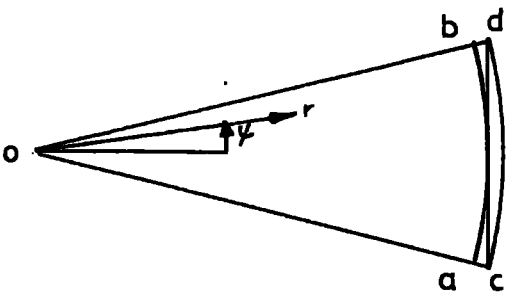

FIG. 3.3.2, SECTOR LIMITS

From elasticity theory

$$C = \frac{2}{\theta}\int_0^a \int_{-\alpha/2}^{\alpha/2} \phi\, r\, d\psi\, dr$$

a = radius of sector

where ϕ is the stress function given by

$$\phi = \frac{G\theta}{2}\left[-v^2\left(1 - \frac{\cos 2\psi}{\cos\alpha}\right) + \frac{16a^2\alpha^2}{\pi^3}\sum_{n=1,3,5}^{\infty}(-1)^{\frac{n+1}{2}}\left(\frac{v}{a}\right)^{\frac{n\pi}{\alpha}}\frac{\cos\frac{n\pi\psi}{\alpha}}{n\left(n+\frac{2\alpha}{\pi}\right)\left(n-\frac{2\alpha}{\pi}\right)}\right]$$

It is found that terms in the series beyond n = 5 are negligible, and therefore substituting the expression for ϕ in the equation for C and integrating gives

$$C = 2Ga^4\left\{\frac{\tan\alpha - \alpha}{8} + \frac{16\alpha^3}{\pi^4}\left[-\sum_{n=1,3,5}^{\infty}\frac{1}{n^2\left(\frac{n\pi}{\alpha}+2\right)\left(n+\frac{2\alpha}{\pi}\right)\left(n-\frac{2\alpha}{\pi}\right)}\right]\right\}$$

from which C for the two sectors may be calculated.

4. Approximate stress function for a narrow isosceles triangle[3]

Duncan, Ellis and Scruton have obtained an approximate stress function for an isosceles triangle using Ritz's variational technique. The expression produced for C is exact for the equilateral triangle and the fractional error tends to vanish as α tends to zero.

If ψ be the torsional stress function for the section, then the integral

$$U = \iint\left\{\frac{1}{2}\left(\frac{\partial\psi}{\partial x}\right)^2 + \frac{1}{2}\left(\frac{\partial\psi}{\partial y}\right)^2 - 2\psi\right\} dx\, dy$$

is stationary for small variations of ψ which vanish on the boundary.

It is assumed that for the section in Fig (3.3.1) bounded by

$$y = \pm mx$$

$$x = c$$

$$\psi = \frac{m^2x^2 - y^2}{1-m^2} f(x)$$

where $f(c) = 0$

Application of the calculus of variations results in the approximate stress function

$$\psi = \frac{m^2x^2 - y^2}{1-m^2}\left(1 - \left(\frac{x}{c}\right)^r\right)$$

where $r = \frac{\sqrt{6m^2+10}}{2m} - 2$

from which

$$C = \frac{2Gm^3c^4}{3(1-m^2)}\left(1 - \frac{4}{r+4}\right)$$

5. Alternative variational method[4]

The total potential energy of a rod of length l, shear modules G, twisted through an angle θ radians per unit length is given by

$$U = \frac{l}{2G}\iint_R \left[\left(\frac{\partial\phi}{\partial x}\right)^2 + \left(\frac{\partial\phi}{\partial y}\right)^2 - 4G\theta\phi\right] dx\,dy \qquad \text{—— 3.3.1}$$

where $\phi(x,y)$ is the stress function which must satisfy Poisson's equation for torsion:

$$\frac{\partial^2\phi}{\partial x^2} + \frac{\partial^2\phi}{\partial y^2} = \nabla^2\phi = -2G\theta \qquad (3.3.2)$$

The usual procedure adopted is to determine a stress function $\phi(x,y)$ which satisfies (3.3.2) and has zero value along the boundary of the cross section.

Nuttall[4], however, determines a function $\phi_r(x,y)$ which has zero value along the boundary and satisfies the equation

$$\nabla^2\phi_r(x,y) = -\lambda_r^2\phi_r(x,y) \qquad (3.3.3)$$

If λ_r^2 and λ_s^2 are eigenvalues corresponding to the eigenvectors ϕ_r and ϕ_s, an application of Green's theorem gives,

$$\iint_R \left[\phi_r \nabla^2\phi_s - \phi_s \nabla^2\phi_r\right] dx\,dy = \left(\lambda_r^2 - \lambda_s^2\right)\iint_R \phi_r\phi_s\,dx\,dy$$

$$= \int_C \left[\phi_r \frac{\partial\phi_s}{\partial n} - \phi_s \frac{\partial\phi_r}{\partial n}\right] ds$$

$$= 0$$

as $\phi_r = \phi_s = 0$ along the boundary

If, therefore $\lambda_r^2 \neq \lambda_s^2$ the orthogonal relationship

$$\iint_R \phi_r\phi_s\,dx\,dy = 0$$ is satisfied.

If the stress function is now expanded in the form

$$\phi = \sum_r A_r \phi_r$$

and substituted in equation (3.3.1) and ie.

$$U = \frac{l}{2G}\left[\sum_r A_r^2 \lambda_r^2 \iint_R \phi_r^2 \, dx\,dy - 4G\theta \sum_r A_r \iint_R \phi_r \, dx\,dy\right]$$

the condition $\frac{\partial U}{\partial A_i} = 0$ that U shall be stationary provides the equations for determining A_r:

ie. $$A_r = 2G\theta \frac{k_r^2}{\lambda_r^2} \iint_R \phi_r \, dx\,dy$$

where $$k_r^2 \iint \phi_r^2 \, dx\,dy = 1$$

The stress function ϕ may therefore be written as

$$\phi = 2G\theta \sum_r \left[\frac{k_r^2}{\lambda_r^2} \iint \phi_r \, dx\,dy\right] \phi_r$$

By this method, Nuttall obtained solutions for rods of (amongst others) equilateral and right angled isosceles triangular sections. These exact solutions are further modified to produce Rayleigh-Ritz approximate solutions for cross sections of any isosceles triangular shape.

In each case the approximate stress function ϕ is written in the form $\phi = \sum A_r \phi_r$ where ϕ_r is given by one or other of the following expressions:

$$\phi_r(x,y) = \frac{2 \sin \pi n x \cos \pi n y}{3ba} - \frac{\sin 2\pi n x}{3b} \quad \text{— 3.3.4}$$

where height = 3b, width = 2a

$$\phi_r(x,y) = \cos\left[\frac{\pi}{6b}(m+n)x\right]\cos\left[\frac{\pi}{2a}(m-n)y\right]$$

$$-\cos\left[\frac{\pi}{6b}(m-n)x\right]\cos\left[\frac{\pi}{2a}(m+n)y\right] \quad \begin{matrix} m \text{ odd} \\ n \text{ even} \end{matrix}$$

Each of these functions has zero value along the boundary, and (3.3.4) is exact in the case of the equilateral triangle, while (3.3.5) is exact for the right angled isosceles triangle.

The solution corresponding to (3.3.4) gives

$$C = 3\cdot6\,\frac{G a^3 b^3}{a^2+3b^2} \qquad (3.3.6)$$

and that corresponding to (3.3.5) gives

$$C = \frac{55{,}296\, G a^3 b^3}{\pi^6(a^2+9b^2)} \sum_{\substack{m \\ \text{odd}}} \sum_{\substack{n \\ \text{even}}} \frac{n^2}{m^2(m^4-n^4)(m^2-n^2)+\frac{32}{\pi^4}\left(\frac{a^2-9b^2}{a^2+9b^2}\right)m^4n^2}$$

(3.3.7)

It is stated that in the range $\alpha \leq 60°$ equation (3.3.6) should be used and in the range $\alpha \geq 90°$ equation (3.3.7) is more accurate. For $60° < \alpha < 90°$ the equations serve as a check on each other.

6. Empirical formula for C

Scholes and Slater[5] commented that Griffith's formula for very thin sections:

$$C = \frac{G}{J}\int_0^c 8y^3\,dx \qquad \text{Fig. (3.3.1)}$$

or

$$C = \frac{GI}{J}$$

tended to give results which are rather high, even after the

modification described previously. Hence an empirical formula was presented which allows for the reduction in stiffness at the ends of the section.

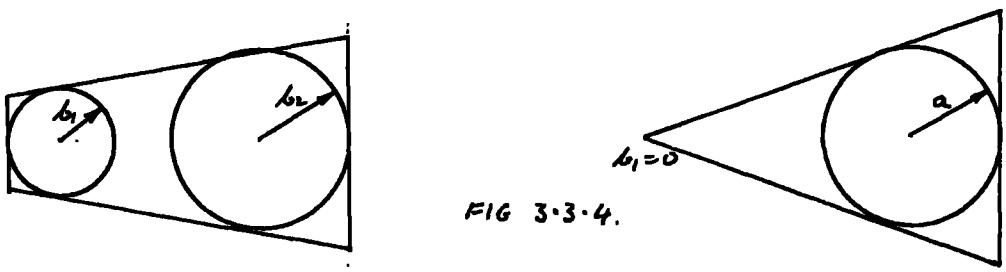

FIG 3·3·4.

The reduction in stiffness is assumed to depend on the end radius (for a round ended bar) or the radius of the local inscribed circle (for a square ended bar) Fig. (3.3.4)

The formula thus derived is of the form

$$C = G\left\{ I/3 - k_{1,2} \left(b_1^4 + b_2^4 \right) \right\}$$

where k_1 is a factor for round eded bars, and k_2 applies to square ended bars.

From published data it is stated that

$k_1 = 0.068$

$k_2 = 0.106$

Thus for the thin isosceles triangular section

$$C = G\left\{ I/3 - 0.106\, a^4 \right\}$$ where a = radius of inscribed circle.

(b_1 or $b_2 = 0$ for pointed ends)

3.4 Position of the centre of flexure

1. Determination by soap film analogy[2]

A force W is applied at the centre of flexure, c, of a section symmetrical about the Y axis. (Fig 3.4.1)

The general theory of elasticity is applied which gives the shear stresses Xz, Yz by

$$Xz = \frac{W}{Ak^2_{yy}} \left(\frac{\partial \psi}{\partial y} - \frac{x^2}{2} + \frac{\nu y^2}{2(1+\nu)} \right) \qquad (3.4.1)$$

$$Yz = -\frac{W}{Ak^2_{yy}} \frac{\partial \psi}{\partial x} \qquad (3.4.2)$$

in terms of a function $\psi(x,y)$

As $W r_y + \iint (x Y_3 - y X_3)\, dx\, dy = 0$,

$$\therefore r_y = \frac{1}{Ak^2_{yy}} \iint \left(x \frac{\partial \psi}{\partial x} + y \frac{\partial \psi}{\partial y} - \frac{x^3}{2} + \frac{\nu x y^2}{2(1+\nu)} \right) dx\, dy \qquad (3.4.3)$$

From the boundary condition, it is deduced that

$$\psi = \frac{1}{2} \int x^2\, dy - \frac{\nu}{2(1+\nu)} \frac{y^3}{3} + \text{const.} \qquad (3.4.4)$$

which gives the value of ψ on the boundary of the section.

Suppose that a hole is now cut in a piece of metal such that its projection on the XY plane has the same shape as the section, while the Z coordinates represent to some scale, the values of ψ given in equation (3.4.4) Fig. (3.4.2)

If a soap film is now stretched over the hole with zero pressure difference between the two sides and the z coordinates of the film are

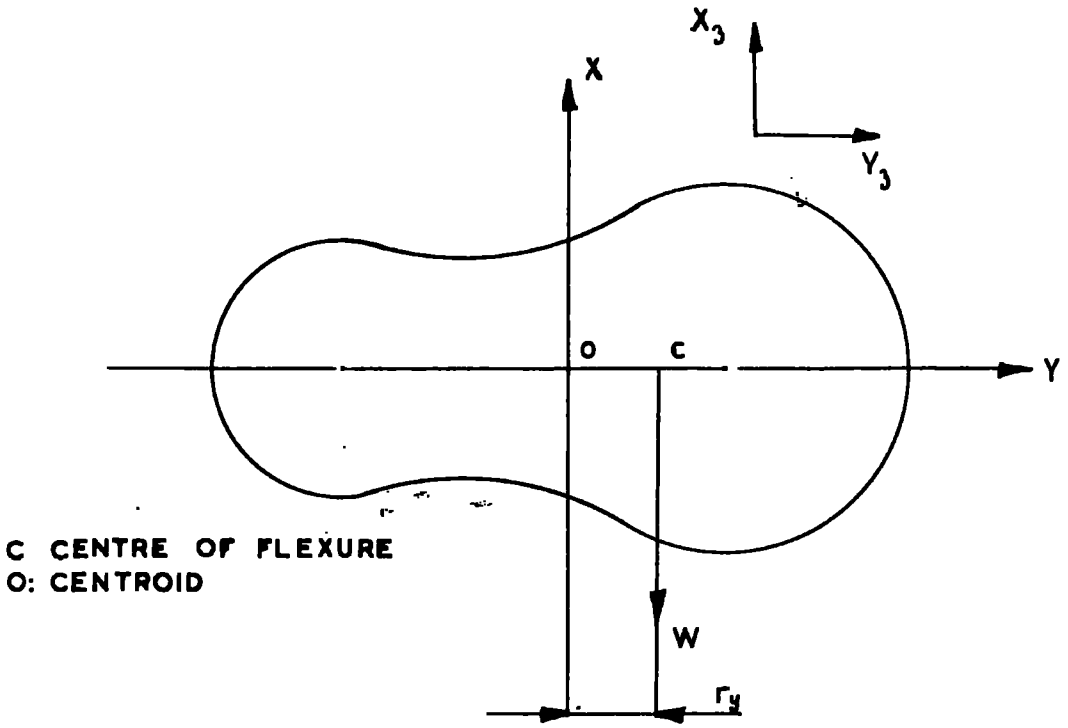

FIG. 3 4 1

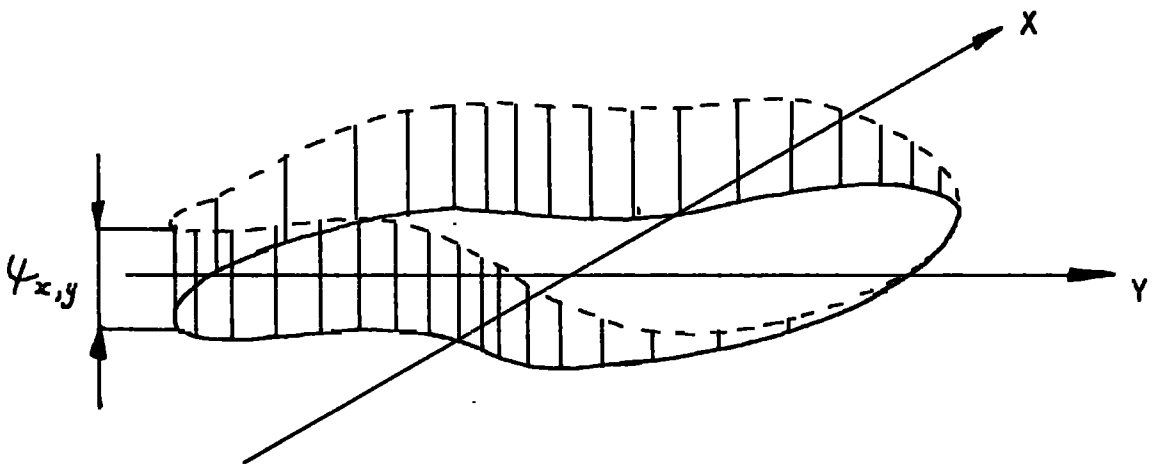

FIG. 3.4.2

sufficiently small in comparison with the x and y dimensions, then the z coordinates of the film represent the value of at all points in the cross section. Hence contour lines of the film may be drawn and Xz and Yz determined.

During the soap film measurements, it was noted that if the section is bounded by curves which are nearly parallel of separation t, then if t is small certain lines on the soap film may be assumed to be straight.

Applying this assumption to the theory, Xz, Yz and r_y become

$$Xz = -\frac{\omega}{Ak^2_{yy}} \frac{1}{t} \frac{dx}{ds} \left(\int t\left(x - \frac{t_1}{2}\right) ds + c \right)$$

$$Yz = -\frac{\omega}{Ak^2_{yy}} \frac{1}{t} \frac{dy}{ds} \left(\int t\left(x + \frac{t_1}{2}\right) ds + c \right)$$

$$r_y = \frac{1}{Ak^2_{yy}} \int \left[\int t\left(x - \frac{t_1}{2}\right) ds + c \right] \left(x\frac{dy}{dx} - y\frac{dx}{ds} \right) ds \quad (3.4.5)$$

where $t_1 = t\frac{ds}{dy}$

From (3.4.5), for a thin beam

$$r_y = \frac{1}{2Ak^2_{yy}} \iint y(t^2 - x^2)\, dx\, dy = \frac{\int t^3 y\, ds}{\int t^3 dy} \quad (8)$$

2. Determination of r_y by an approximate stress function

Duncan, similarly, derives the fundamental theory of flexure resulting in the equations for the shear stresses: (Fig. 3.4.1)

$$Yz = -\frac{\omega}{Ak^2_{yy}} \frac{\partial \psi'}{\partial x}$$

$$Xz = \frac{\omega}{Ak^2_{yy}} \left\{ \frac{\partial \psi'}{\partial y} - \frac{1}{2}x^2 + \frac{\nu y^2}{2(1-\nu)} \right\} \quad (3.4.6)$$

in terms of a function $\psi'(x, y)$

A stress function Ω is introduced where

$$\Omega = \psi' - B(y) \qquad \text{which vanishes on the boundary if}$$

$$B(y) = \int_0^y t^2 dy - \frac{\nu (y^3 - a^3)}{6(1+\nu)}$$

Also as $\nabla^2 \psi' = 0$

$$\therefore \nabla^2 \Omega + \frac{d^2 B}{dy^2} = 0 \qquad (3.4.8)$$

To obtain the approximate stress function, Ω is expanded in the form

$$\Omega = f^0(y) + x^2 f'(y) + x^4 f^2(y) \cdots\cdots$$

and as Ω vanishes on the boundary $x=t$

$$\therefore \quad 0 = f^0(y) + t^2 f'(y) + t^4 f^2(y) \cdots\cdots$$

Hence $$\Omega = \sum_1^\infty (t^{2n} - x^{2n}) f^n(y)$$

Substitution in (3.4.8) gives

$$D^2 \sum_1^\infty t^{2n} f^n(y) - \sum_1^\infty x^{2n} D^2 f^n(y) - \sum_1^\infty 2n(2n-1) x^{2n-2} f^n(y) + D^2 B = 0 \qquad (3.4.9)$$

where $D = \frac{d}{dy}$

Equating to zero the coefficients of x^2 and higher powers, the recurrence relation

$$f^n(y) = \frac{2(-1)^{n-1}}{(2n)!} D^{2n-2} f'(y) \qquad (3.4.10)$$

The superscript in $f'(y)$ may now be omitted. The terms in (3.4.9) independent of x become on substitution from (3.4.10),

$$D^2 B + 2 D^2 \sum_1^\infty t^{2n} \frac{(-1)^{n-1}}{(2n)!} D^{2n-2} f(y) - 2f(y) = 0$$

giving $$f(y) = \Delta^2\left\{ \tfrac{1}{2}B + \sum_{1}^{\infty} t^{2n}\frac{(-1)^{n-1}}{(2n)!}\Delta^{2n-2} f(y)\right\} \qquad (3.4.11)$$

The function B(y) is the sum of a term dependent on x and one independent of x.

If $B_0 = \dfrac{\nu(a^3 - y^3)}{6(1+\nu)}$

and $B_2 = \tfrac{1}{2}\int_0^y t^2\,dy$

then $B(y) = B_0 + B_2$

and the first approximation of f(y) arises from B_0 on the right hand side of (3.4.11)

Hence $f_1(y) = \tfrac{1}{2}\Delta^2 B_0 = \dfrac{-\nu y}{2(1+\nu)}$

From (3.4.10) the exact expression for Ω is

$$\Omega = 2\sum_{1}^{\infty}\frac{(-1)^{n-1}}{(2n)!}(t^{2n} - x^{2n})\Delta^{2n-2} f(y)$$

and the first approximation to Ω

is $\Omega_{ap.} = (t^2 - x^2) f_1(y)$

$$= \frac{-\nu(t^2 - x^2)y}{2(1+\nu)} \qquad (3.4.12)$$

As r_y is the distance from the centroid to the centre of flexure, then

$$W r_y = -\iint (x Y_3 - y X_3)\,dx\,dy$$

$$= \frac{-W}{Ah^3 I_y}\iint\left\{\frac{y}{2}(t^2 - x^2) + y\frac{\partial \Omega_{ap}}{\partial y} + x\frac{\partial \Omega_{ap}}{\partial x}\right\}dx\,dy$$

——— 3.4.13.

$$\iint \frac{y}{2}(t^2 - x^2)\,dx\,dy = \frac{2}{3}\int y t^3\,dy$$

and from Green's theorem

$$\iint \left(y\frac{\partial \Omega}{\partial y} + x\frac{\partial \Omega}{\partial x}\right)dx\,dy = -2\iint \Omega\,dx\,dy \qquad (3.4.14)$$

Therefore from 3.4.13 and 3.4.14, taking the first approximation to Ω as given by (3.4.12), as this is the limiting case for thin sections,

$$r_y = \frac{1+3\nu}{1+\nu}\,\frac{\int y t^3\,dy}{\int t^3\,dy}$$

3. Approximation to the sector of a circle.

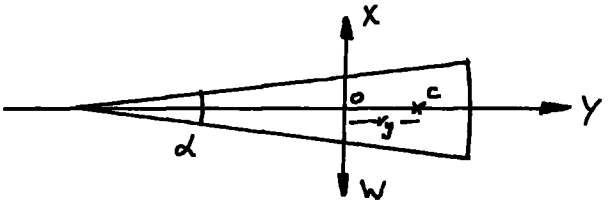

(3.4.4)

Young, Elderton and Pearson[9] consider the torsion produced in a sector by a force W applied at the centroid at right angles to the axis of symmetry. (It is not, of course strictly applicable to the triangle, but has been included very briefly for completeness).

The torsion produced per unit length is given by

$$\theta = \frac{Wa}{EI_{yy}} \qquad \text{——} \quad 3.4.15$$

Where K is a constant dependent upon ν and α, and may be calculated from formulae given in the paper.

The torsional stiffness per unit length, by definition, is given by

$$C = \frac{T}{\theta}$$

where T is the applied torque

$$= \frac{W r_y}{\theta}$$

$$\therefore \quad \theta = \frac{W r_y}{C} \qquad (3.4.16)$$

Hence from (3.4.15) and (3.4.16)

$$r_y = \frac{C_a \kappa}{E I_{yy}}$$

3.5. Torsional oscillations of asymmetric sections

It is not strictly valid to consider an asymmetric section executing purely torsional oscillations as the motion will always be coupled with transverse motion in the direction of either or both principal axes. However, if the predominantly torsional frequency differs from the nearest bending mode frequency by more than 20%, the influence of the bending mode is very small and the section may be considered to be oscillating in torsion alone.

Consider a section of cantilever beam of narrow isosceles triangular cross-section at a point some distance from the root. Fig.3.5.1.

Under the action of a force F applied at the centroid in the positive X direction and an equal and opposite force applied at the centre of flexure, C, the section will rotate about C by definition, as it is under the influence of a pure couple.

However, it does not follow from this static argument that the

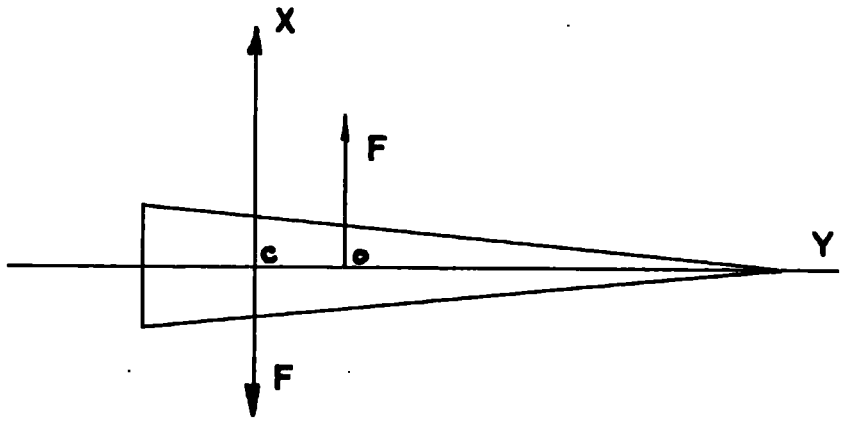

FIG 3.5.1

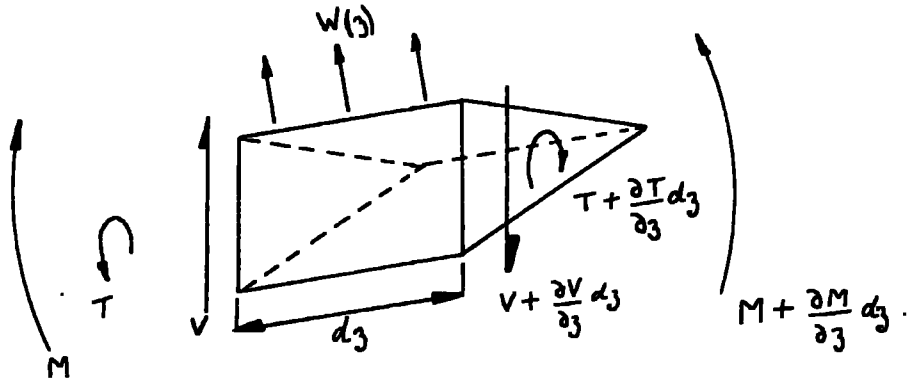

FIG 3.5.2

section oscillating in torsion does so about the centre of flexure.

Consider the equilibrium of an element of the beam of length d_z at some distance z from the root. (Fig.3.5.2)

Net. torque across the element :-

$$= T + \frac{\partial T}{\partial z} dz - T$$

$$= C \frac{\partial^2 \theta}{\partial z^2} dz \qquad \text{as } d\theta = \frac{T dz}{C}$$

Rotary inertia couple (applying d'Alembert's Principle)

$$= m k^2 \frac{\partial^2 \theta}{\partial t^2} dz$$ when k is the radius of gyration about axis of rotation.

Net bending force across element

$$= w(z)\, dz \quad = \frac{\partial V}{\partial z} \quad = \frac{\partial^2 M}{\partial z^2}$$

$$= EI \frac{\partial^4 x_c}{\partial z^4} dz$$

Linear inertia

$$= m\, dz \frac{\partial^2 x_0}{\partial t^2}$$

Assume that the section oscillates about the centre of flexure C, (Fig.3.5.3)

Taking moments about C :

$$m r_g\, dz\, \ddot{x}_0 + m k_c^2 \ddot{\theta}\, dz - C\theta''\, dz = 0$$

but resolving vertically produces the impossible situation

$$m\, dz\, \ddot{x}_0 \cos\theta = 0$$

hence the section cannot be oscillating about C.

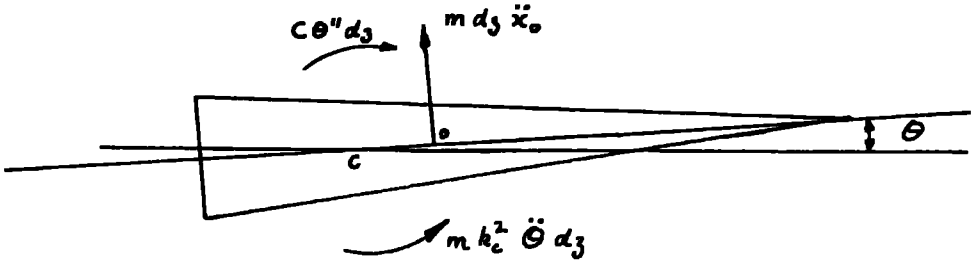

FIG 3.5.3

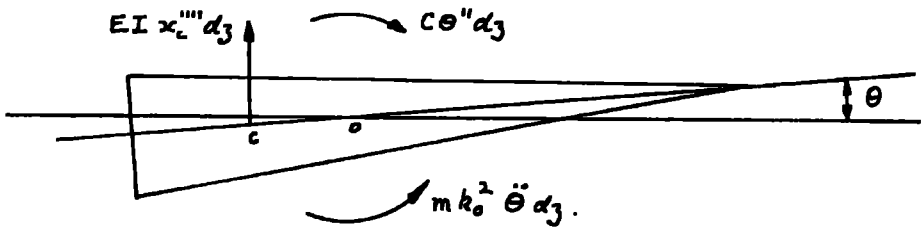

FIG 3.5.4

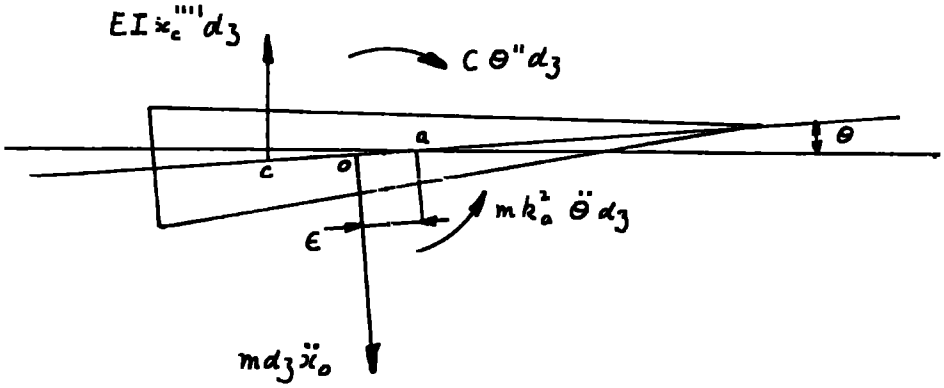

FIG 3.5.5

Assume therefore that the section oscillates about the centroid O : (Fig.3.5.4).

Taking moments about O

$$m k_o^2 \ddot{\Theta}\, dz - C\Theta''\, dz - EI x_c''''\, dz\, r_y \cos\Theta = 0$$

but resolving vertically produces

$$EI x_c''''\, dz = 0$$

which cannot be true.

In order to obtain a valid equilibrium condition, therefore, the section must oscillate about some point which does not lie between O and C. Suppose this point is at A (Fig. 3.5.5) a distance ϵ from O on the side remote from C .

Taking moments about A

$$m k_A^2 \ddot{\Theta}\, dz + m\epsilon\, dz\, \ddot{x}_o - C\Theta''dz - EI x_c''''dz\,(r_y+\epsilon)\cos\Theta = 0$$

and resolving vertically

$$EI x_c''''\, dz = m\, dz\, \ddot{x}_o \cos\Theta \qquad (3.5.1)$$

Now, if Θ is small, $\cos\Theta \simeq 1$,

$$x_c'''' = (r_y + \epsilon)\Theta''''$$

$$\ddot{x}_o = \epsilon\ddot{\Theta} = \epsilon p^2 \Theta$$

and assuming the first mode of torsional oscillation ie.

$$p^2 = \frac{\pi^2}{4L^2}\frac{C}{mk_A^2}$$

$$\Theta = \hat{\Theta}\sin\frac{\pi z}{2L}$$

then on substitution for x_c and x_o, 3.5.1 becomes

$$EI(r_y+\epsilon)\frac{\pi^4}{16L^4}\hat{\theta}\sin\frac{\pi z}{2L}\,dz = m\,dz\,\epsilon\frac{\pi^2}{4L^2}\frac{C}{k_\eta^2}\hat{\theta}\sin\frac{\pi z}{2L}$$

hence $\epsilon =$

$$\frac{\frac{EI\pi^2}{4L^2}}{\frac{C}{k_\eta^2}-\frac{EI\pi^2}{4L^2}} \times r_y$$

and it is shown in Appendix 6 that for a typical beam considered in this work

$$\frac{C}{k_\eta^2} \gg \frac{EI\pi^2}{4L^2}$$

and hence A lies at a very small distance from O on the side remote from C, and may in fact be considered to be coincident with O.

Deflection measurements across the section (Chapter 4 and Appendix 8) confirm this, and frequency measurements indicate that I_{cg} should be used in place of I_{cf} in equation 3.1.

CHAPTER 4

EXPERIMENTAL METHOD

To confirm the theoretical predictions of frequency and mode shape of coupled torsion bending vibration, five beams of suitable size for laboratory testing were manufactured. Four were machined from 43.5 mm x 12.7 mm steel bar and one from 'duralumin' designed (App. 7) so that the frequencies of the fourth and fifth modes of vibration (ie.3rd XX and 1st torsional modes) coincided at a length between about 0.3 and 0.4 m. These overall dimensions were sufficient to ensure that effects due to shear deformation and rotary inertia were negligible.(18)

For testing, a beam was clamped securely to a cast iron bedplate mounted on a concrete plinth which could be raised about 10-15 mm on four air springs to minimise the effect of floor transmitted vibrations. This was found to be particularly necessary during experiments to determine the deflected shape.

4.1 Development of the apparatus.

Bright (cold-rolled) steel bar was found to be unsuitable for the beams as the release of residual stresses during machinery produced considerable distortion. The beams were therefore machined from black (hot-rolled) steel bar or ' duralumin ', which do not distort. Steel was chosen for the majority of the beams for the purely practical reason of ready availability.

For accurate work the means of excitation and the measurement of response must contribute as little as possible to the mass or stiffness of

the beam. This prohibited excitation by any contacting method, and an infinitely variable oscillator (Dawe type 440 B) driving a coil (with a power amplifier for modes above 200 Hz) was employed here. (The means of excitation may be different for steel and ' duralumin '. In the former case, the effect may be predominantly ferromagnetic as opposed to an eddy current effect. The core of the coil was not a permanent magnet and therefore an opposite pole was induced in the beam every half cycle of the input resulting in two attractive pulses to the beam every cycle. In the case of the 'duralumin' the excitation was by eddy currents which induced a like pole in the beam every half cycle. In both cases therefore the beam was excited at twice the frequency of the input to the coil.)

The response of the beam was indicated by a barium titanate piezo-electric crystal glued near the root off the line of centroids. This detected all the modes satisfactorily and the output was both displayed on the Y axis of an oscilloscope and measured quantitatively using a valve voltmeter.

The resonant frequency was assumed to be that at maximum amplitude, as damping was negligible, and was accurately determined by applying a "Muirhead" decade oscillator (type D-890-B) to the X axis of the oscilloscope and obtaining Lissajou's figures.

During the experiments to obtain the mode shapes it was found that the valve voltmeter reading fluctuated by about 10%. This was unsatisfactory as it produced scatter in the readings and may have been caused by "beating" i.e. the driving frequency not coinciding exactly with the resonant frequency, or variation in the level of the power supply to the

coil. Once the resonant frequency had been determined, the problem was overcome by using the Muirhead, which permitted much finer frequency control, to power the coil in place of the Dawe.

Initially, attempts were made to measure the deflection at the apex and base using 'Vibrometer' inductive transducers, but it was soon found that these were being influenced by the magnetic field generated by the coil. This effect was independent of the beam material and only slightly dependent on the position of the coil relative to the transducers. A method of excitation similar to the 'tuning fork' principle used by Slyper[14] was investigated, in an attempt to isolate the exciter coil from the transducers, but the response obtainable was insufficient and the method was much less easy to operate.

Any contacting method of deflection measurement would be unsatisfactory as it would produce localised distortion. The method employed was therefore required to be non-contacting, and in order to detect torsion/bending coupling, be able to measure the deflection along both edges of the beam, and detect any phase change between the two edges or along either edge.

Carnegie, Dawson and Thomas[21] described a method which employed a stroboscope and travelling microscope, and used it to determine the deflected shape of the trailing edge of a pretwisted aerofoil sectioned beam. The method, though, had the disadvantage that it could not detect any change of phase.

Capacitive probes, however, are unaffected by a magnetic field, and it is shown below that a change of phase was easily detected by

displaying the carrier signal to the probes on the oscilloscope.

In principle, the probes were mounted with the faces parallel to the surface of the beam. A capacitance was thus formed between the beam (earth) and the probe itself. Variation of the separation of the probe and beam varied the capacitance which modulated the 7 Volt (r.m.s) 50 KHz carrier signal from the supply meter (Wayne-Kerr Type B 731 B) to give (according to the size of the probe) a static, or mean dynamic, distance reading and peak to peak amplitude of oscillation of the structure. To give an accurate static deflection the face of the probe must be parallel to the structure surface, but it was found that the amplitude readings were not affected by small degrees of non-alignment.

4.2 Preliminary tests. (Appendix 8)

Using a single probe, the following preliminary tests were made:

1). Axis of torsional oscillation. Fig. A 8 (1)

This experiment was performed to confirm the conclusion drawn in part 5 Chapter 3 (p. 49) that torsional oscillations take place about a point very close to the centroid.

A single probe was moved across the beam surface at right angles to the beam axis and its position across the surface determined by a vernier depth gauge. Amplitude readings taken at small intervals across the surface confirmed the theoretical conclusion and also illustrate the linearity of the deflection across the surface. This information was required so that the computer results in terms of the deflection of the

centre of flexure and the section rotation could be related to apex and base deflections.

2). Relation of piezo-electric crystal response to probe amplitude reading Fig. A 8 (2).

The purpose of this test was to find the amplitude which could conveniently be obtained within the limits of the exciter coil. From this the probe with the most suitable full scale deflection was selected. Also, had the results not been repeatable, ie. had they shown excessive scatter, it would have shown that the piezo-electric crystal and voltmeter system would be unsatisfactory as a monitor of constant amplitude.

The results show that the sensitivity of the crystal was satisfactory.

During this experiment the resonant frequency was found to be invariant with amplitude.

3). Position of exciter coil.

For constant piezo-electric crystal response the probe amplitude reading was found to be invariant with coil position (Appendix 8). The input power to the coil to produce a given response of course varied considerably with coil position.

4.3. Measurement of base and apex deflections.

Two probes were used, supported in a mounting block above the beam as shown in Fig. 4.1. Both were connected through a junction box (JB731B) to the vibration meter.

The bottom surface and side A of the probe mounting block (Fig. 4.1) were ground and the holes for the probes drilled perpendicular to

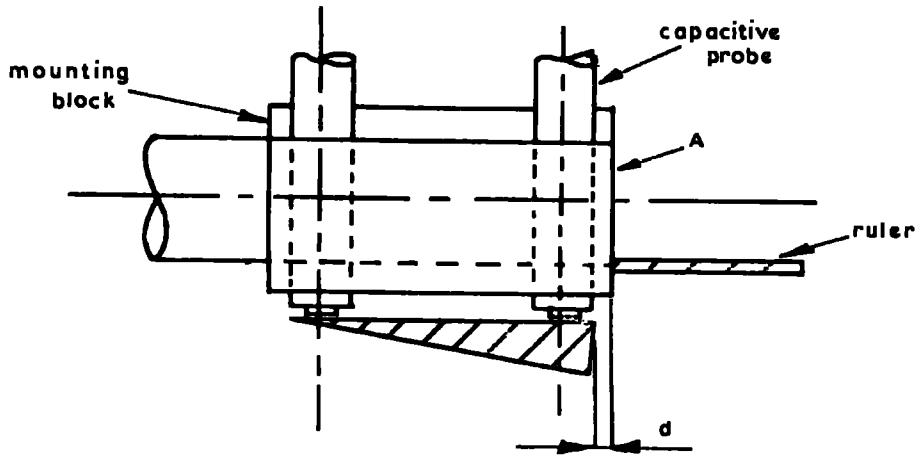

FIG. 4.1

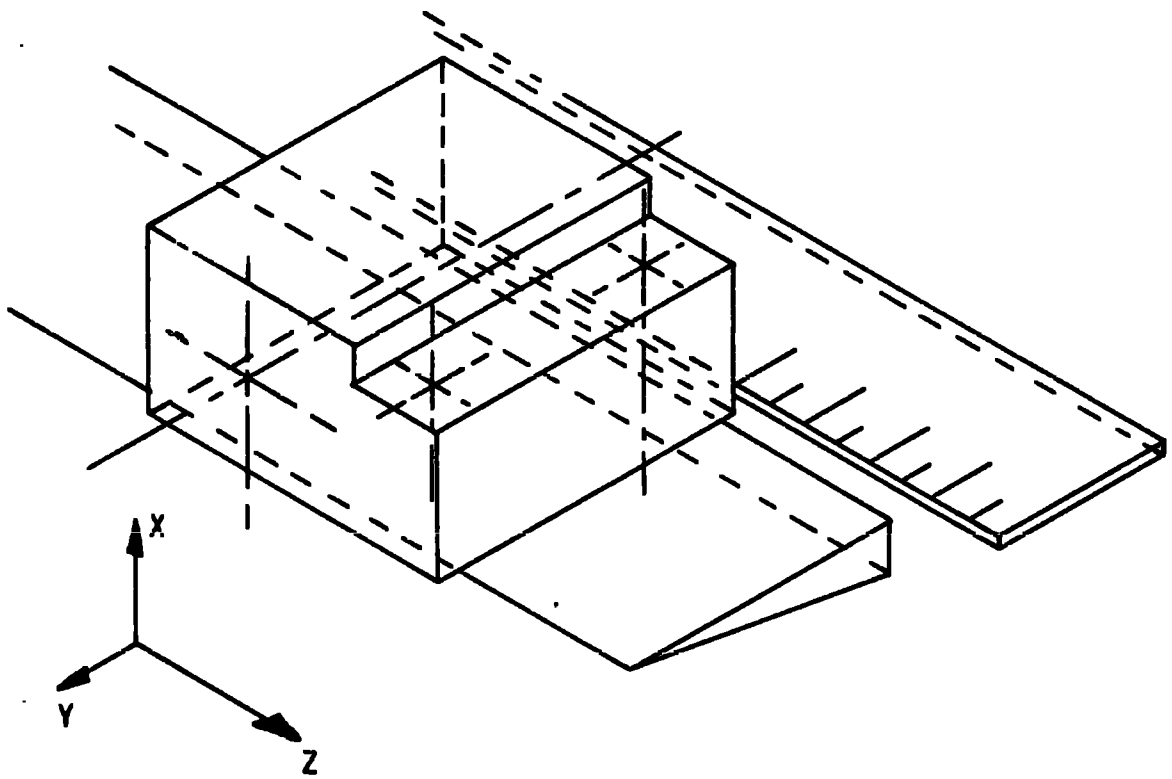

FIG. 4.2

the bottom surface in positions such that a line joining the centres was at right angles to side A. Using slip gauges the probes were inserted and clamped so that they protruded equally from the underside of the block.

With the beam to be tested clamped in position, a ruler was mounted slightly above and to one side of it. The ruler was set up using a travelling microscope so that both probes were above the beam with side A in contact with the ruler and the distance d from ruler to beam edge constant to within 0.1 m along the beam.

4.3.1 Support of the probes.

The method of supporting the probes must meet the following requirements (Fig. 4.2.).

1. Freedom to move along the Z axis in order to traverse the beam length.

2. Fine rotational adjustment about an axis parallel to Z so that the probes are an equal distance from the beam surface.

3. Fine rotational adjustment about an axis parallel to Y so that the probes are perendicular to the beam surface.

4. Fine linear adjustment in the X direction to bring both probes within their operating range.

For the modes of interest to this work the maximum deflection was approximately 75 x 10^{-6}m, hence probes of 125 x 10^{-6}m full scale deflection were used, necessitating the fineness of the adjustments described above.

All the requirements were met using a precision variable height clamp and attaching the probe block with variable angle clamps giving the fine rotational movement. The whole clamp assembly was then placed with the side A of the block in the required position against the ruler, and the adjustments made so that:

1). The static deflection readings for each probe were within 10% of full scale deflection of each other. This also ensures that the probes are parallel to the XZ plane.

2). The underside of the block was parallel to the beam surface, i.e. parallel to the YZ plane. Preliminary tests showed that vibration measurements were independent of probe rotation about an axis parallel to Y (or Z) within the limits of visual accuracy.

3). The static deflection of each probe was approximately 80% of full scale deflection. This distance was governed by rules described in the probe operating instructions, but in general the amplitude of the motion must not be such that the beam comes into contact with the probes.

Both the top surface of the cast iron bedplate and the bottom surface of the precision clamp were machined and the whole assembly (having fairly substantial mass) was found to be perfectly stable in all positions.

4.3.2 Change of phase.

The vibration meter gives a direct reading of peak to peak amplitude of each probe, but with this information alone it was impossible to distinguish between cases A and B below:

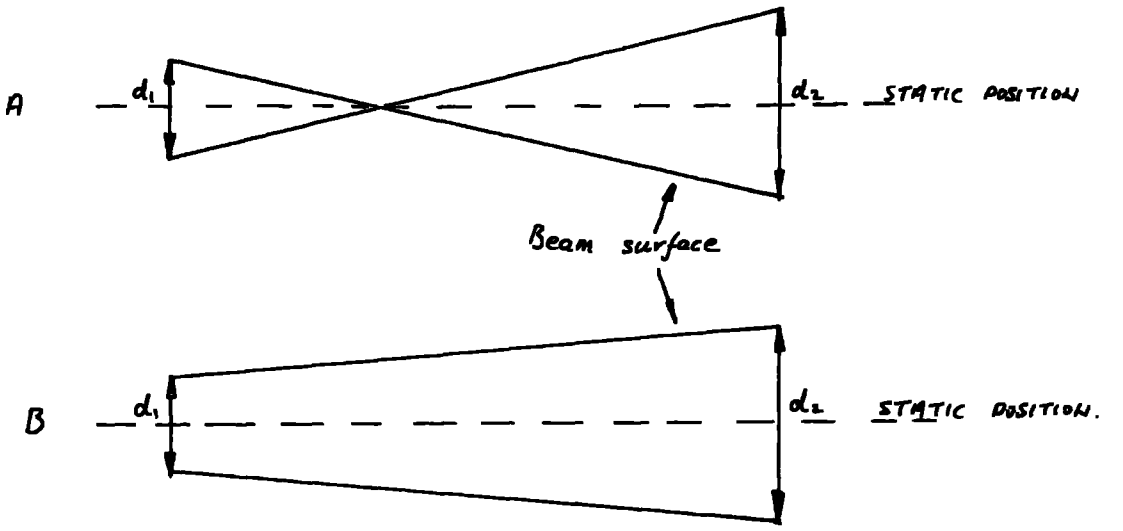

In each case the probe readings would be d_1 and d_2 as indicated, but in case A there is a change of phase. In pure bending or pure torsional vibrations it is known intuitively which type of motion is taking place, but for coupled motion the distinctions are blurred and the exact type of motion by no means obvious.

Additional information was obtained, however, by displaying the piezo-electric crystal output and the amplitude modulated 50 KHz of the carrier signal to the probes on an oscilloscope. The amplitude of the carrier signal is proportional to the separation of the probe and structure, and was therefore amplitude modulated at the frequency of oscillation. From this the phase may be obtained and an arbitrary convention adopted:

C.

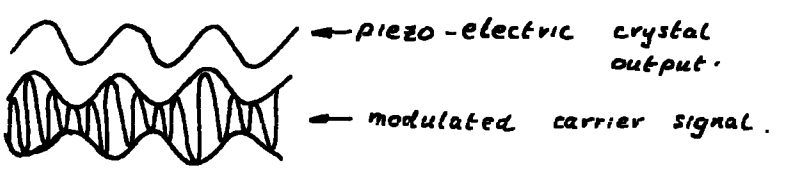

D.

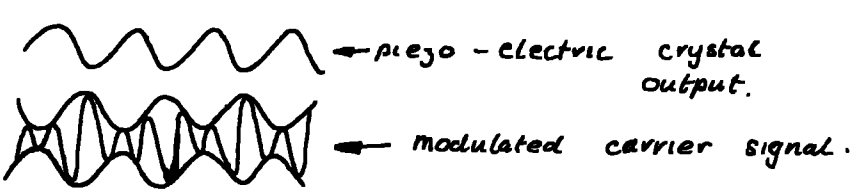

C and D were said to be in phase and out of phase respectively, and hence the magnitude and phase of the displacements at the apex and base of the triangle were determined.

The amplitude of vibration must be held constant for readings to be free from scatter, and some initial trouble in this respect has been mentioned (p. 56). It was found, though, that provided the reading was taken when the monitor voltmeter was at its predetermined value to within visual accuracy the results obtained were repeatable and as can be seen (Chapter 5) almost completely free from scatter. It would be an improvement to have the amplitude held constant automatically by a suitable control loop, which would considerably shorten the experimental time, as great care must be taken to ensure that the monitor signal is exactly set on the predetermined value. The refinement of the control loop is of course not necessary.

CHAPTER 5

RESULTS AND DISCUSSION

5.1 Determination of material properties (Appendix 9)

Suitable specimens were manufactured from the black-bar steel for the determination of Young's Modulus E, the shear modulus G, Poisson's Ratio ν , and the density ρ .

Density

The density was obtained by accurately shaping and grinding a rectangular block which was weighed and measured.

This gave $\rho = 7.82 \times 10^3$ Kg/m^3

Young's Modulus and Poisson's ratio

1). A tension test using an extensometer and 'Denison' type T42B4 testing machine gave the value $E = 2.09 \times 10^{11}$ N/m^2. All the experimental results were analysed by linear regression. (Appendix 9).

2). A similar test to the above, but with the extensometer replaced by two foil strain gauges on the principal axes gave

$E = 2.09 \times 10^{11}$ N/m^2

$\nu = 0.28$

Shear Modulus

1). A torsion test using a torsiometer with the load measured by a spring release on a torque arm gave $G = 8.49 \times 10^{10}$ N/m^2

2). The above test repeated using a B.P.A. load cell (type D90) and transducer meter (type C52) in place of the spring balance :

$G = 8.53 \times 10^{10}$ N/m^2

However, E, ν and G are interdependent and the values above are not compatible.

The above value of E must be accepted as correct, as both the strain gauges and extensometer agree. The Denison testing machine conformed to Grade A1 of B.S.S. 1610 (1964), and its accuracy was confirmed using a calibration proving ring.

Similarly, the values of G obtained by the two methods are within 0.5% of each other, which is acceptable.

Attempts were also made to obtain G by measuring the frequency of torsional oscillations of rectangular sectioned beams of differing thickness: Appendix 9.

Length = 0.30 m.

Width = 0.04334 m.

THICKNESS	G, N/m^2
0.01275	8.21×10^{10}
0.00948	8.33×10^{10}
0.00640	8.44×10^{10}

As the thickness decreases, the calculated G appears to converge to the static value. This indicates that the relative improvement of the root fixing as the thickness decreases yields values of G which are closer to the static value.

Accepting, therefore, the values of $E = 2.09 \times 10^{11}$ N/m^2 and $G = 8.53 \times 10^{10}$ N/m^2 gives $\nu = 0.23$, which is lower than expected.

Poisson's ratio is, however, extremely difficult to obtain directly by experiment, and little confidence is attached to the value of 0.28 given by the strain gauges.

It is concluded that, therefore, the values

$E = 2.09 \times 10^{11}\ N/m^2$

$\nu = 0.23$

$G = 8.53 \times 10^{10}\ N/m^2$

$\rho = 7.82 \times 10^{3}\ Kg/m^3$

must be accepted.

5.2. Variation of torsional stiffness with apex angle.

In this section the terms " in defect " and " in excess " are used when a value is respectively less than or greater than a given value.

The calculations based on the two sectors of a circle (Fig. 5.2.1 b) are exact solutions and, particularly at small apex angles, give a useful standpoint for the comparison of other methods.

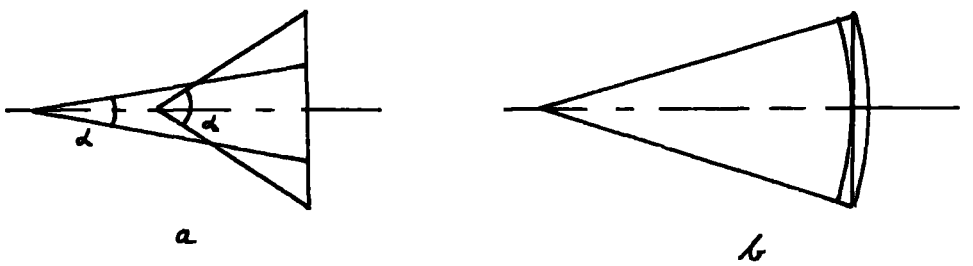

5.2.1

Figure 5.2.2 is plotted by varying the apex angle such that the cross sectional area is constant (at an arbitrary value). This means

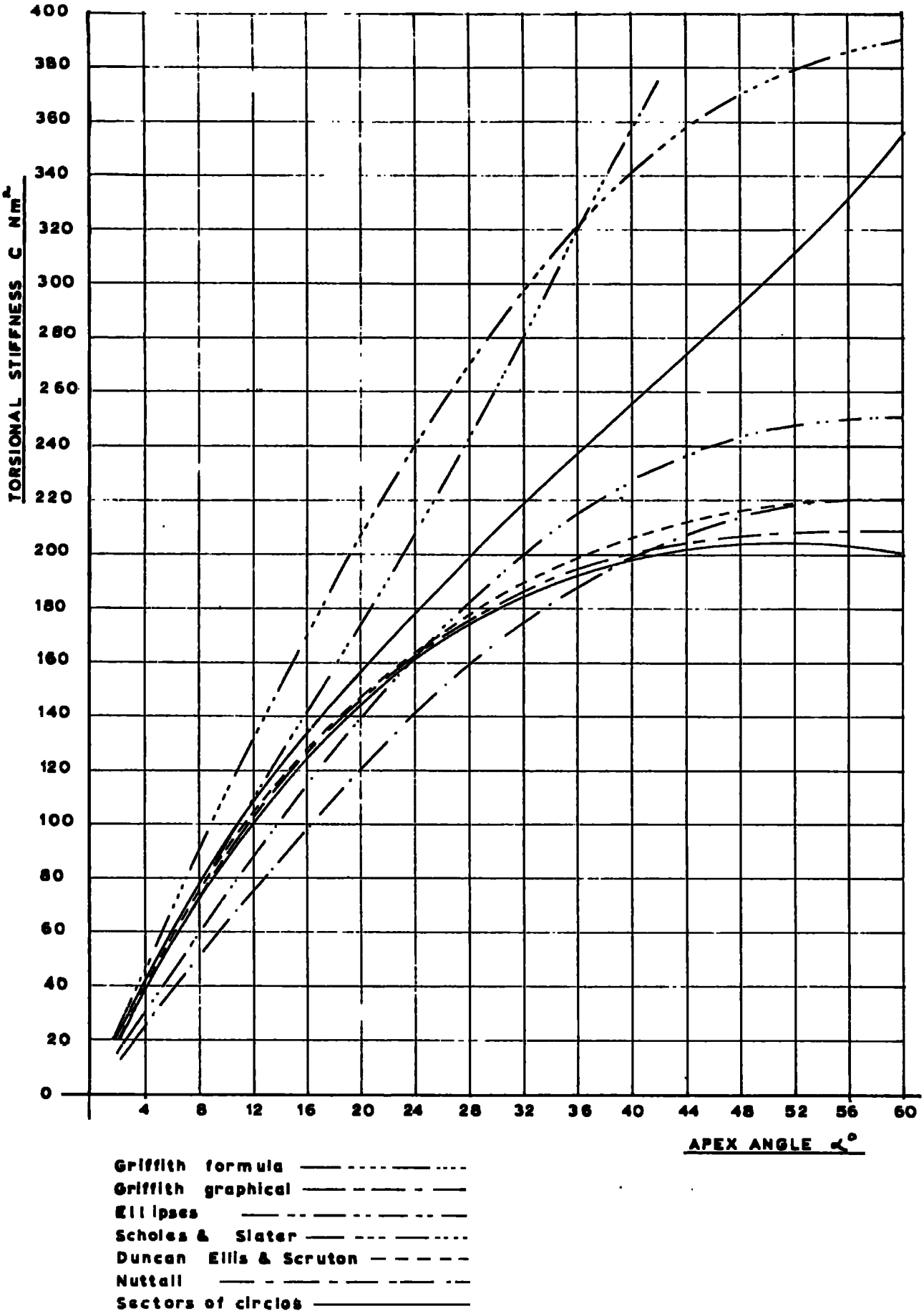

FIG 5.2.2 VARIATION OF TORSIONAL STIFFNESS WITH APEX ANGLE

that the volume of material per unit length is constant and the graphs represent the variation of torsional constant with shape alone.

For apex angles of less than 3° it is seen that Nuttall's method and the elliptical approximation are in defect of the sector limits by 38% and 29% respectively. All other methods are in good agreement to within 5%. In particular, Scholes and Slater, and Duncan, Ellis and Scruton are only just outside the exact range, the discrepancy being less than one part in two thousand.

At the other end of the range, $\alpha = 60^\circ$, both Nuttall and Duncan, Ellis and Scruton give exact solutions for the equilateral triangle. The elliptical approximation is in excess of the exact solution by 14%, and Griffith's graphical method is in defect by only 4.5%. Obviously the formulae inteded for small angles only are invalid here.

In the range $2^\circ \leq \alpha \leq 60^\circ$ only Duncan, Ellis and Scruton remains exactly within the sector limits, but Griffith's graphical method and Schole's and Slater's formula is seen to be much more accurate than Griffith's for small apex angles: at $\alpha = 10^\circ$, Schole's and Slater's is only 3.3% above the accepted range, whereas Griffith's is almost 20% above. Nuttall and the elliptical approximation give very low values throughout.

Above $\alpha = 10^\circ$, the section can no longer justifiably be termed thin, and Scholes and Slater's formula, while remaining closer than Griffith's, becomes increasingly inaccurate. Griffith's graphical method and the formula by Duncan, Ellis and Scruton remain within the bounds of the sectors for increasing α up to $\alpha = 60^\circ$. Throughout

$20^\circ \leq \alpha \leq 30^\circ$ the elliptical approximation is probably within 5% of the truth, being in defect for $\alpha < 20^\circ$ and in excess for $\alpha > 30^\circ$. Nuttall remains in defect of the lower sector limit by over 5%.

In general, therefore, as far as isosceles triangular sections are concerned, the formula due to Duncan, Ellis and Scruton is probably most accurate throughout the total range. It is stated by Nuttall[4] that his formula is probably in defect by 4% when $\alpha = 40^\circ$: applying this correction yields a value which is within 0.5% of Duncan, Ellis and Scruton.

Throughout the total range Griffith's graphical method remains within 5% of Duncan, Ellis and Scruton, which, in view of its claimed general application would inspire confidence in its use when considering more complex cross-sectional shapes.

5.3 Variation of centroid/centre of flexure distance: r_y

	$\alpha = 14.98^\circ$	13.10°	9.75°	6.86°
GRIFFITH	0.528	0.529	0.550	0.530
DUNCAN	0.725	0.729	0.755	0.727
10° SECTOR OF CIRCLE	-	-	0.455	-
YOUNG; ELDERTON AND PEARSON	0.784 0.829	0.789 0.803	0.892 0.914	0.909 0.919

FIG. 5.3.1, VALUES OF r_y ($\times 10^{-2}$ m) CALCULATED BY EACH METHOD (WHERE APPLICABLE.)

Griffith's and Duncan's formulae are specifically for thin sections, in which case $\alpha = 14.98^\circ$ and 13.10° are probably outside the range.

With that limitation, both are independent of α , whereas the formula due to Young, Elderton and Pearson (from which the values of r_y for the limiting sectors are calculated) is dependent upon α , and it is seen that this formula gives higher values of r_y than Duncan's or Griffith's throughout the range. The discrepancy decreases with increase in α .

Griffith states[6] that by soap film measurement the centre of flexure of a 10° sector of a circle is 0.78 of the radius from the apex. This is applied to the 9.75° triangle giving $r_y = 0.455 \times 10^{-2}$m.

5.4 Effect of coupling on beam frequencies and mode shapes.

Introduction.

If two independent vibrating systems having nearly equal natural frequecies are coupled together, the resulting system has one natural frequency above the higher and one below the lower of the two uncoupled frequencies.

This is readily demonstrated in the case of the simple spring-mass system and its extension to the coupling by pretwisting of XX and YY direction bending modes of rectangular sectioned cantilevers is illustrated specifically by Rosard and Lester[15].

The present results show the same effect in the case of coupled torsion/bending modes.

A total of five beams are investigated: one symmetrical about the X axis (Fig. 5.4.1) and four of varying apex angle symmetrical about the Y axis. The frequency results are presented as a logarithmic plot

(to base 10) of frequency against length in the region where the uncoupled first torsion and 3rd XX bending modes coincide.

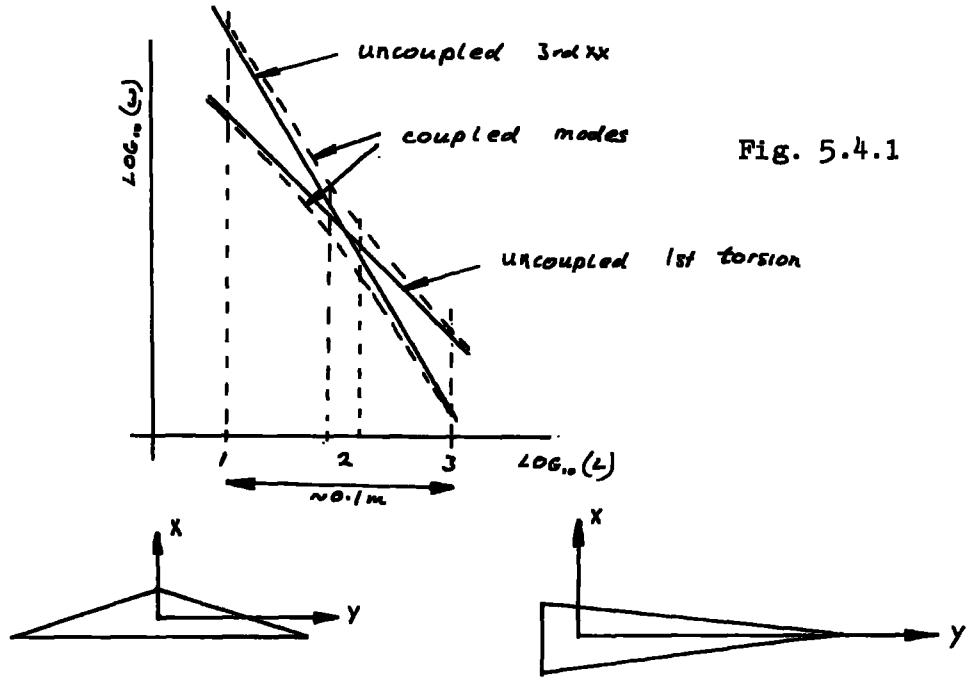

Fig. 5.4.1

In the case of the beam symmetrical about the X axis, $r_y = 0$ and no coupling exists between the 3rd XX and 1ist torsion modes. Hence progressive shortening of the beam from point 3 to point 1 yields the uncoupled straight lines of 3rd XX and 1st torsion. (Fig. 5.4.2).

In the cases of the other four beams, however, $r_y \neq 0$, and the frequencies are separated around the critical length (point 2 Fig. 5.4.1) into two curves representing the fourth and fifth modes of the beam - the first three being 1st XX, 2nd XX and 1st YY, in ascending order.

These fourth and fifth modes possess both 3rd XX and 1st torsion mode shape characteristics.

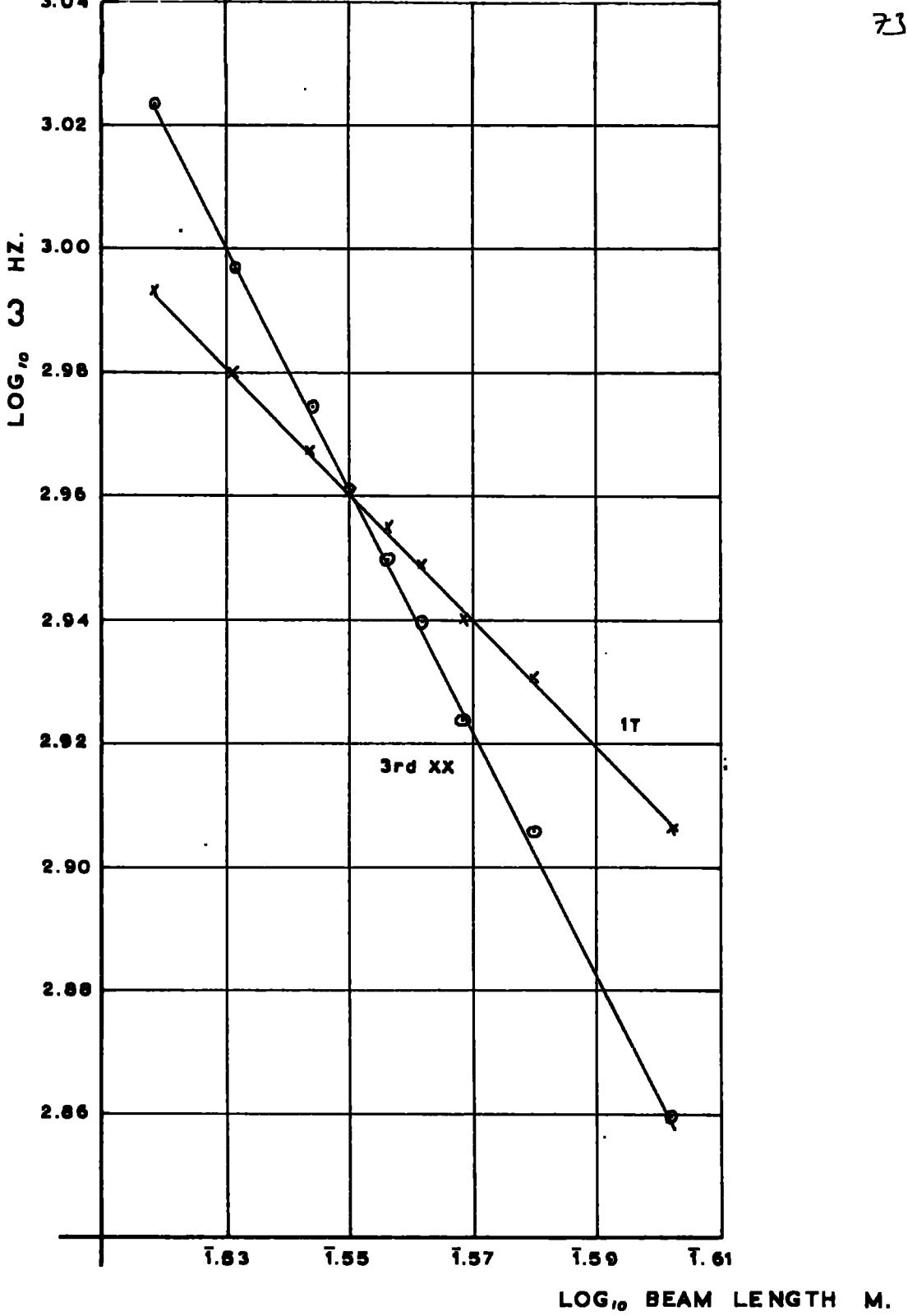

FIG 5.4.2 UNCOUPLED 3RD XX AND 1T MODES

Mode shape presentation and normalisation.

The output from the eigenvalue solution routine gives the deflection of the centre of flexure and the rotation about the z axis at the nodes of the elements. This must be related to the experimental deflections of the apex and base.

There are two alternatives. The deflection of the centre of flexure and the rotation of the section may be calculated from the experimental apex and base deflections and the ratio deflection / rotation calculated for each point. Provided the units of deflection and rotation agree with the theoretical, this should correspond to the theoretical deflection / rotation ratios. Alternatively, the theoretical results may be converted to apex and base deflections and both theory and experiment plotted according to some normalisation convention.

The latter procedure, apart from presenting a better visual picture, is preferable mathematically as the first involves subtracting two experimental observations which may be nearly equal. Any error may thus become a substantial part of the result:

For the calculation of the deflection / rotation ratios, the deflection is calculated by taking a weighted average of the apex and base readings. In the worst case, assuming the error in both readings is $+\epsilon$ then the deflection δ is given by

$$\delta = k_1 x_1 + k_2 x_2 + (k_1 + k_2)\epsilon$$

where x_1 and x_2 are the apex and base deflections and k_1 and k_2 constants such that

$$k_1 + k_2 = 1$$

$$\therefore \quad \delta = k_1 x_1 + k_2 x_2 + \epsilon$$

The rotation is calculated by taking the difference, and in the worst case the errors are opposite in sign:

$$x_1 + \epsilon \; ; \quad x_2 - \epsilon$$

$$\text{rotation } \phi = \quad x_1 - x_2 + 2\epsilon$$

Hence the final error may be twice the observational error, and would be particularly significant where $x_1 \simeq x_2$.

The normalisation convention adopted initially was that of making the apex deflection at the tip of the beam unity. In most cases this is satisfactory, but can give rise to erroneous results if that deflection is very small. Hence the improved method of making the sum of the moduli of the apex and base deflections at the tip unity is adopted for all the mode-shapes presented:

If x_{1T} and x_{2T} are the tip apex and base deflections then

$$\text{let} \quad K = |x_{1T}| + |x_{2T}|$$

which normalises the other readings to

$$\frac{x_1}{K} \; , \; \frac{x_2}{K} \quad \text{etc}$$

In the z direction the length is taken to be one unit. (Appendix 10 shows the calculation of the theoretical apex and base deflections.)

Comparison of theoretical and experimental results

The results obtained from the finite element solution were identical (to within 0.5 Hz) with those obtained from the Laplace Transform

theory, releasing the former program for use only when both the frequencies and mode shapes were required: at points 1,2 and 3 (Fig. 5.4.1), thus economising on computer time. The solution system of the finite element theory is part of the computer software library and both the eigenvalues and eigenvectors are produced automatically.

The first theoretical results assumed a value of $E = 2.09 \times 10^{11} N/m^2$ and the value of C calculated by the formula of Duncan, Ellis and Scruton assuming $G = 8.53 \times 10^{10} N/m^2$. This gave an agreement between theory and experiment of + 1.78% to - 1.93% in 3rd XX modes over the four beams for which $r_y \neq 0$, but at + 4.07% to - 5.9% based on Duncan, Ellis and Scruton the range of error of torsional modes is greater. It was suspected that this discrepancy could be due to the root fixing and on completion of all the tests an examination (as far as possible) of the variation in experimental error with length, thickness and mode number was made.

APEX ANG α° / AREA A m^2	6.86 / 0.949 x10⁻⁴	9.75 / 1.46 x10⁻⁴	13.10 / 1.82 x10⁻⁴	16.99 / 2.08 x10⁻⁴
1st XX	+5.1%	+2.6%	(not taken)	−2.7%
2nd XX	+2.7%	−0.16%	+1.45%	−1.65%
3rd XX	+1.76%	−1.93%	−0.02%	−1.78%
1st TORSION	+4.07%	+1.13%	+0.33%	−5.9%

FIG 5.4.3.

The table (in Fig. 5.4.3) shows the variation in experimental error (positive when the experimental value exceeds the theoretical) averaged over the lengths taken for the beams vibrating in the first three XX and 1st torsion modes. The variation with length was less

than 0.5% and there was no correlation of error with length. This indicates consistency of clamping for each beam.

However, for the bending modes it can be seen that there is a significantly greater variation in error with mode number. This applies to all the beams except the thickest where the values are generally low and closer together.

Similarly it can be seen from all the rows of the table that the error algebraically greater for the thinner beams, decreasing algebraically with increasing thickness. The bending modes of the two beams in the middle of the range are anomalous in this respect, but there was an error in the manufacture of the beam of $\alpha = 9.75^{\circ}$ which necessitated the root being trimmed down on a grinder after the machining of the triangular section. This was not thought to be significant before testing, but may account for the anomalous behaviour here.

It is suggested therefore that the root fixing becomes less effective with higher modes, and with increasing thickness. In retrospect therefore, duralumin would have been the better material for all the beams as the root reaction to a given cantilever deflection is much less for a beam of duralumin than for one of steel.

At some distance from the critical point (points 3 or 1) the effect of one mode on the other due to coupling is very small, and an error in either frequency compared to the theoretical prediction based on measured values of the material properties does not produce a significant error in the mode shapes. In the critical region, 2, however, for accurate prediction of the mode shapes the experimental and theoretical estimates of the critical length must be within 1%.

To show therefore that good agreement of the mode shapes can be obtained, it is thought to be justifiable to choose an effective value of E based on the experimental frequencies at lengths which differ considerably from the critical. Similar reasoning applies to the selection of an effective value of the torsional constant C, which incorporates any error in the determination of G and the inaccuracy of the method of calculation. Choosing an effective value of C is therefore, in the absence of an exact solution, more easily justified but the variation required of C is greater than that of E. The two mid-range beams $\alpha = 9.75^{\circ}$, 13.10° both have effective values of C which are within 1% of the sector of circle limits, but the thinnest beam gives a value 7.3% above the limit, and the thickest a value 10.8% below.

Assuming therefore the effective values of E and C shown (Fig. 5.4.4) the frequency / length graphs and modal curves for each beam were drawn for varying r_y.

BEAM α =	EFFECTIVE E x 10 N /m^2	EFFECTIVE C N /m^2	C by DUNCAN ELLIS and SCRUTON	C, SECTOR of CIRCLE
6.86°	2.16	28.67	26,48	26.46 26.65
9.75°	2.01	85.47	83.57	83.41 84.63
13.10°	2.09	164.5	163.42	163.12 167.5
14.99°	2.01	207.00	234.74	233.59 241.75

Measured E = 2.09 x 10^{11} N/m^2 Fig. 5.4.4

Discussion of results

Frequency / length curves.

Figures (5.4.5 to 5.4.8) show the effect of coupling on the frequency of 3rd XX and 1st torsion modes of the four beams for which $r_y \neq 0$.

With the exception of the fifth mode at lengths which are less than the critical, which shows a decrease in frequency with increase of r_y, the figures show that the frequency of the fourth mode is reduced and that of the fifth mode is increased with increase of r_y. This separation effect decreases with distance away from the critical point. The anomalous behaviour of the fifth mode at the shorter lengths cannot be readily accounted for as the frequency of the next highest torsional mode is almost three times that of the mode in question, but the effect must undoubtably be due to coupling. The figures also show that the true value of r_y appears to be less than that given by either Duncan's or Griffith's formula. For the beam of apex angle 9.75° the experimental value of r_y deduced by Griffith gives close agreement (Fig. 5.4.6). This is discussed later with relation to the mode shape curves and the views of other authors.

The separation due to torsional coupling is not as significant as the separation of adjacent bending frequencies due to pretwist. For the beams considered the change in either frequency is not greater than 2%, whereas for in rectangular sectioned beam of dimension ratios $1\frac{1}{2}$ x 4 x 11 the frequencies of the second mode in the flexible direction and the first in the stiff direction are nearly equal, and an applied pretwist of 40° decreases the lower frequency by 25% and increases the higher by

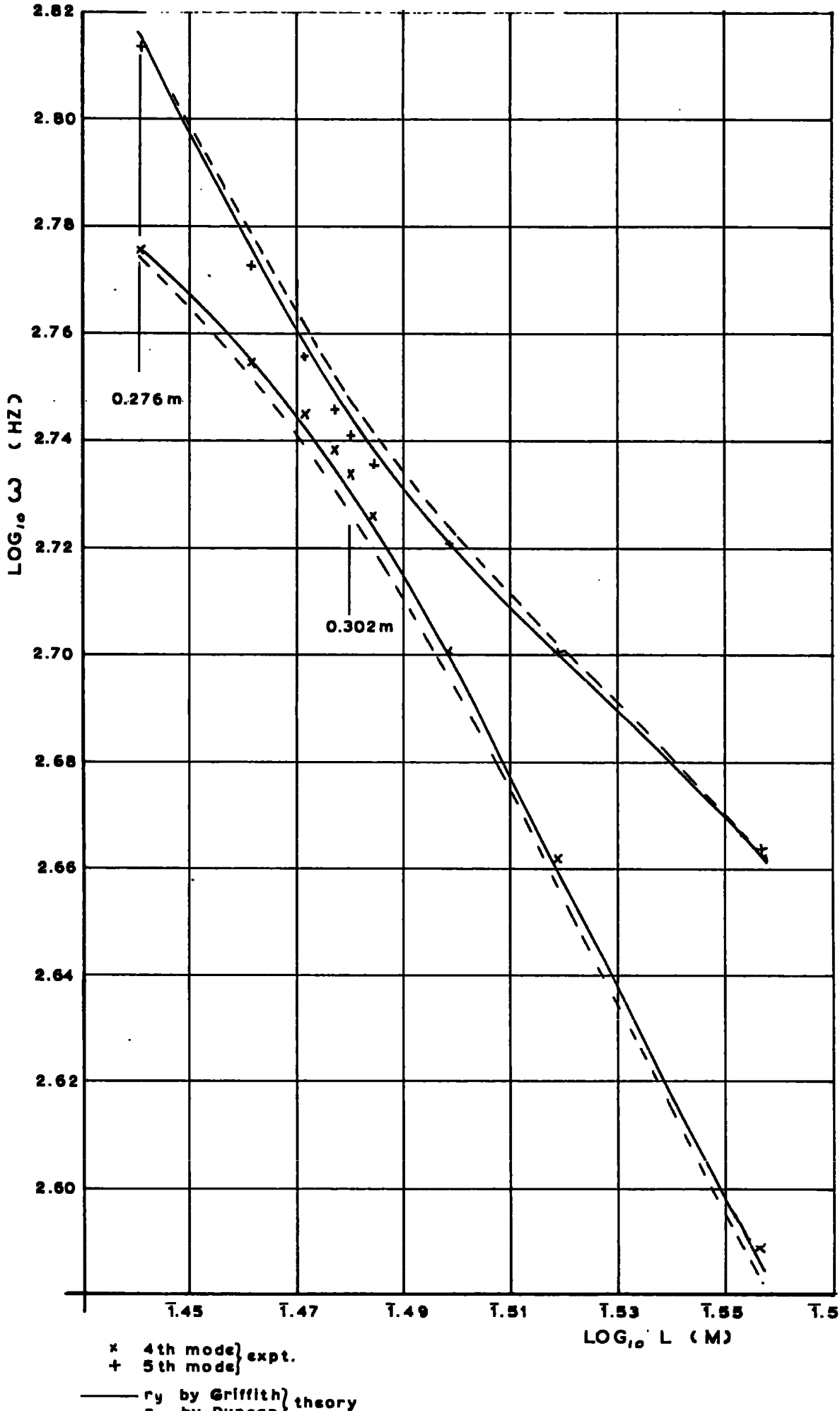

FIG. 5.4.5

4TH AND 5TH MODES $\alpha = 6.86°$

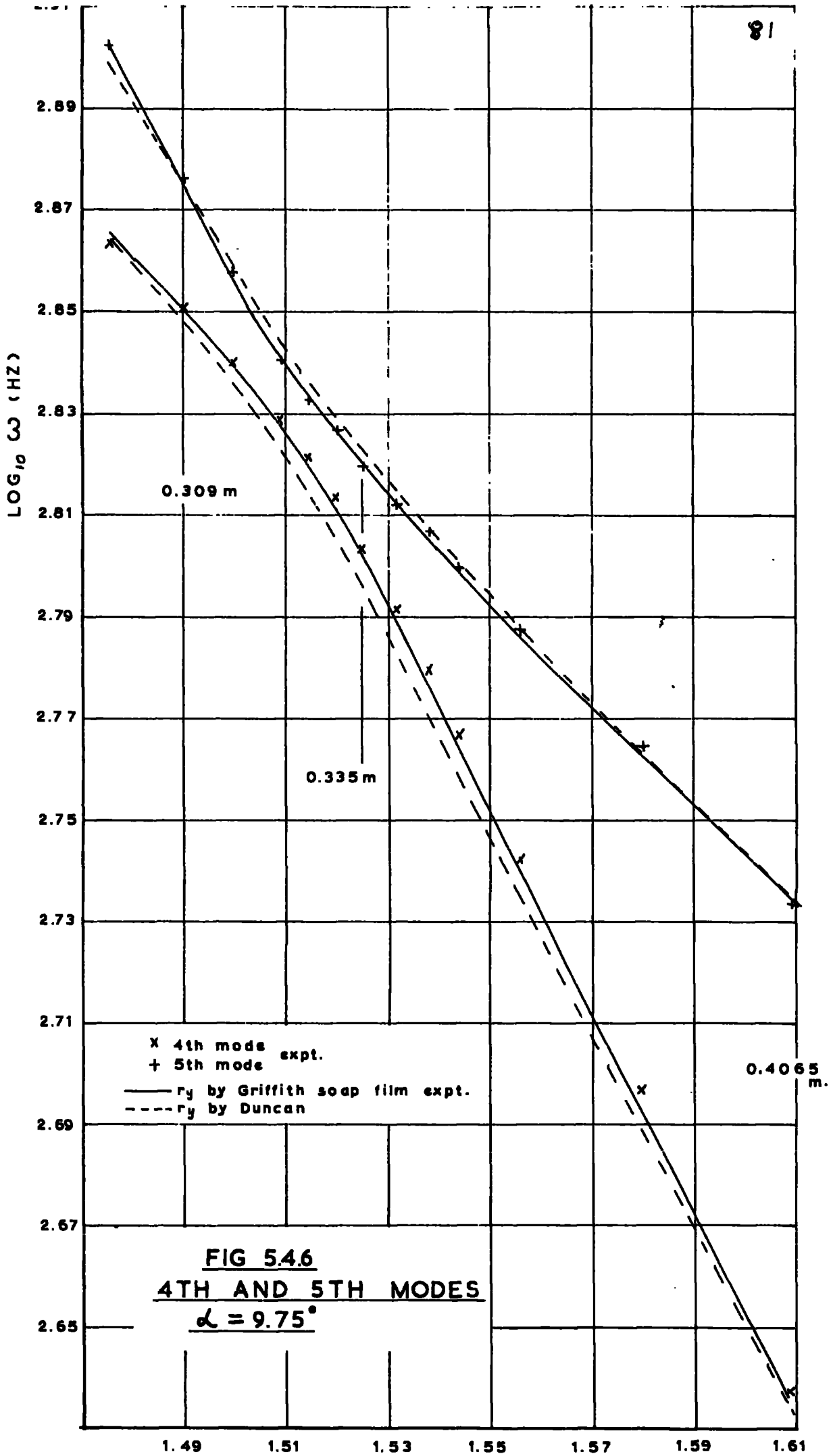

FIG 5.4.6
4TH AND 5TH MODES
$\alpha = 9.75^{\circ}$

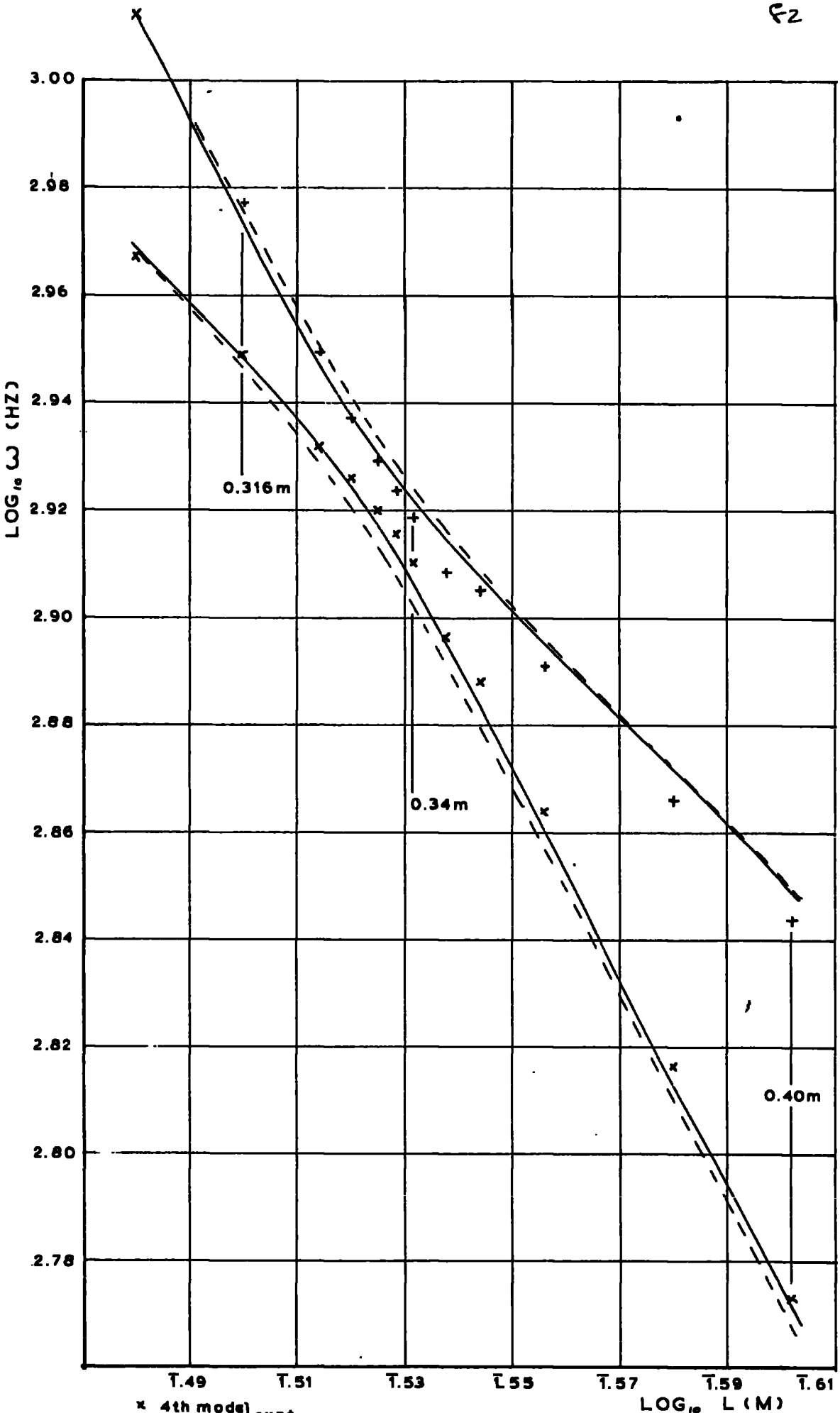

FIG 5.4.7
4TH AND 5TH MODES
$\alpha = 13.10°$

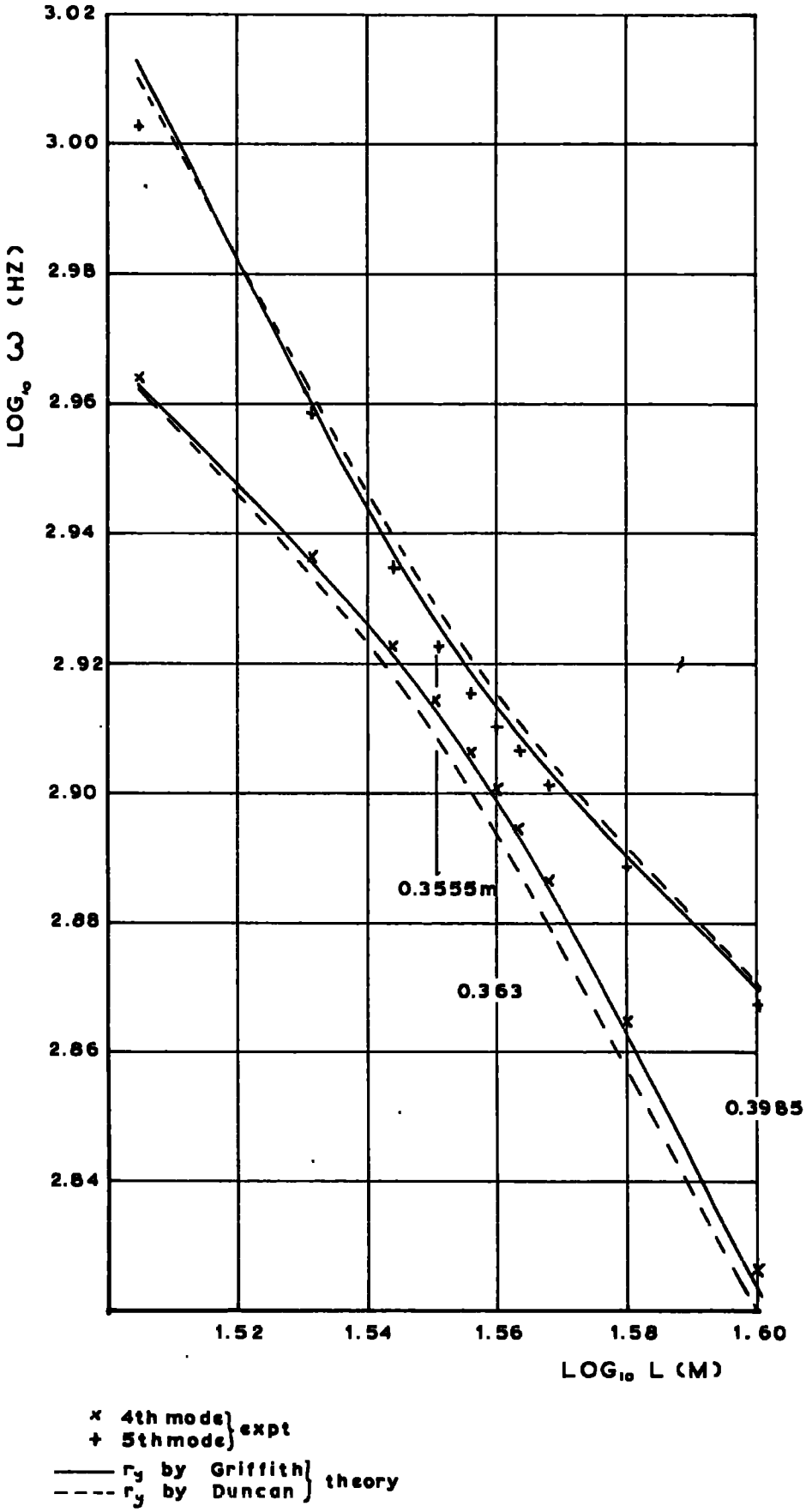

FIG 5.4.8

4TH AND 5TH MODES $\alpha = 14.99^\circ$

30%[15]. The effect of torsional coupling is therefore small compared with the effect of pretwist.

Mode shape curves

Figures 5.4.9 to 5.4.21 show experimental and theoretical mode shape curves for each beam at points 1 and 3 (Fig. 5.4.1) either side of the critical length and at point 2 in the critical region itself.

At point 1 the fourth mode is predominantly torsional but a slight introduction of 3rd XX bending may be seen in the apex and base deflections (5.4.4 to 5.4.9). Similarly at point 3 the fourth mode is predominantly 3rd XX but the presence of torsion is shown by the edge deflections not being coincident (5.4.12 to 5.4.14).

In the critical region 2 the fourth mode shape is a hybrid of 3rd XX and 1st torsion: both lines have a marked 3rd XX characteristic but are not coincident, indicating torsion. (Fig. 5.4.15 to 5.4.17). It is therefore possible to see a progressive change in the fourth mode shape from 1st torsion to 3rd XX with increasing length. (5.4.18 , 5.4.19).

Comparing the fourth and fifth modes a t a given length and noting that the apex line is drawn so that it lies more on the positive side of the z axis, it is seen that there is a change of phase between the two modes. This is demonstrated by all the figures (5.4.9 to 5.4.17) where it is shown that the fourth mode consists of A superimposed upon B. Fig. 5.4.22.

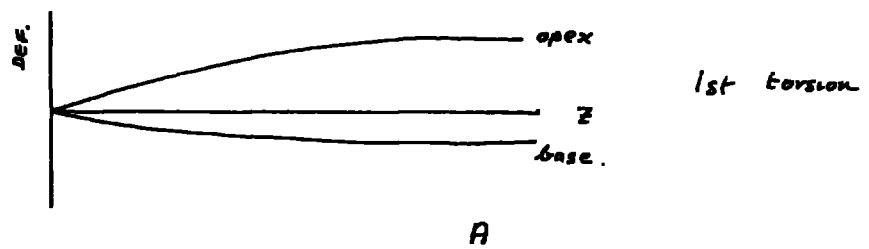

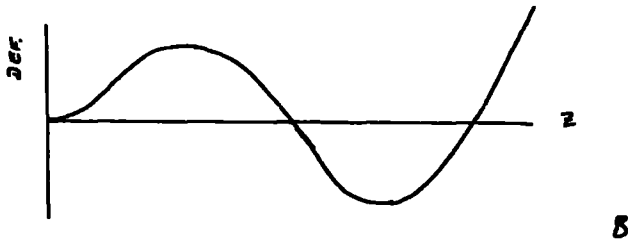

Fig. 5.4.22

whereas the fifth mode consists of A superimposed upon C.

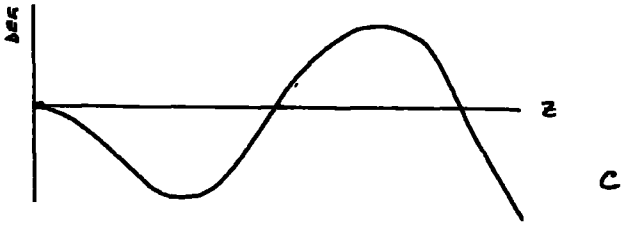

Fig. 5.4.22

To show the variation of the mode shape with the degree of coupling, the theoretical curves are drawn for different values of r_y. From these it is seen that for a given mode, if the coupling is increased by increasing r_y the effect is to increase the proportion of the other mode in the deflected shape.

Graphs 5.4.9 to 5.4.11 for example show the fourth and fifth mode shapes at lengths appreciably less than the critical. The fourth is therefore predominantly torsional but with evidence of 3rd XX coupling. It can be seen that increasing the degree of coupling increases the bending characteristics. Similarly, in the case of the predominantly 3rd XX fifth mode at lengths less than the critical, an increase of r_y increases the separation of the apex and base deflections indicating a greater proportion of the torsional fourth mode.

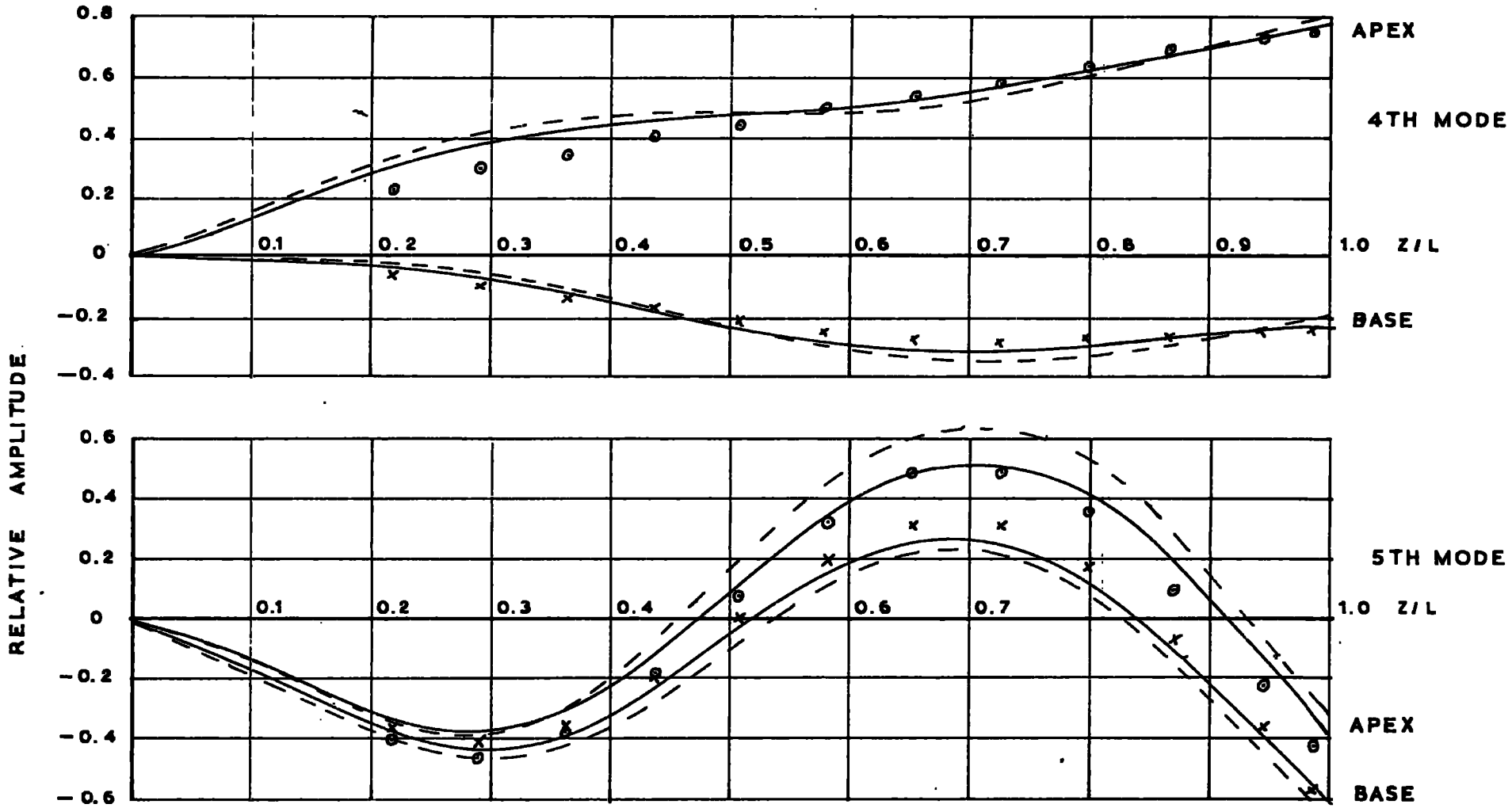

FIG 5.4.9 MODE SHAPES

$\alpha = 6.86$ L = 0.276 M

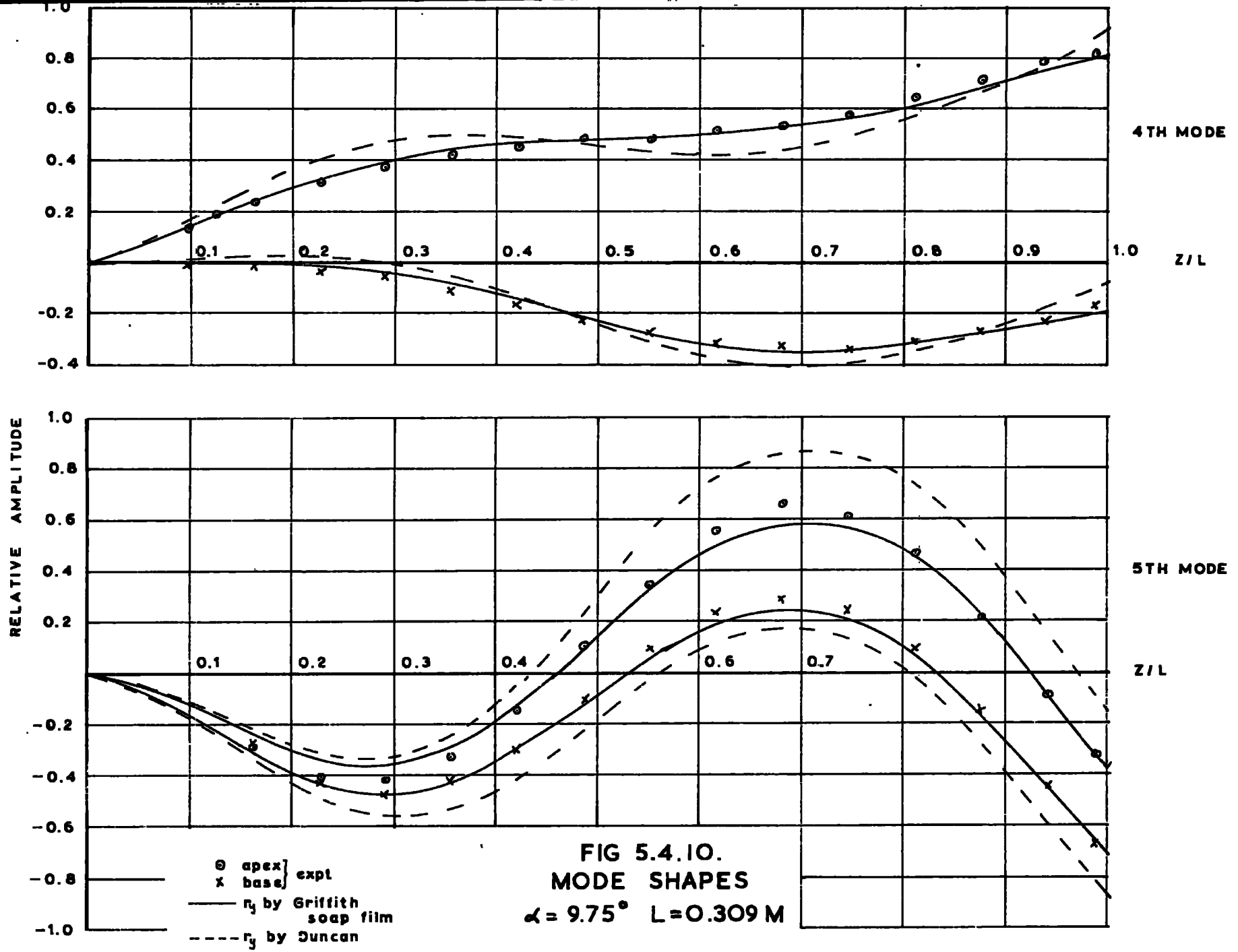

FIG 5.4.10.
MODE SHAPES
$\alpha = 9.75°$ L=0.309 M

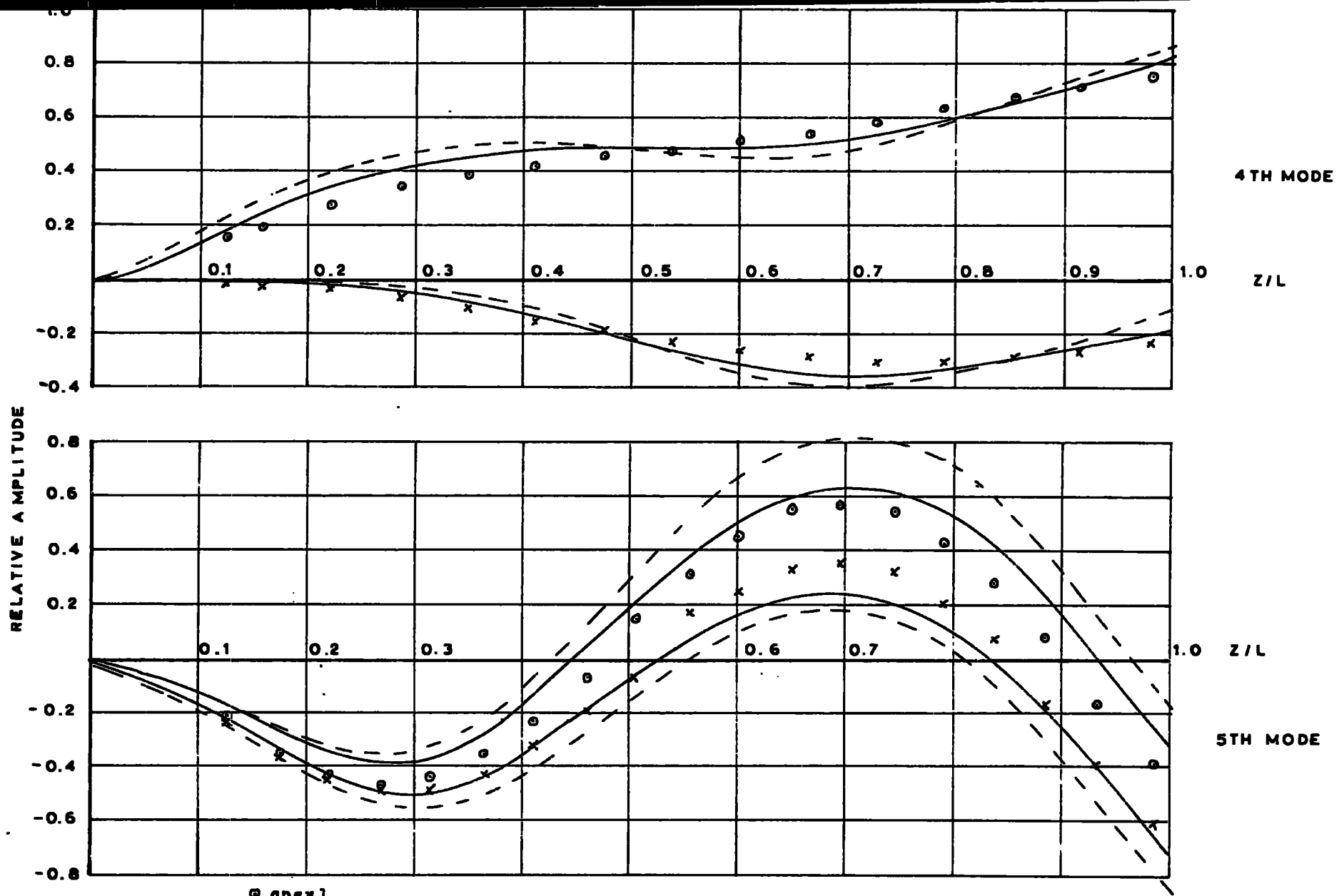

FIG 5.4.11
MODE SHAPES
$\alpha = 13.10^\circ$ L=0.316 M.

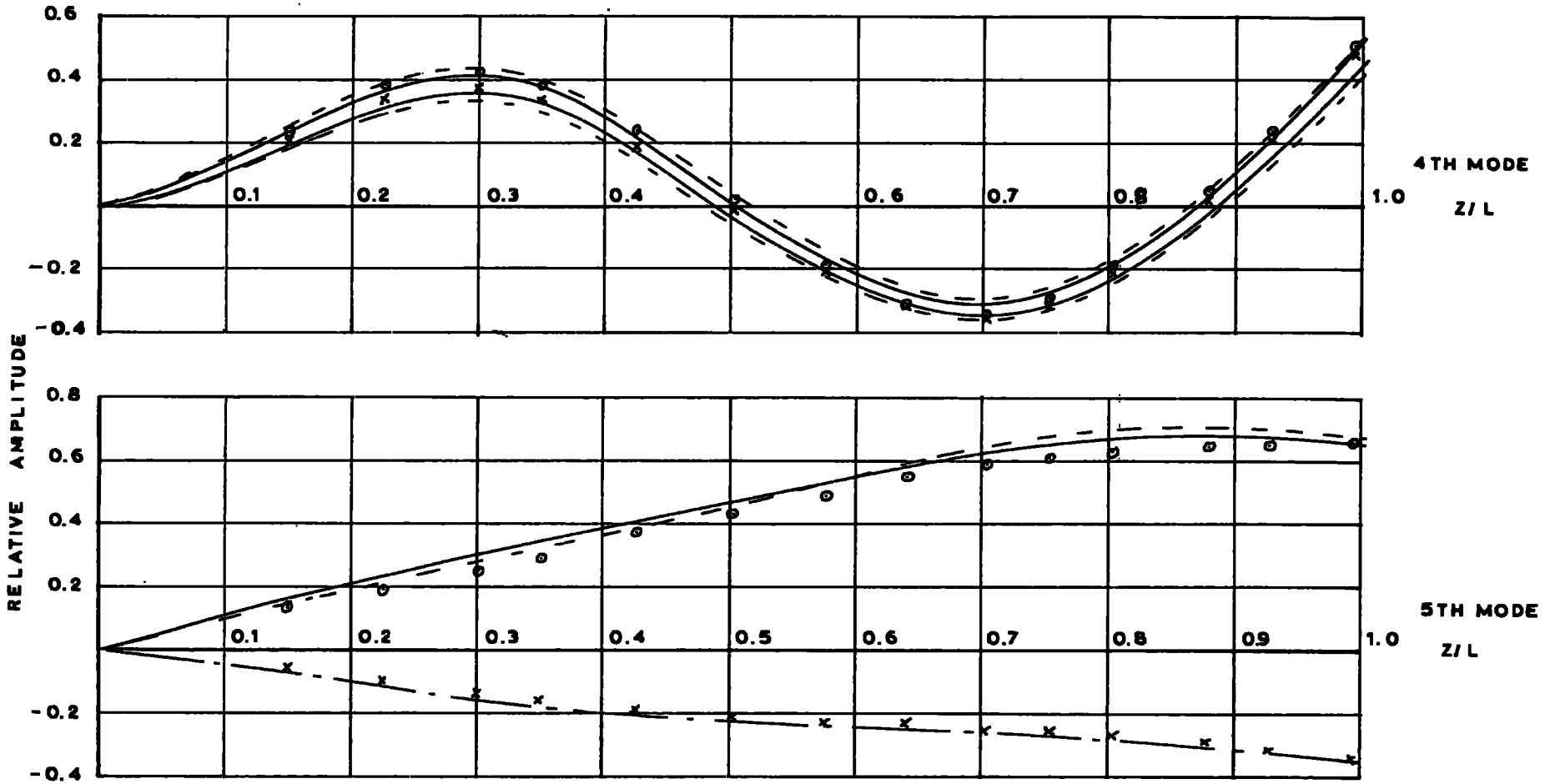

⊙ apex
× base
} expt

——— r_y by Griffith
- - - - r_y by Duncan
} theory

FIG 5.4.12
MODE SHAPES
α = 6.86 L = 0.399 M.

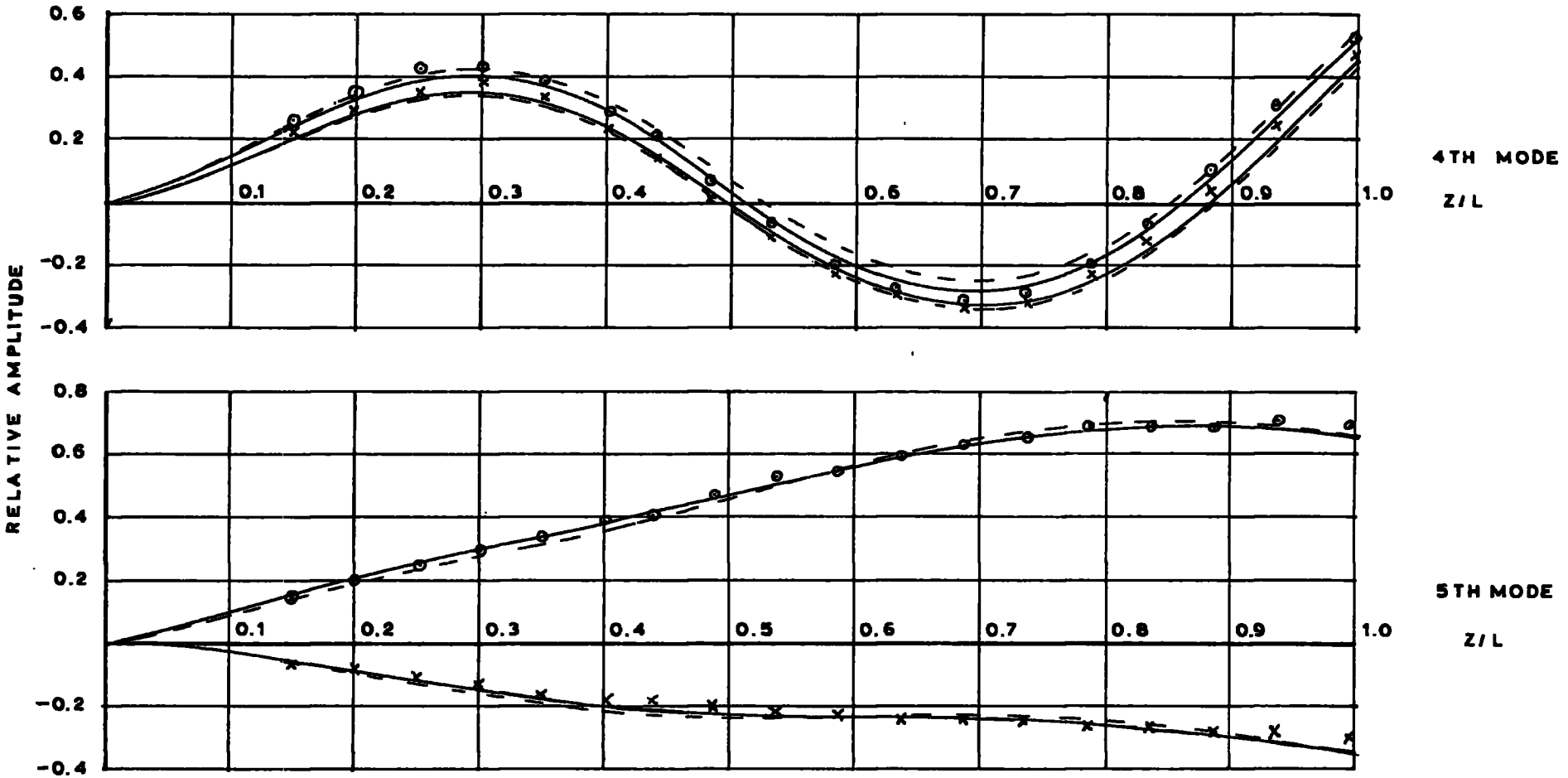

⊙ apex } expt
× base }

——— r_y by Griffith } theory
- - - - r_y by Duncen }

FIG 5.4.13
MODE SHAPES
α = 13.10 L = 0.400 M

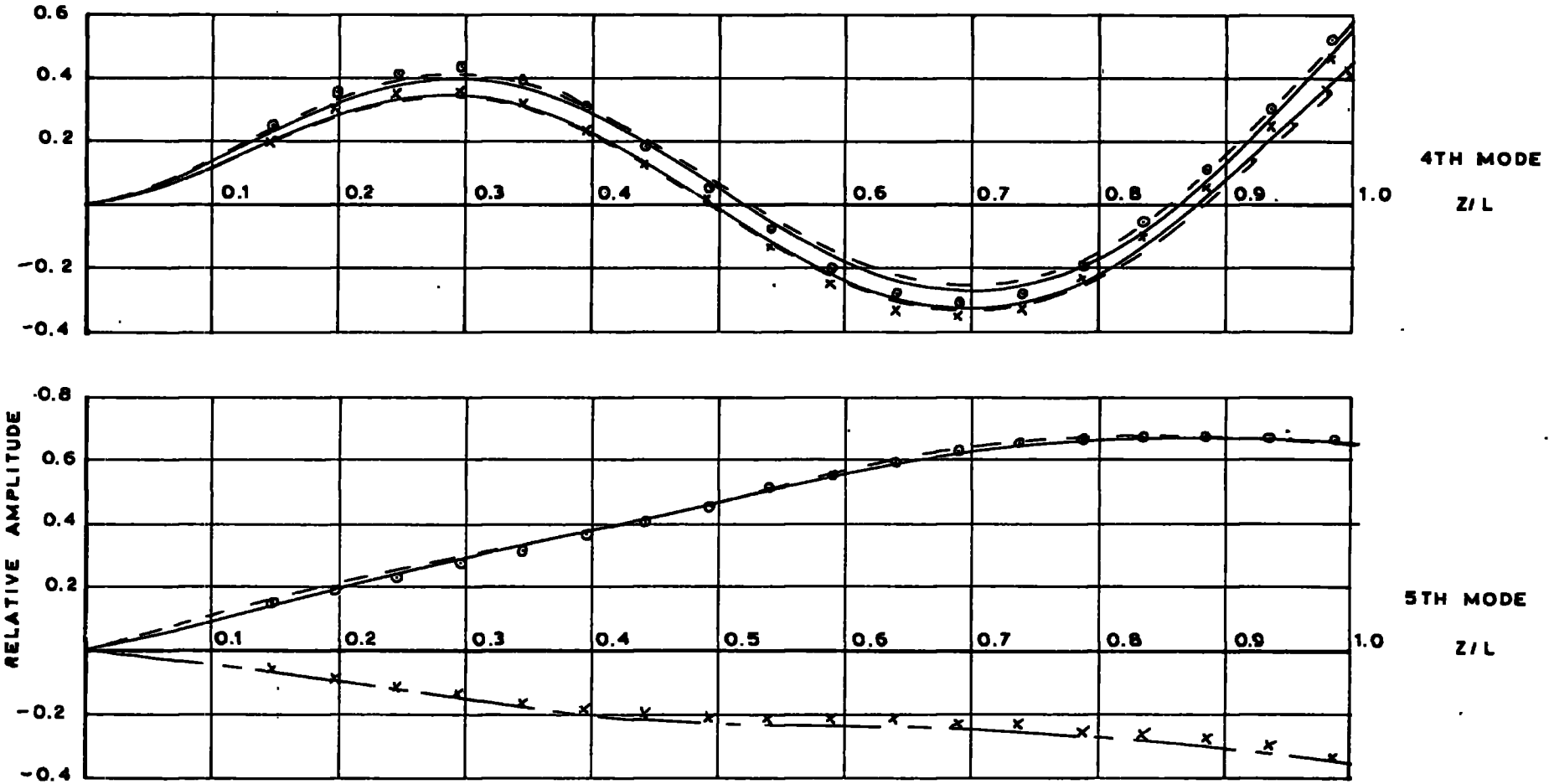

o apex } expt
x base }

——— r_y by Griffith soap film } theory
– – – r_y by Duncan }

FIG 5.4.14.
MODE SHAPES
$\alpha = 9.75^\circ$ L = 0.4065 M

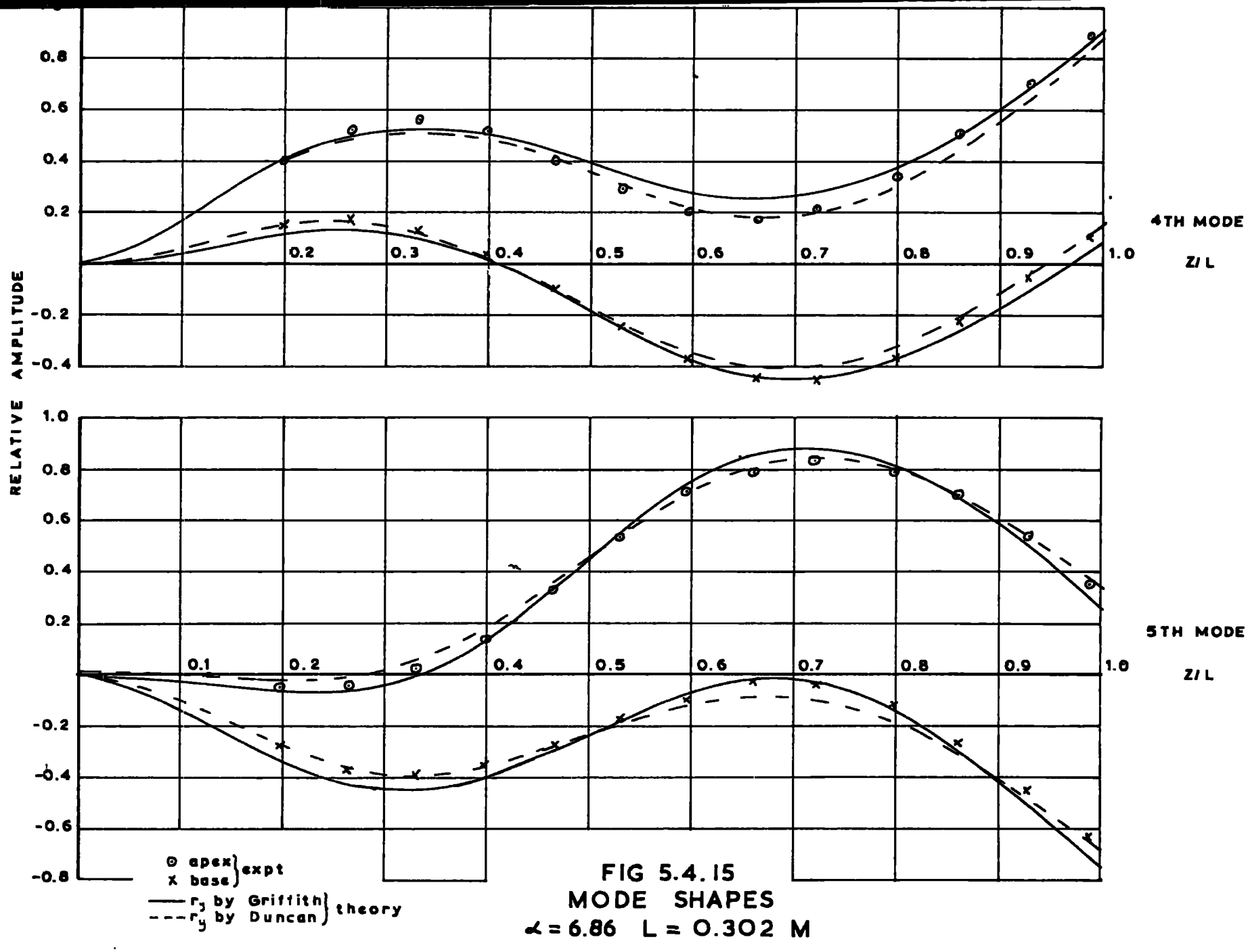

FIG 5.4.15
MODE SHAPES
$\alpha = 6.86$ L = 0.302 M

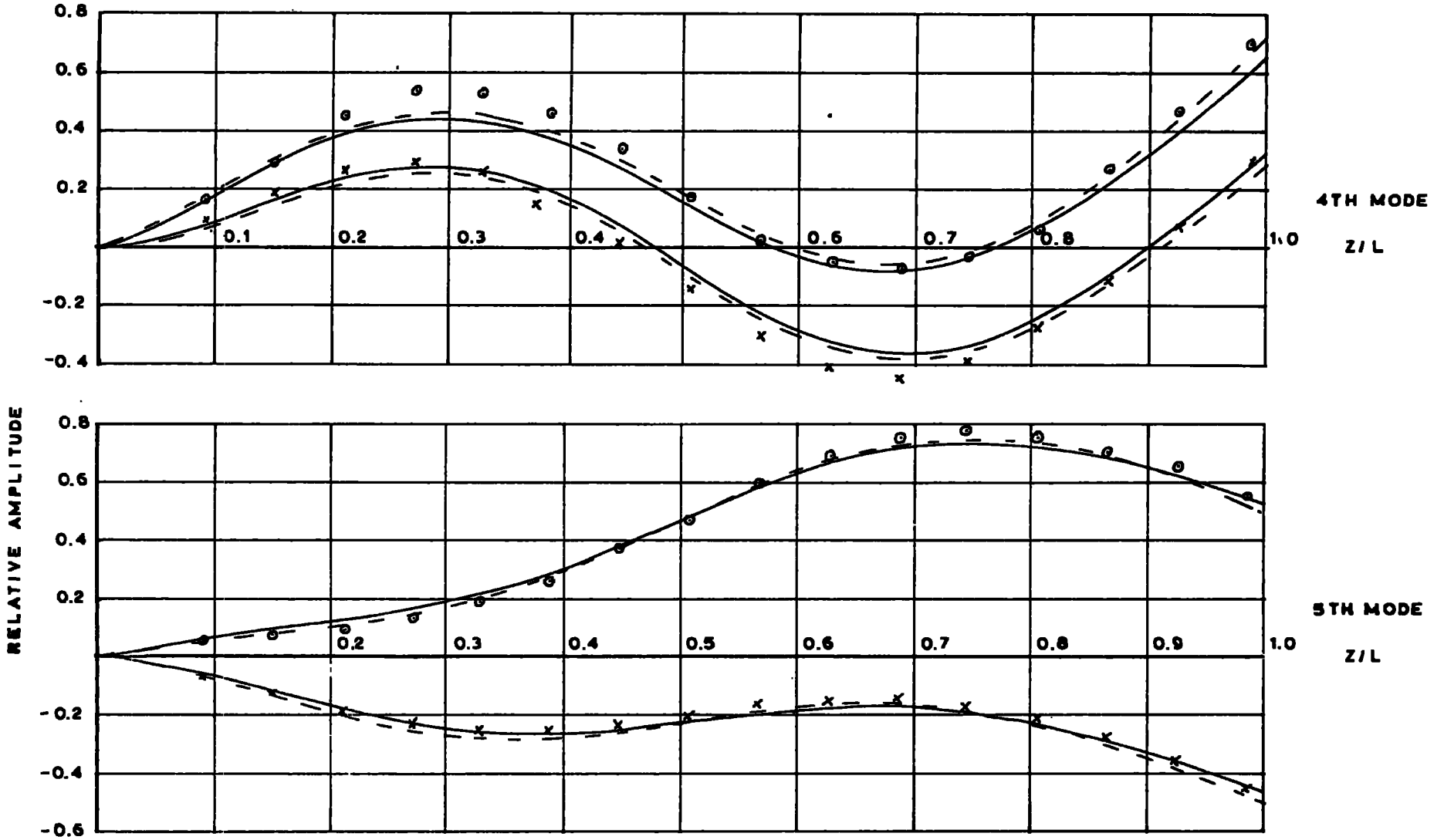

o apex } expt
x base }

——r_y by Griffith soap film } theory
---r_y by Duncan

FIG 5.4.16
MODE SHAPES
$\alpha = 9.75^\circ$ L=0.335 M

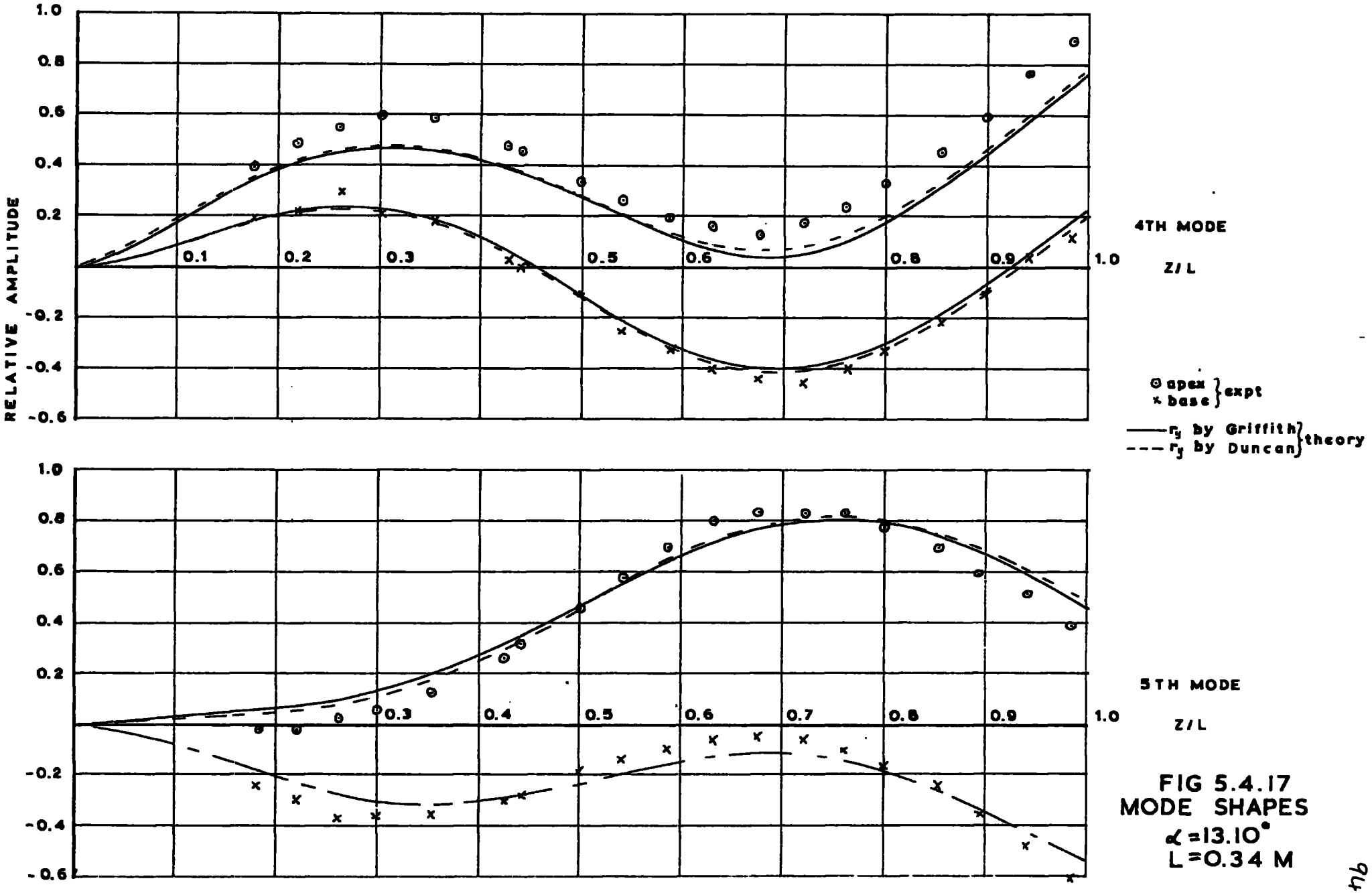

FIG 5.4.17
MODE SHAPES
$\alpha = 13.10^{\circ}$
L = 0.34 M

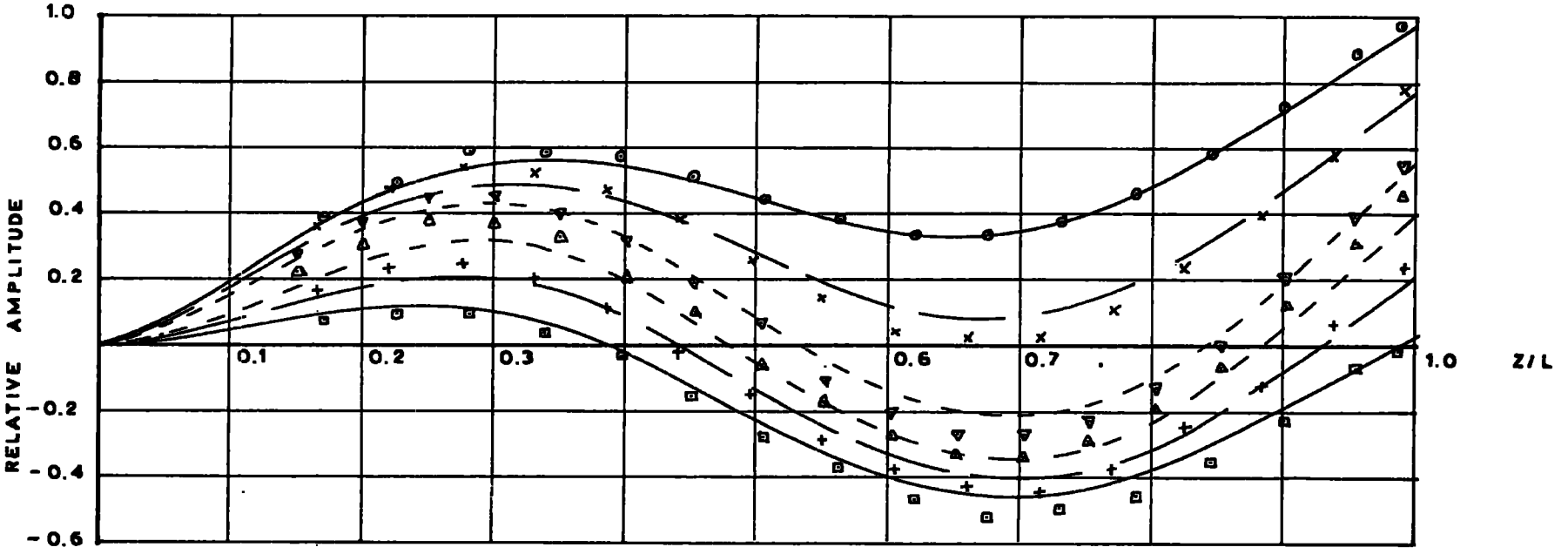

L=0.3555 M ⊖ apex, ⊡ base } expt —— r_y by Griffith (theory)

L=0.363 M × apex, + base } expt —— $-r_y$ by Griffith (theory)

L=0.3985 M ▽ apex, △ base } expt ---- r_y by Griffith (theory)

FIG 5.4.18 VARIATION OF 4TH MODE WITH LENGTH, $\alpha = 14.99°$

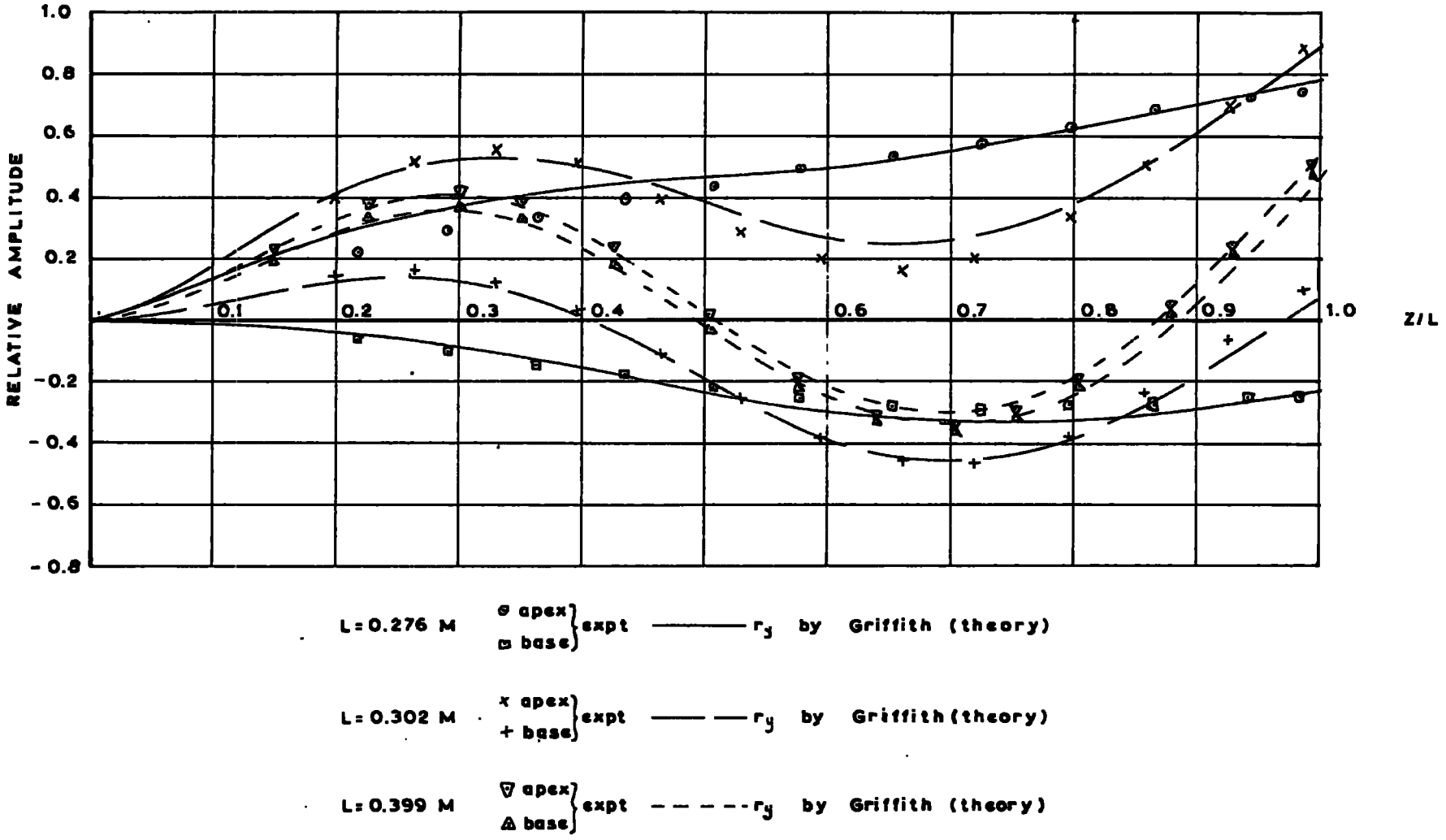

FIG 5.4.19 VARIATION OF 4TH MODE WITH LENGTH, $\alpha = 6.86^\circ$

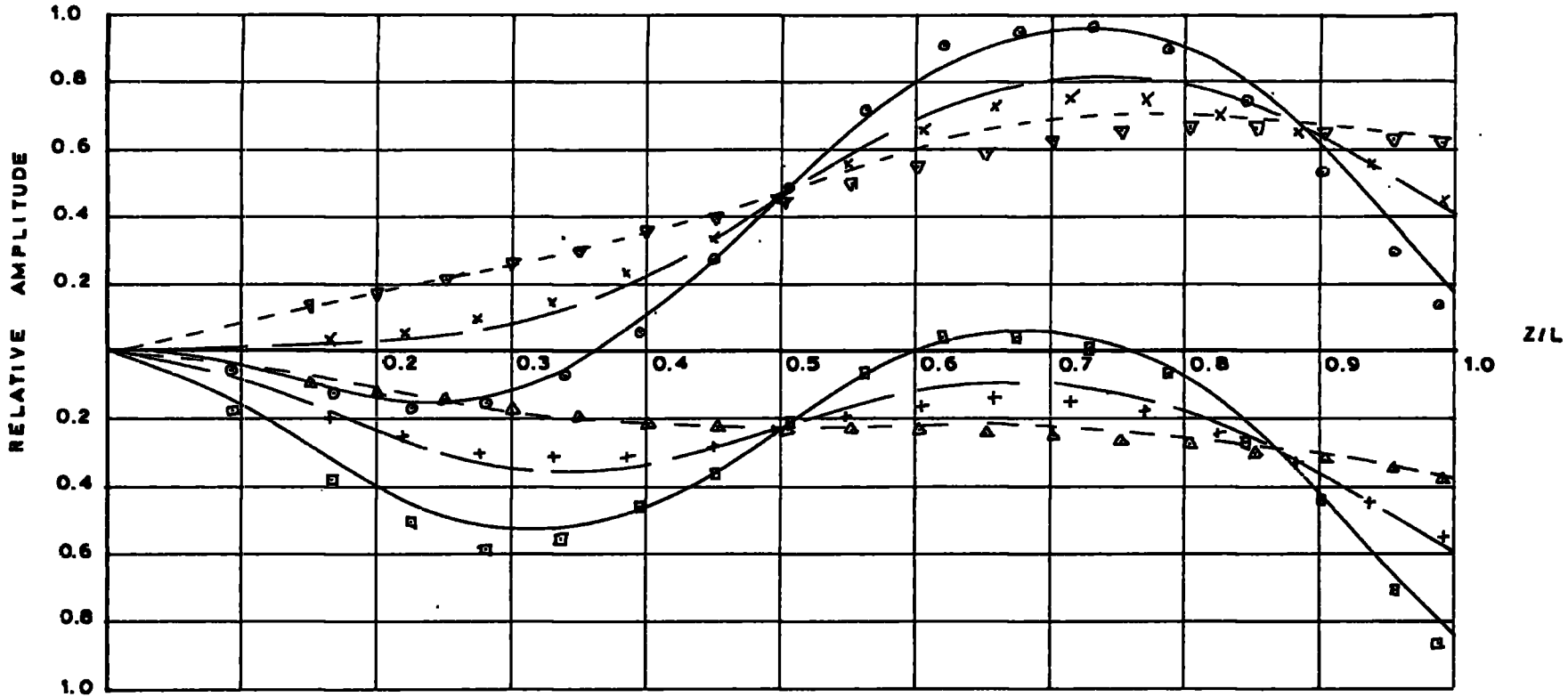

L=0.3555 M ⊙ apex, □ base } expt ——— r_y by Griffith (theory)

L=0.363 M × apex, + base } expt — — r_y by Griffith (theory)

L=0.3985 M ▽ apex, △ base } expt - - - - r_y by Griffith (theory)

FIG 5.4.20 VARIATION OF 5TH MODE WITH LENGTH, α=14.99°

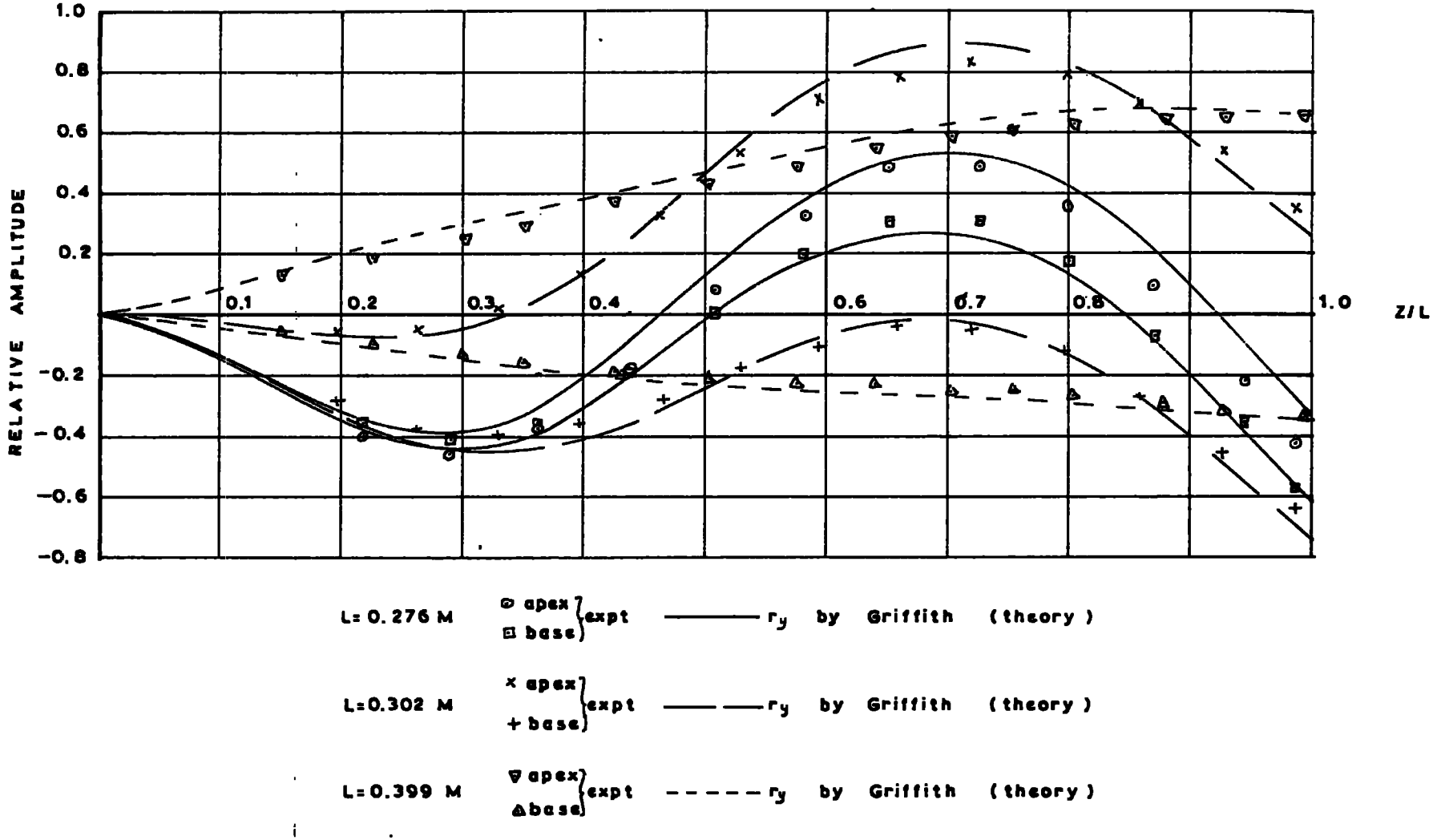

FIG 5.4.21 VARIATION OF 5TH MODE WITH LENGTH, $\alpha = 6.86^\circ$

With the possible exception of Fig. 5.4.15 in which the theoretical results based on r_y calculated by Duncan's formula agree more closely with the experimental, all the mode shape and frequency / length curves indicate that Griffith's formula gives a better approximation for r_y than that due to Duncan. The same conclusion is drawn by Scholes and Slater[5] who state that the formula by Griffith gives a better fit to their static results.

The present curves show, though, that for each beam the true value of r_y is less than that predicted by either formula: in the case of the beam of apex angle 9.75° the experimental value of r_y deduced by Griffith gives close agreement of frequency length and mode shape curves. Morley (communication to 22) makes an interesting comment in stating that for propellor and compressor blades the theoretical shear centre lies between the centroid and the leading edge, but measured shear centres tend to lie between the centroid and the trailing edge. Approximating the thin isosceles triangular section to an aerofoil such that the base of the triangle corresponds to the leading edge, there may be a general conclusion to be drawn that measured shear centres appear to be displaced away from the leading edge towards the trailing edge - possibly due to root effects.

5.5. Error Analysis.

5.5.1 Frequency.

This section considers the variation in observed frequency due to error in the measurement of physical quantities.

Bending modes

$$\omega_{1mKv} = \frac{(7.855)^2}{2\pi L^2}\sqrt{\frac{E k^2_{yy}}{\rho}}$$

Error in L

This is most likely to occur in setting up the beam in the clamping block, but may also be introduced by failure to square off the tip after reducing the length.

In the worst case, the error ϵ_L is estimated at 0.5 mm over a length of 300 mm.

$$\therefore \epsilon_L = \pm\ 0.166\%$$

Hence error in $L^2 = 0.33\%$

Error in $\sqrt{k^2_{yy}}$

$$k^2_{yy} = \frac{(\text{width})^2}{6}$$

Variation of micrometer readings over total length of beam showed an error of $\pm$ 0.86%

Hence error in $\sqrt{k^2_{yy}} = \pm\ 0.86\%$

Error in $\frac{1}{\sqrt{\rho}}$

Variation in dimensions of rectangular block with surfaces ground $\simeq$ 0.1%

Variation in volume $\simeq \pm$ 0.3%

Mass of block accurate to within $\pm$ 0.001%

Hence error in $\frac{1}{\sqrt{\rho}} \simeq \pm$ 0.15%

Accuracy of decade oscillator

At frequencies producing stationary Lissajou's figures with reference to the internal crystal oscillator the accuracy is specified at ±0.005%. At other frequencies the accuracy is specified at ± 0.05%.

In the worst case therefore the error in frequency ω may be

$$\pm (0.33 + 0.86 + 0.15 + 0.05) \%$$

$$= \pm 1.39\%$$

Torsion modes

$$\omega_{1T} = \frac{1}{4L}\sqrt{\frac{C}{\rho A k^2_g}}$$

Error in L

As before the error is estimated at ± 0.17%

Error in $\frac{1}{\sqrt{A}}$

Area A = $\frac{1}{2}$ (width) x (height)

Error in width, as before, = ± 0.86%

The error in the height of the cross section = ±1.46% which is fairly large due to the difficulty of holding the beam accurately during the machining of the narrow angle along the apex.

Error in A = ± (1.46 + 0.86) %

= ±2.32%

Error in $\frac{1}{\sqrt{A}}$ = ±1.16%

Error in $\sqrt{k^2_{cg}}$

$$k^2_{cg} = k^2_{xx} + k^2_{yy}$$

As $k^2_{xx} \gg k^2_{yy}$ then for the estimation of error

$k^2_{cg} \simeq k^2_{xx}$

Hence the error in $\sqrt{k^2_{cg}}$ = ± 1.46%

The total error in $\omega_{1,T}$ is therefore

$$\pm (0.17 + 1.16 + 1.46 + 0.05)\%$$ including possible error in the decade oscillator

$$= \pm 2.84\%$$

The error in torsion is much larger than that in bending principally because of the large error in the height dimension. In practice, though, with the small apex angle, the amount of material involved is very small and the error is not therefore as significant as the above calculations imply.

5.5.2 Mode shape error analysis

A quantitative analysis of the total error in the mode shape readings would serve little general purpose as the error varies with each figure. This is inherent in the method of normalisation, and it has been shown that the method of normalisation is chosen so as to minimise the error in plotting the shapes.

The good general agreement and lack of scatter confirms the acceptability of the method of probe support, the alignment of the support block and ruler using a travelling microscope, and the sensitivity of the probes.

CHAPTER 6

CONCLUSIONS

The assumption of a cubic polynomial variation in torsional displacement along an element in the finite element idealisation has been shown to be valid in the study of coupled torsion / bending vibration. Also, the accuracy and stability of the Laplace Transform solution is adequate provided double precision arithmetic is employed.

Cold rolled steel bar cannot be used for the manufacture of beams for testing because of distortion due to the release of residual stresses. Hot rolled steel bar and duralumin (neither of which distort) are equally suitable for electromagnetic excitation and response measurement by capacitive probes, but duralumin is preferable as a better encastré root fixing in steel may be obtained.

For constant cross sectional area the torsional stiffness of an isosceles triangular cross-section increases with apex angle . All the methods of calculation considered give an approximately linear increase up to $\alpha = 10^{\circ}$. Within the range $2^{\circ} \leq \alpha \leq 60^{\circ}$ the formula by Duncan, Ellis and Scruton is probably the most accurate, but the graphical method by Griffith is within 5% of the former, and is claimed to be applicable to any cross-sectional shape. It should therefore give at least a good first approximation to the torsional stiffness of more complex sections.

The static result: that an asymmetric cross section of a cantilever under the influence of a pure couple in its plane rotates about the centre of flexure has been shown to be inapplicable to an asymmetric section performing torsional oscillations. As far as it can be stated that an asymmetric section performs pure torsional oscillations about a point,

the point has been shown to be on the axis of symmetry (for an isosceles triangular section) at a small distance from the centroid on the side remote from the centre of flexure. The displacement of the point from the centroid has been shown theoretically to be extremely small and the point may be assumed to be coincident with the centroid.

As with the coupling of bending modes by pretwisting, the effect of coupling on the frequencies of otherwise distinct torsion and bending modes whose frequencies are within 10% of each other is to separate the two frequencies into coupled modes. These coupled modes both possess torsion and bending characteristics.

The separation increases with increase on r_y and decreases away from the critical length. It is not as significant, as far as the usual turbine blade shape is concerned, as the separation of adjacent bending frequencies due to pretwist.

For the beams considered, the fourth mode changes from a predominantly first torsion mode to a 3rd XX bending mode with increase in length, whereas the fifth mode does the reverse. At one particular length, therefore, the fourth and fifth modes must consist of torsion and bending characteristics in equal proportions, but may be distinguished by a phase change of 180° in the torsion / bending combination.

The overall conclusion on the position of the centre of flexure, drawn from the frequency / length and mode shape curves, is that Griffith's formula gives a better approximation for the centroid / centre of flexure coordinate than that due to Duncan, Griffith's experimental value of r_y,

deduced by soap film measurements gives particularly close agreement.

The results do, however, support Morley's observation that experimentally determined positions of the centre of flexure are displaced further from the leading edge than the theoretical.

APPENDIX 1

Bibliography

1. Griffith, A.A. " Determination of Torsional Stiffness and strength of cylindrical bars of any shape". Rep. Memo. Advis. Comm. Aero. 1917 No.334 New Series.

2. Timoshenko, S.P. and Goodier, J.N. " Theory of Elasticity " 2nd Ed. 1957 Eng. Sci. monographs McGraw Hill p.278.

3. Duncan, W.J., Ellis, D.L., and Scruton, C. " The flexural centre and centre of twist of an elastic cylinder ". Phil. Mag. 7th Series 1933 Vol.16 p.201.

4. Nuttall, H., " Torsion of uniform rods with particular reference to rods of triangular cross-section ". A.S.M.E. paper no. 52 - APM - 27 1952.

5. Scholes, A., and Slater, D.J., " Torsional stiffness of long steam turbine blades ". Journal of Strain Analysis Vol. 5, No.4 1970, p.242.

6. Griffith, A.A., and Taylor, G.I., " Problem of flexure and its solution by the soap film method ". Rep. Memo. Advis. Comm. Aero. 1917 No. 399.

7. Timoshenko, S.D., and Goodier, J.N., op. cit., p. 259.

8. Duncan, W.J., " Torsion and flexure of cylinders and tubes ". Report no. 1444 Aeronautical Research Council, 1932.

9. Young, A.W., Elderton, E.M., and Pearson, K., " On the torsion resulting from flexure in prisms with cross-sections of non-axial symmetry only". Drapers Co. Research Memoirs, Tech. Series No. 7 C.U.P. 1918.

10. Troesch, A., Anliker, M., and Ziegler, H., " Lateral vibrations of twisted rods " 1954 Quarterly Journal of Applied Mathematics Vol. 12 No. 2 p. 163.

11. Warburton, G.B., " The dynamical behaviour of structures " Pergamon Press 1964 p. 87.

12. Carnegie, W., " Vibrations of pretwisted cantilever blading " Proc. Inst. Mech. Engrs. 1959 Vol. 173, No. 12

13. Carnegie W., " Static bending of pretwisted cantilever blading" Jour. Mech. Eng. Sci., Vol. 171 No. 32 1957.

14. Slyper, M.A., " Coupled bending vibration of pretwisted cantilever Jour. Mech. Eng. Sci. Vol. 4 No. 4 1962.

15. Rosard, D.D., and Lester, A.A., " Natural frequencies of twisted cantilever beams ". Trans. A.S.M.E. No. 52 - A - 15 1952.

16. Isakson, G., and Eisley, G.J., " Natural frequencies in coupled bending and torsion of twisted rotating and non rotating bars ". N.A.S.A. 1964 Grant No. N 56 - 27 - 59 University of Michigan.

17. Gendler, A., and Mendelsohn, A., " Analytical and Experimental investigation of effect on twist on vibrations of cantilever beams. " N.A.C.A. Tech. Note 2300, 1951.

18. Dawson, B., Ghosh, N.G., and Carnegie W., " Effect of slenderness ratio on the natural frequencies of pretwisted cantilever beams of uniform rectangular cross-section " Jour. Mech. Eng. Sci. Vol. 13, No. 1 1971.

19. Dokumaci, E., Thomas, J., and Carnegie W., " Matrix displacement analysis of coupled bending- bending vibrations of pretwisted blading ". Jour. Mech. Eng. Sci. Vol.9 No. 4, 1967.

20. Ahmad, S., Anderson, R.G., and Zienkiewicz, O.C., " Vibration of thick curved shells, with particular reference to turbine blades ". Journal of Strain Analysis Vol.5, No. 3, 1970.

21. Carnegie, W., Dawson, B., and Thomas, J., " Vibration characteristics of cantilever blading ". Proc. Inst. Mech. Engrs. 1965 - 66 Vol. 180 Pt. 3I.

22. Carnegie, W. " Vibrations of pretwisted cantilever blading: an additional effect due to torsion ". Proc. Inst. Mech. Engrs. Vol. 176, No. 13, 1962.

23. Timoshenko, S.P., and Goodier, J.N., op. cit. p. 245.

APPENDIX 2

The effect of fibre bending on the first torsional mode

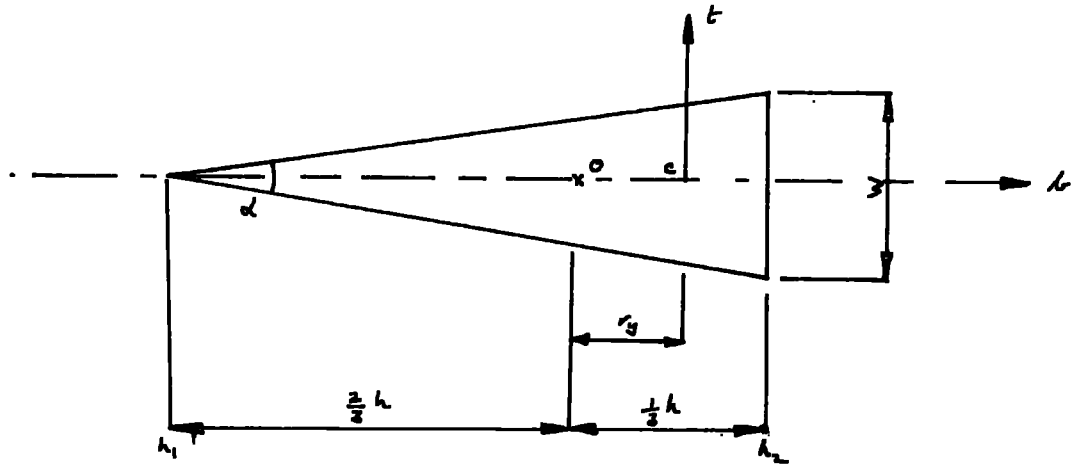

The factor $^{(F)}$ by which the first torsional mode is raised when fibre bending is taken into account is given by Carnegie (22) as

$$F = \sqrt{1 + \frac{E\pi^2 C_1}{4CL^2}}$$

where $C_1 = \frac{1}{12}\int_{h_1}^{h_2} b^2 t^3 \, db$ and is constant for the section.

In this case $t = f(b)$

Suppose $t = mb + k$ where m and k are constants

at h_1 $\quad 0 = m\left(-\frac{2}{3}h - r_y\right) + k$

and at h_2 $\quad \frac{w}{2} = m\left(\frac{1}{3}h - r_y\right) + k$

$$\therefore k = m\left(\frac{2}{3}h + r_y\right)$$

and $m = \frac{w}{2h}$

hence $t = \frac{w}{2h}b + \frac{1}{3}w + \frac{wr_y}{2h}$

The total thickness at a given value of b = 2t as the section is symmetrical

$$2t = \frac{w}{h} b + \left(\frac{2}{3} w + \frac{w r_g}{h} \right)$$

$$= A.b + B \quad \text{for brevity}$$

where $A = \frac{w}{h}$ and $B = w\left(\frac{2}{3} + \frac{r_g}{h} \right)$

Hence

$$C_1 = \frac{1}{12} \int_{h_1}^{h_2} (A^3 b^5 + 3A^2 B b^4 + 3AB^2 b^3 + B^3 b^2)\, db$$

$$= \frac{1}{12} \left\{ \frac{A^3}{6}(h_2^6 - h_1^6) + \frac{3}{5} A^2 B (h_2^5 - h_1^5) + \frac{3}{4} AB^2 (h_2^4 - h_1^4) + \frac{B^3}{3}(h_2^3 - h_1^3) \right\}$$

Taking the extremes of thickness of the beams considered (Appendix 11) at L = 0.3m and C calculated by the formula of Duncan, Ellis and Scruton, then for the thickest beam (α = 14.986°).

A = 0.2631

B = 8.365×10^{-3}

h_2 = 7.94×10^{-3}

h_1 = -3.178×10^{-2}

Hence F = $\sqrt{1.0068}$ = 1.0034

Hence the frequency is raised by 0.34%

Similarly, for the thinnest beam α = 6.858°

A = 1.198×10^{-1}

B = 3.815×10^{-3}

$h_2 = 7.967 \times 10^{-3}$

$h_1 = -3.183 \times 10^{-2}$

hence $F = \sqrt{1.0008} = 1.0004$

Hence the frequency is raised by 0.04%

It is seen therefore that the effect is greatest for the thickest beam, and increases with decrease in length. Hence for all the lengths of the beams considered the maximum effect will be 0.34%

S_1	C_1										
C_1	$-S_1$										
ϕC_1	$-\phi S_1$	S_1	C_1								
$-\phi S_1$	$-\phi C_1$	C_1	$-S_1$								
				1							
					1						
S_2	C_2	ℓS_2	ℓC_2			$\ell^2 S_2$	$\ell^2 C_2$	$\ell^3 S_2$	$\ell^3 C_2$		
C_2	$-S_2$	ℓC_2	$-\ell S_2$			$\ell^2 C_2$	$-\ell^2 S_2$	$\ell^3 C_2$	$-\ell^3 S_2$		
ϕC_2	$-\phi S_2$	$S_2 + \ell\phi C_2$	$C_2 - \ell\phi S_2$			$2\ell S_2 + \ell^2\phi C_2$	$2\ell C_2 - \ell^2\phi S_2$	$3\ell^2 S_2 + \ell^3\phi C_2$	$3\ell^2 C_2 - \ell^3\phi S_2$		
$-\phi S_2$	$-\phi C_2$	$C_2 - \ell\phi S_2$	$-S_2 - \ell\phi C_2$			$2\ell C_2 - \ell^2\phi S_2$	$-2\ell S_2 - \ell^2\phi C_2$	$3\ell^2 C_2 - \ell^3\phi S_2$	$-3\ell^2 S_2 - \ell^3\phi C_2$		
				1	ℓ					ℓ^2	ℓ^3
					1					2ℓ	$3\ell^2$

$s_{1,2}$ denotes $\sin \chi_{1,2}$
$c_{1,2}$ " $\cos \chi_{1,2}$
(unspecified elements are zero)

APPENDIX 3: MATRIX [D]

$\beta\phi^4\ell$	0	$\beta\phi^4\frac{\ell^2}{2}$	$2\beta\phi^3\ell$	0	0	$\beta\phi^2\left(\phi^2\frac{\ell^3}{3}-2\ell\right)$	$\beta\phi^3\ell^2$	$\beta\phi^2\left(\phi^2\frac{\ell^4}{4}-3\ell^2\right)$	$2\beta\phi^3\ell^3$	0	0
	$\alpha\phi^4\ell$	$2\alpha\phi^3\ell$	$\alpha\phi^4\frac{\ell^2}{2}$	0	0	$2\alpha\phi^3$	$\alpha\phi^2\left(\phi^2\frac{\ell^3}{3}-2\ell\right)$	$-2\phi^3\alpha\ell^3$	$\alpha\phi^2\left(\phi^2\frac{\ell^4}{4}-3\ell^2\right)$	0	0
		$-4\alpha\phi^2\ell+\beta\phi^4\frac{\ell^3}{3}$	$\beta\phi^3\ell^2-\alpha\phi^3\ell^2$	0	0	$-4\alpha\phi^2\ell^2+\phi^2\beta\left(\phi^2\frac{\ell^4}{4}-\ell^2\right)$	$2\alpha\phi\left(2\ell-\phi^2\frac{\ell^3}{3}\right)+4\beta\phi^3\frac{\ell^3}{3}$	$4\alpha\phi^2\ell^3+\beta\phi^2\left(\phi^2\frac{\ell^5}{5}-2\ell^3\right)$	$2\alpha\phi\left(3\ell^2-\phi^2\frac{\ell^4}{4}\right)+3\phi^3\beta\frac{\ell^4}{2}$	0	0
			$\alpha\phi^4\frac{\ell^3}{3}+4\beta\phi^2\ell$	0	0	$4\alpha\phi^3\frac{\ell^3}{3}-2\beta\phi\left(2\ell-\phi^2\ell^3/3\right)$	$\alpha\phi^2\left(\phi^2\frac{\ell^4}{4}-\ell^2\right)+2\beta\phi^2\ell^2$	$-3\alpha\phi^3\frac{\ell^4}{2}-2\beta\phi\left(3\ell^2-\phi^2\ell^4/4\right)$	$\alpha\phi^2\left(\phi^2\frac{\ell^5}{5}-2\ell^3\right)+4\beta\phi^2\ell^3$	0	0
				0	0	0	0	0	0	0	0
					$C\ell$	0	0	0	0	$C\ell^2$	$C\ell^3$
						$-16/3\left(\alpha\phi^2\ell^3\right)+\beta\left(4\ell-\frac{\phi^4\ell^5}{5}-\frac{4\phi^2\ell^3}{3}\right)$	$4\alpha\phi\left(\ell^2-\phi^2\frac{\ell^4}{6}\right)-4\beta\phi\left(\ell^2-\phi^2\frac{\ell^4}{4}\right)$	$6\alpha\phi^2\ell^4+\beta\left(6\ell^2-2\phi^2\ell^4+\frac{\phi^4\ell^6}{6}\right)$	$4\alpha\phi\left(2\ell^3-\phi^2\frac{\ell^5}{5}\right)-6\beta\phi\left(2\frac{\ell^3}{3}-\phi^2\frac{\ell^5}{5}\right)$	0	0
							$\frac{16}{3}\beta\phi^2\ell^3+\alpha\left(4\ell-\phi^4\frac{\ell^5}{5}-4\phi^2\frac{\ell^3}{3}\right)$	$6\alpha\phi\left(2\frac{\ell^3}{3}-\phi^2\frac{\ell^5}{5}\right)-4\beta\phi\left(2\ell^3-\phi^2\frac{\ell^5}{5}\right)$	$\alpha\left(6\ell^2-2\phi^2\ell^4+\phi^4\frac{\ell^6}{6}\right)+6\beta\phi^2\ell^4$	0	0
								$\frac{36}{5}\alpha\phi^2\ell^5+\beta\left(12\ell^3-\frac{12}{5}\phi^2\ell^5+\frac{\phi^4\ell^7}{7}\right)$	$6\alpha\phi\left(\frac{3\ell^4}{2}-\phi^2\frac{\ell^6}{6}\right)-6\beta\phi\left(\frac{3\ell^4}{2}-\phi^2\frac{\ell^6}{6}\right)$	0	0
									$\alpha\left(12\ell^3-\frac{12}{5}\phi^2\ell^5+\phi^4\frac{\ell^7}{7}\right)+36\beta\phi^2\frac{\ell^5}{5}$	0	0
										$\frac{4}{3}C\ell^3$	$\frac{3}{2}C\ell^4$
											$9C\frac{\ell^5}{5}$

(symmetric)

$\alpha = EI_{xx}$

$\beta = EI_{yy}$

APPENDIX 3: MATRIX [k]

l	0	$l^2/2$	0	$r_y l$	$l^2 r_y/2$	$l^3/3$	0	$l^4/4$	0	$r_y l^3/3$	$r_y l^4/4$
	l	0	$l^2/2$	$r_x l$	$l^2 r_x/2$	0	$l^3/3$	0	$l^4/4$	$r_x l^3/3$	$r_x l^4/4$
		$l^3/3$	0	$r_y l^2/2$	$r_y l^3/3$	$l^4/4$	0	$l^5/5$	0	$r_y l^4/4$	$r_y l^5/5$
			$l^3/3$	$r_x l^2/2$	$r_x l^3/3$	0	$l^4/4$	0	$l^5/5$	$r_x l^4/4$	$r_x l^5/5$
				$[\,]l$	$[\,]l^2/2$	$r_y l^3/3$	$r_x l^3/3$	$r_y l^4/4$	$r_x l^4/4$	$[\,]l^3/3$	$[\,]l^4/4$
					$[\,]l^3/3$	$r_y l^4/4$	$r_x l^4/4$	$r_y l^5/5$	$r_x l^5/5$	$[\,]l^4/4$	$[\,]l^5/5$
						$l^5/5$	0	$l^6/6$	0	$r_y l^5/5$	$r_y l^6/6$
							$l^5/5$	0	$l^6/6$	$r_x l^5/5$	$r_x l^6/6$
								$l^7/7$	0	$r_y l^6/6$	$r_y l^7/7$
									$l^7/7$	$r_x l^6/6$	$r_x l^7/7$
										$[\,]l^5/5$	$[\,]l^6/6$
											$[\,]l^7/7$

(symmetric)

$[\quad] \equiv (r_x^2 + r_y^2 + k_{cg}^2)$

APPENDIX 3: MATRIX [m]

APPENDIX 4

Listing of programs and notes on running.

Both programs are written in Fortran 4.

1. Finite element solution

The beam is divided into 8 elements, which is more than necessary to satisfy convergence, but enables the mode shapes to be drawn more accurately. The difference in frequency of the 3rd XX bending mode is less than 0.2% when run with 6 elements or 8.

The program is assembled thus:

LINE

8 Number of elements (NELEM) read in. If a number other than 8 is required, it is only necessary to change NELEM and the dimensions of the matrices in line 7 from 54 to (NELEM + 1) x 6 and NODE to (NELEM, 2)

12 Beam dimensions.

- ALL - total beam length
- HEIGHT - dimension in XX direction metres
- WIDTH - dimension in YY direction
- PRTWST - pretwist over total length (radians) anticlockwise positive looking from root.

17 RX, RY are coordinates of the centroid from the centre of flexure (metres).

21 C = torsional stiffness per unit length

44 E, DENS Youngs Modulus E (N/m^2) and Density ρ Kg / m^3

As listed, the program is limited to isosceles triangular sections symmetrical about the YY axis, as EI_{xx} and EI_{yy} (A and B respectively) are calculated with that assumption.

51 - 195 The matrices [k] and [m] (ie. AKK(I,J) and AMM(I,J) are assembled. Both are symmetric, hence only the upper or lower triangular needs to be specified.

196 - 257 The matrix [D] is assembled and inverted (line 257) by the Gauss - Jordan method.

261 - 268 [N] and [M] (AN(I,J) and AM(I,J)) calculated from $[\Delta^{-1}]^T[k][\Delta^{-1}]$ and $[\Delta^{-1}]^T[m][\Delta^{-1}]$

272 - 292 Matrices [ΣN] and [ΣM] (SAN (I,J) and SAM (I,J)) are formed from [N] and [M] according to the NODE matrix which defines the alignment of the elements in the structure.

296 - 310 The boundary conditions are applied. If any or all of the degrees of freedom at a node are to be constrained, it is done by setting the appropriate row and column of the stiffness and mass matrices to zero, and making the point on the leading diagonal of the stiffness matrix unity. NBOUND is the number of nodes to be constrained (which in this case = 2). ND (I) is the matrix of constrained nodes (nodes 1 and 9 in this case). IDN (I,J) is the matrix which defines the constraint at each node. Its six columns refer to the degrees of

freedom at each constrained node. An element of IDN which = 0 indicates that that particular movement of the node is fixed at zero. A non zero value indicates that it is free.

314 The eigenvalue problem is solved by a variation on the Jacobi Diagonalisation procedure. (W.W. Cooley and P.R. Lohnes, Multivariate procedures for the Behavioural Sciences, Wiley 1962, Chapter 3.) This yields XL(I,J), the matrix of eigenvalues, and X(I,J) the corresponding eigenvectors. The eigenvalues are printed columnwise as the mode shapes in order y, x, $\frac{dy}{dz}$, $\frac{dx}{dz}$, θ, $\frac{d\theta}{dz}$ at each node.

LAPLACE TRANSFORM SOLUTION

In principle the program is an iterative process, which, given three frequencies which are less than that of the fourth mode, in between the fourth and fifth modes, and greater than the fifth mode, converges to the fourth and fifth modes.

The subroutine ' CONDIT' calculates ' COND ', the value of the determinant for a given frequency (u).

LINE

74 - 77 The coefficients of the polynomial in s are calculated and

78 by means of the subroutine POLRT the roots (α, β, γ) of the equation are found by the Newton - Raphson process.

79 - 120 From the roots the terms of the matrix in equation 3.1.13 are calculated.

121 - 125 The value of the determinant calculated and returned to the main program.

The theory is derived specifically for the solution of the equations governing the coupled torsion / bending frequencies of straight uniform cantilever beams having one axis of symmetry (YY). Hence the pretwist (χ) and r_x are zero. Otherwise the data input is similar to that of the finite element program:

6 Beam length (AL), height, width and r_y read in as before.

11 CS - torsional stiffness per unit length.

18 Three initial frequencies read in, in ascending order. The frequencies are read in and printed out in Hertz, but the program works with all frequencies in radians / second.

Preliminary tests showed that for frequencies below that of the fourth mode and above that of the fifth COND was negative. At frequencies between those of the fourth and fifth modes COND was positive.

38 - 41 Before iteration is begun, it is confirmed that the

initial frequencies produce values of COND which are respectively negative, positive, negative.

42 - 57 Two iterations are performed, taking the mean of the first and second frequency to find the fourth mode, and the mean of the second and third to find the fifth. Each iteration was terminated when $|\ \text{COND}\ | \leq 5$, whereupon the frequency had converged to within 0.2 Hz.

Occasionally it was found that the iteration was unstable, and | COND |would remain constant at a value greater than 5. This was thought to be due to round - off error, and was overcome by employing double precision arithmetic. Usually the process had converged after about ten iterations.

```
>      1      C            D,T&C, PAPER ---ADAPTED FOR TORSION
>      2      C
>      3      C
>      4            IMPLICIT REAL*8(A-H,O-Z)
>      5            DIMENSION AKK(12,12),AMM(12,12), D(12,12),
>      6           *AM(12,12), AN(12,12), L(12), M(12), ND(2),
>      7           *SAN(54,54),SAM(54,54),NODE(8,2),IDN(2,5),XL(54),X(54,54)
>      8            READ(5,111) NELEM
>      9            WRITE(6,112) NELEM
>     10          111 FORMAT(I3)
>     11          112 FORMAT(' ','NO. OF ELEMENTS=',I3)
>     12            READ(5,113) ALL,HEIGHT,WIDTH,PRTWST
>     13            WRITE(6,114)  ALL,HEIGHT,WIDTH,PRTWST
>     14          113 FORMAT(4F9.6)
>     15          114 FORMAT(' ','LENGTH=',F9.6,3X,'HT=',F9.6,3X,'WIDTH=',F9.6,3X,'PRTW
>     16             &ST=',F9.6)
>     17            READ(5,115) RX,RY
>     18            WRITE(6,116) RX,PY
>     19          115 FORMAT(2E10.3)
>     20          116 FORMAT(' ','RX=',E10.3,3X,'RY=',E10.3)
>     21            READ(5,117) C
>     22          117 FORMAT(F7.2)
>     23            WRITE(6,118) C
>     24          118 FORMAT(' ','TORSIONAL STIFFNESS / UNIT LENGTH=',F7.2)
>     25            TH1=0.0
>     26            PHI=PRTWST/NELEM
>     27            TH2=PHI
>     28            MAT=(NELEM+1)*6
>     29            NBOUND=2
>     30            DO 119 J=1,5
>     31            IDN(2,J)=1
>     32          119 IDN(1,J)=0
>     33            IDN(1,6)=1
>     34            IDN(2,6)=0
>     35            DO 120 I=1,NELEM
```

```
>     36            NODE(I,1)=I
>     37          120 NODE(I,2)=I+1
>     38            ND(1)=1
>     39            ND(2)=NELEM+1
>     40            AL=ALL/NELEM
>     41            DEP=WIDTH/2.0
>     42            RG=DSQRT(((HEIGHT**2)/18.0)+((DEP**2)/6.0))
>     43            AREA=0.5*WIDTH*HEIGHT
>     44            READ(5,115) E,DENS
>     45            WRITE(6,122) E,DENS
>     46          122 FORMAT(' ','E=',E10.3,3X,'DENSITY=',E10.3)
>     47            A=E*AREA*(HEIGHT**2)/18.0
>     48            B=E*AREA*((DEP**2)+DEP*(WIDTH-DEP)+((WIDTH-DEP)**2))/18.0
>     49            AMU=AREA*DENS
>     50        C
>     51        C               SET UP AKK MATRIX
>     52            DO 1 I=1,6
>     53            AKK(I,5)=0.0
>     54            AKK(I,6)=0.0
>     55            AKK(5,(I+6))=0.0
>     56          1 AKK(6,(I+6))=0.0
>     57            DO 2 I=1,10
>     58            AKK(I,12)=0.0
>     59          2 AKK(I,11)=0.0
>     60            AKK(6,6)=C*AL
>     61            AKK(6,11)=C*(AL**2)
>     62            AKK(6,12)=C*(AL**3)
>     63            AKK(11,11)=(4.0*C*(AL**3)/3.0)
>     64            AKK(11,12)=(3.0*C*(AL**4)/2.0)
>     65            AKK(12,12)=(9.0*C*(AL**5)/5.0)
>     66            AKK(1,1)=B*AL*(PHI**4)
>     67            AKK(1,2)=0.0
>     68            AKK(1,3)=B*(AL**2)*(PHI**4)/2.0
>     69            AKK(1,4)=2.0*B*AL*(PHI**3)
>     70            AKK(1,7)=B*(PHI**2)*(((PHI**2)*(AL**3)/3.0)-2.0*AL)
>     71            AKK(1,8)=2.0*B*(PHI**3)*(AL**2)
>     72            AKK(1,9)=B*(PHI**2)*(((PHI**2)*(AL**2)/4.0)-3.0*(AL**2))
```

```
>     73            AKK(1,10)=2.*B*(PHI**3)*(AL**3)
>     74            AKK(2,2)=A*AL*(PHI**4)
>     75            AKK(2,3)=2.0*A*AL*(PHI**3)
>     76            AKK(2,4)=A*(PHI**4)*(AL**2)/2.0
>     77            AKK(2,7)=2.0*A*(PHI**3)*(AL**2)
>     78            AKK(2,8)=A*(PHI**2)*(((PHI**2)*(AL**3)/3.0)-2.0*AL)
>     79            AKK(2,9)=-2.0*(PHI**3)*A*(AL**3)
>     80            AKK(2,10)=A*(PHI**2)*(((PHI**2)*(AL**4)/4.0)-3.0*(AL**2))
>     81            AKK(3,3)=-4.0*A*AL*(PHI**2)+B*(PHI**4)*(AL**3)/3.0
>     82            AKK(3,4)=(B-A)* (PHI**3)*(AL**2)
>     83            AKK(3,7)=4.0*A*(PHI**2)*(AL**2)+(PHI**2)*B*(((PHI**2)*(AL**4)/4.0)
>     84           8-(AL**2))
>     85            AKK(3,8)=2.0*A*PHI*((2.0*AL)-((PHI**2)*(AL**3)/3.0))+4.0*B*(PHI**3
>     86           8)*(AL**3)/3.0
>     87            AKK(3,9)=4.0*A*(PHI**2)*(AL**3)+B*(PHI**2)*(((PHI**2)*(AL**5)/5.0)
>     88           8-2.0*(AL**3))
>     89            AKK(3,10)=2.*A*PHI*((3.0*(AL**2))-(PHI**2)*(AL**4)/4.0)+1.5*3*(PHI
>     90           8**3)*(AL**4)
>     91            AKK(4,4)=(A*(PHI**4)*(AL**3)/3.0)+4.0*B*(PHI**2)*AL
>     92            AKK(4,7)=(4.0*A*(PHI**3)*(AL**3)/3.0)+2.0*B*PHI*(((PHI**2)*(AL**3)
>     93           8/3.0)-2.0*AL)
>     94            AKK(4,8)=A*(PHI**2)*(((PHI**2)*(AL**4)/4.0)-(AL**2))+2.0*B*((PHI*
>     95           8AL)**2)
>     96            AKK(4,9)=(-6.0*A*(PHI**3)*(AL**4)/4.0)-2.0*B*PHI*((3.0*(AL**2))-(
>     97           8PHI**2)*(AL**4)/4.0)
>     98            AKK(4,10)=A*(PHI**2)*(((PHI**2)*(AL**5)/5.)-2.0*(AL**3))+4.0*3*(
>     99           8PHI**2)*(AL**3)
>    100            AKK(7,7)=(16.0*A*(PHI**2)*(AL**3)/3.0)+B*(4.0*AL-((PHI**4)*(AL**5)
>    101           8/5.0)-(4.0*(PHI**2)*(AL**3)/3.0))
>    102            AKK(7,8)=4.0*PHI*((AL**2)-(PHI**2)*(AL**4)/4.0)*(A-B)
>    103            AKK(7,9)=6.0*A*(PHI**2)*(AL**4)+B*(6.0*(AL**2)-2.0*(PHI**2)*(AL**4
>    104           8)+((PHI**4)*(AL**5)/6.0))
>    105            AKK(7,10)=4.*A*PHI*(2.0*(AL**3)-(PHI**2)*(AL**5)/5.0)-6.0*B*PHI*
>    106           8((2.0*(AL**3)/3.0)-((PHI**2)*(AL**5)/5.0))
>    107            AKK(8,8)=(16.0*B*(PHI**2)*(AL**3)/3.0)+A*(4.0*AL-((PHI**4)*(AL**5)
>    108           8/5.0)-(4.0*(PHI**2)*(AL**3)/3.0))
```

```
>    109            AKK(8,9)=6.0*A*PHI*((2.0*(AL**3)/3.0)-((PHI**2)*(AL**5)/5.0))-4.0*
>    110           8B*PHI*(2.0*(AL**3)-((PHI**2)*(AL**5)/5.0))
>    111            AKK(8,10)=A*(5.*(AL**2)-(2.0*(PHI**2)*(AL**4))+((PHI**4)*(AL**6)/
>    112           86.0))+6.0*B*(PHI**2)*(AL**4)
>    113            AKK(9,9)=(36.0*A*(PHI**2)*(AL**5)/5.0)+B*(12.0*(AL**3)-(12.0*(PHI*
>    114           8*2)*(AL**5)/5.0)+((PHI**4)*(AL**7)/7.0))
>    115            AKK(9,10)=6.*PHI*(1.5*(AL**4)-((PHI**2)*(AL**6)/8.0))*(A-B)
>    116            AKK(10,10)=A*(12.*(AL**3)-(12.*(PHI**2)*(AL**5)/5.0)+((PHI**4)*(AL
>    117           8**7)/7.0))+(36.0*B*(PHI**2)*(AL**5)/5.0)
>    118            N=2
>    119            DO 11 I=1,11
>    120            DO 12 J=N,12
>    121         12 AKK(J,I)=AKK(I,J)
>    122            N=N+1
>    123         11 CONTINUE
>    124      C           SET UP AMM MATRIX
>    125            DO 31 I=1,12
>    126            DO 31 J=1,12
>    127         31 AMM(I,J)=0.0
>    128            AMM(1,1)=AL
>    129            AMM(1,3)=(AL**2)/2.0
>    130            AMM(1,5)=AL*RY
>    131            AMM(1,6)=(AL**2)*RY/2.0
>    132            AMM(1,7)=(AL**3)/3.0
>    133            AMM(1,9)=(AL**4)/4.0
>    134            AMM(1,11)=RY*(AL**3)/3.0
>    135            AMM(1,12)=RY*(AL**4)/4.0
>    136            AMM(2,2)=AL
>    137            AMM(2,4)=(AL**2)/2.0
>    138            AMM(2,5)=AL*RX
>    139            AMM(2,6)=RX*(AL**2)/2.0
>    140            AMM(2,8)=(AL**3)/3.0
>    141            AMM(2,10)=(AL**4)/4.0
>    142            AMM(2,11)=RX*(AL**3)/3.0
>    143            AMM(2,12)=RX*(AL**4)/4.0
>    144            AMM(3,3)=(AL**3)/3.0
```

```
>    145            AMM(3,5)=RY*(AL**2)/2.0
>    146            AMM(3,6)=RY*(AL**3)/3.0
>    147            AMM(3,7)=(AL**4)/4.0
>    148            AMM(3,9)=(AL**5)/5.0
>    149            AMM(3,11)=RY*(AL**4)/4.0
>    150            AMM(3,12)=RY*(AL**5)/5.0
>    151            AMM(4,4)=(AL**3)/3.0
>    152            AMM(4,5)=RX*(AL**2)/2.0
>    153            AMM(4,6)=RX*(AL**3)/3.0
>    154            AMM(4,8)=(AL**4)/4.0
>    155            AMM(4,10)=(AL**5)/5.0
>    156            AMM(4,11)=RX*(AL**4)/4.0
>    157            AMM(4,12)=RX*(AL**5)/5.0
>    158            BRAC=(RX**2)+(RY**2)+(RG**2)
>    159            AMM(5,5)=AL*BRAC
>    160            AMM(5,6)=BRAC*(AL**2)/2.0
>    161            AMM(5,7)=RY*(AL**3)/3.0
>    162            AMM(5,8)=RX*(AL**3)/3.0
>    163            AMM(5,9)=RY*(AL**4)/4.0
>    164            AMM(5,10)=RX*(AL**4)/4.0
>    165            AMM(5,11)=BRAC*(AL**3)/3.0
>    166            AMM(5,12)=BRAC*(AL**4)/4.0
>    167            AMM(6,6)=BRAC*(AL**3)/3.0
>    168            AMM(6,7)=RY*(AL**4)/4.0
>    169            AMM(6,8)=RX*(AL**4)/4.0
>    170            AMM(6,9)=RY*(AL**5)/5.0
>    171            AMM(6,10)=RX*(AL**5)/5.0
>    172            AMM(6,11)=BRAC*(AL**4)/4.0
>    173            AMM(6,12)=BRAC*(AL**5)/5.0
>    174            AMM(7,7)=(AL**5)/5.0
>    175            AMM(7,9)=(AL**6)/6.0
>    176            AMM(7,11)=RY*(AL**5)/5.0
>    177            AMM(7,12)=RY*(AL**6)/6.0
>    178            AMM(8,8)=AMM(7,7)
>    179            AMM(8,10)=(AL**6)/6.0
>    180            AMM(8,11)=RX*(AL**5)/5.0
```

```
>   181            AMM(8,12)=RX*(AL**6)/6.0
>   182            AMM(9,9)=(AL**7)/7.0
>   183            AMM(9,11)=RY*(AL**6)/6.0
>   184            AMM(9,12)=RY*(AL**7)/7.0
>   185            AMM(10,10)=AMM(9,9)
>   186            AMM(10,11)=RX*(AL**6)/6.0
>   187            AMM(10,12)=RX*(AL**7)/7.0
>   188            AMM(11,11)=BRAC*(AL**5)/5.0
>   189            AMM(11,12)=BRAC*(AL**6)/6.0
>   190            AMM(12,12)=BRAC*(AL**7)/7.0
>   191            N=2
>   192            DO 42 I=1,11
>   193            DO 43 J=N,12
>   194         43 AMM(J,I)=AMM(I,J)
>   195         42 N=N+1
>   196      C     SET UP  D  MATRIX AND INVERT
>   197            DO 41 I=1,12
>   198            DO 41 J=1,12
>   199         41 D(I,J)=0.0
>   200            S=DSIN(TH1)
>   201            C=DCOS(TH1)
>   202            D(1,1)=S
>   203            D(1,2)=C
>   204            D(2,1)=C
>   205            D(2,2)=-S
>   206            D(3,1)=PHI*C
>   207            D(3,2)=-PHI*S
>   208            D(3,3)=S
>   209            D(3,4)=C
>   210            D(4,1)=-PHI*S
>   211            D(4,2)=-PHI*C
>   212            D(4,3)=C
>   213            D(4,4)=-S
>   214            D(5,5)=1.0
>   215            D(6,6)=1.0
>   216            S=DSIN(TH2)
```

```
>    217            C=DCOS(TH2)
>    218            D(7,1)=S
>    219            D(7,2)=C
>    220            D(7,3)=AL*S
>    221            D(7,4)=AL*C
>    222            D(7,7)=(AL**2)*S
>    223            D(7,8)=(AL**2)*C
>    224            D(7,9)=(AL**3)*S
>    225            D(7,10)=(AL**3)*C
>    226            D(8,1)=C
>    227            D(8,2)=-S
>    228            D(8,3)=AL*C
>    229            D(8,4)=-AL*S
>    230            D(8,7)=(AL**2)*C
>    231            D(8,8)=-D(7,7)
>    232            D(8,9)=D(7,10)
>    233            D(8,10)=-D(7,9)
>    234            D(9,1)=PHI*C
>    235            D(9,2)=-PHI*S
>    236            D(9,3)=S+AL*PHI*C
>    237            D(9,4)=C-AL*PHI*S
>    238            D(9,7)=2.0*AL*S+(AL**2)*PHI*C
>    239            D(9,8)=2.0*AL*C-(AL**2)*PHI*S
>    240            D(9,9)=3.0*(AL**2)*S+(AL**3)*PHI*C
>    241            D(9,10)=3.0*(AL**2)*C-(AL**3)*PHI*S
>    242            D(10,1)=-PHI*S
>    243            D(10,2)=-PHI*C
>    244            D(10,3)=D(9,4)
>    245            D(10,4)=-D(9,3)
>    246            D(10,7)=D(9,8)
>    247            D(10,8)=-D(9,7)
>    248            D(10,9)=D(9,10)
>    249            D(10,10)=-D(9,9)
>    250            D(11,5)=1.0
>    251            D(11,6)=AL
>    252            D(11,11)=(AL**2)
```

```
>    253            D(11,12)=AL**3
>    254            D(12,6)=1.0
>    255            D(12,11)=2.0*AL
>    256            D(12,12)=3.0*(AL**2)
>    257            CALL DMINV(D,12,DET,L,M)
>    258       C
>    259       C                CALCULATE (AN) AND (AM)
>    260       C
>    261            DO 44 I=1,12
>    262            DO 44 J=1,12
>    263            AN(I,J)=0.0
>    264            AM(I,J)=0.0
>    265            DO 44 K=1,12
>    266            DO 44 LL=1,12
>    267            AN(I,J)=AN(I,J)+AKK(K,LL)*D(LL,J)*D(K,I)
>    268         44 AM(I,J)=AM(I,J)+AMM(K,LL)*D(LL,J)*D(K,I)
>    269       C
>    270       C      POST (AN) AND (AM) AND CONSTRAIN;
>    271       C
>    272            DO 33 I=1,MAT
>    273            DO 33 J=1,MAT
>    274            SAN(I,J)=0.0
>    275         33 SAM(I,J)=0.0
>    276            DO 34 I=1,NELEM
>    277            DO 34 J=1,2
>    278            K1=(NODE(I,J)-1)*6
>    279            K3=(J-1)*6
>    280            DO 34 K=1,2
>    281            K2=(NODE(I,K)-1)*6
>    282            K4=(K-1)*6
>    283            DO 35 JJ=1,6
>    284            K5=K1+JJ
>    285            K7=K3+JJ
>    286            DO 35 KK=1,6
>    287            K6=K2+KK
>    288            K8=K4+KK
```

```
>    280            SAM(K5,K6)=SAM(K5,K6)+AM(K7,K8)
>    290            SAN(K5,K5)=SAN(K5,K6)+AN(K7,K8)
>    291         35 CONTINUE
>    292         34 CONTINUE
>    293      C
>    294      C           CONSTRAINING PROCEDURE
>    295      C
>    296            DO 100 I=1,NBOUND
>    297            NM=(ND(I)-1)*6
>    298            DO 103 J=1,6
>    299            IF(IDN(I,J).NE.0) GO TO 103
>    300      C              NO  IS NOW THE ROW OF THE OVERALL MATRIX TO BE FIXED
>    301            NO=NM+J
>    302            DO 101 K=1,MAT
>    303            SAM(K,NO)=0.0
>    304       101  SAN(K,NO)=0.0
>    305            DO 102 K=1,MAT
>    306            SAM(NO,K)=0.0
>    307       102  SAN(NO,K)=0.0
>    308            SAN(NO,NO)=1.0
>    309       103  CONTINUE
>    310       100  CONTINUE
>    311      C
>    312      C      SOLUTION OF THE EIGENVALUE PROGRAM
>    313      C
>    314            CALL DNROOT(MAT,SAM,SAN,XL,X)
>    315            DO 22 I=1,9
>    316         22 XL(I)=(1.0/6.284)*DSQRT(1.0/(XL(I)*AMU))
>    317            WRITE(6,700)
>    318       700  FORMAT('0','NATURAL FREQUENCIES ARE')
>    319            WRITE(6,701)(XL(I),I=1,9)
>    320       701  FORMAT(' ',9E13.5)
>    321            DO 23 I=1,9
>    322         23 XL(I)=DLOG10(XL(I))
>    323            WRITE(6,707)
>    324       707  FORMAT('0','LOG(10) OF FREQUENCIES')
```

```
>    325           WRITE(6,708)(XL(I),I=1,9)
>    326       708 FORMAT(' ',9F13.4)
>    327           WRITE(6,702)
>    328       702 FORMAT('0','AND CORRESPONDING MODE SHAPES')
>    329           N=1
>    330           DO 703 I=1,MAT
>    331           IF((I-1).EQ.(6*N)) GO TO 704
>    332           WRITE(6,705)(X(I,J),J=1,9)
>    333       705 FORMAT(' ',9E13.3)
>    334           GO TO 703
>    335       704 WRITE(6,706)(X(I,J),J=1,9)
>    336       706 FORMAT('0',9E13.3)
>    337           N=N+1
>    338       703 CONTINUE
>    339           STOP
>    340           END
```

```
>      1      C         PARTIAL DIFFERENTIAL EQNS. OF MOTION
>      2      C            SOLUTION BASED ON LAPLACE TRANSFORMS
>      3      C
>      4            IMPLICIT REAL*8(A-H,O-Z)
>      5            DIMENSION XCOF(4),COF(4),PT(3),ROOTI(3),UU(3),CCOND(3)
>      6            READ(5,1) AL,HEIGHT,WIDTH,RY
>      7          2 FORMAT(' ','LENGTH=',F9.6,3X,'HEIGHT=',F9.5,3X,'WIDTH=',F9.6,3X,'R
>      8           +Y=',E9.2)
>      9          1 FORMAT(3F9.6,E9.2)
>     10            WRITE(6,2) AL,HEIGHT,WIDTH,RY
>     11            READ(5,3) CS
>     12          3 FORMAT(F7.2)
>     13            WRITE(6,4) CS
>     14          4 FORMAT(' ','TORSIONAL STIFFNESS/UNIT LENGTH=',F7.2)
>     15            READ(5,8)(UU(I),I=1,3)
>     16          8 FORMAT(3F8.2)
>     17            WRITE(6,30)(UU(I),I=1,3)
>     18         30 FORMAT(' ','3 INITIAL FREQUENCIES ARE',3F9.2,'HERTZ')
>     19            DO 71 I=1,3
>     20         71 UU(I)=UU(I)*6.284
>     21            DEP=WIDTH/2.0
>     22            RG2=((HEIGHT**2)/18.0)+((DEP**2)/6.0)
>     23            AREA=0.5*WIDTH*HEIGHT
>     24            READ(5,9) E,DENS
>     25          9 FORMAT(2E10.3)
>     26            WRITE(6,10) E,DENS
>     27         10 FORMAT(' ','YOUNGS MOD.=',E10.3,3X,'DENSITY=',E10.3)
>     28            EIYY=E*AREA*((DEP**2)+DEP*(WIDTH-DEP)+((WIDTH-DEP)**2))/18.0
>     29            AMU=AREA*DENS
>     30      C
>     31      C       SET UP THE COEFFICIENTS OF THE POLYNOMIAL IN S
>     32      C
>     33            A=-AMU/EIYY
>     34            B=-AMU*RY/EIYY
>     35            C=AMU*RY/CS
```

```
>     36            D=AMU*((RY**2)+RG2)/CS
>     37      C
>     38            DO 101 I=1,3
>     39            CALL CONDIT   (UU(I),CCOND(I),A,B,C,D,AL)
>     40        101 CONTINUE
>     41            IF(CCOND(1).GT.0.0.OR.CCOND(2).LT.0.0.OR.CCOND(3).GT.0.0) GO TO 99
>     42            UCENT=UU(2)
>     43            L=0
>     44        104 U=(UU(1)+UU(2))/2.0
>     45        102 CALL CONDIT   (U,COND,A,B,C,D,AL)
>     46            UHZ=U/6.284
>     47            WRITE(6,64) UHZ,COND
>     48         64 FORMAT(' ','UHZ=',E16.6,3X,'COND=',E14.4)
>     49            IF(DABS(COND).LE.5.0) GO TO 103
>     50            IF(COND) 51,52,53
>     51         51 UU(1)=U
>     52            U=(UU(2)+U)/2.0
>     53            GO TO 102
>     54         52 GO TO 103
>     55         53 UU(2)=U
>     56            U=(UU(1)+U)/2.0
>     57            GO TO 102
>     58        103 UHZ=U/6.284
>     59            ULOG=DLOG10(UHZ)
>     60            WRITE(6,60) UHZ,COND,ULOG
>     61         60 FORMAT('0','UHZ=',E14.4,3X,'COND',E14.4,3X,'LOG UHZ=',F8.4)
>     62            IF(L.GT.0) GO TO 98
>     63            L=1
>     64            UU(2)=UCENT
>     65            UU(1)=UU(3)
>     66            GO TO 104
>     67         99 WRITE(6,61)(CCOND(I),I=1,3)
>     68         61 FORMAT('0','DATA ERROR:INITIAL CCOND=',3E12.2)
>     69         98 STOP
>     70            END
>     71            SUBROUTINE CONDIT   (U,COND,A,B,C,D,AL)
```

```
>     72            IMPLICIT REAL*8(A-H,O-Z)
>     73            DIMENSION XCOF(4),COF(4),RT(3),ROOTI(3)
>     74            XCOF(1)=(U**4)*(A*D-B*C)
>     75            XCOF(2)=(U**2)*A
>     76            XCOF(3)=(U**2)*D
>     77            XCOF(4)=1.0
>     78            CALL POLRT(XCOF,COF,3,RT,ROOTI,IER)
>     79            A2=0.0
>     80            A3=0.0
>     81            B2=0.0
>     82            B3=0.0
>     83            C2=0.0
>     84            C3=0.0
>     85            D1=0.0
>     86            E1=0.0
>     87            H1=0.0
>     88            DO 20 I=1,3
>     89            MM=I+1
>     90            N=I+2
>     91            IF(N.GT.3) N=N-3
>     92            IF(MM.GT.3) MM=MM-3
>     93            AA=((U**2)*D+RT(I))/((RT(N)-RT(I))*(RT(MM)-RT(I)))
>     94            DD=-(U**2)*B/((RT(N)-RT(I))*(RT(MM)-RT(I)))
>     95            BB=-(U**2)*C/((RT(N)-RT(I))*(RT(MM)-RT(I)))
>     96            CC=((RT(I)**2)+(U**2)*A)/((RT(N)-RT(I))*(RT(MM)-RT(I)))
>     97            IF(RT(I)) 22,23,23
>     98         22 RT(I)=DABS(RT(I))
>     99            ANG=AL*(RT(I)**0.5)
>    100            A2=A2+AA*(-RT(I))*DCOS(ANG)
>    101            A3=A3+AA*(RT(I)**1.5)*DSIN(ANG)
>    102            B2=B2+AA*(RT(I)**0.5)*(-DSIN(ANG))
>    103            B3=B3+AA*(-RT(I))*DCOS(ANG)
>    104            C2=C2+(RT(I)**0.5)*(-DSIN(ANG))*DD
>    105            C3=C3+DD*(-RT(I))*DCOS(ANG)
>    106            D1=D1+BB*(RT(I)**0.5)*(-DSIN(ANG))
>    107            E1=E1+BB*DCOS(ANG)
```

```
>    108            H1=H1+CC*DCOS(ANG)
>    109            GO TO 20
>    110         23 ANG=AL*(RT(I)**0.5)
>    111            A2=A2+AA*RT(I)*DCOSH(ANG)
>    112            A3=A3+AA*(RT(I)**1.5)*DSINH(ANG)
>    113            B2=B2+AA*(RT(I)**0.5)*DSINH(ANG)
>    114            B3=B3+AA*RT(I)*DCOSH(ANG)
>    115            C2=C2+DD*(RT(I)**0.5)*DSINH(ANG)
>    116            C3=C3+DD*RT(I)*DCOSH(ANG)
>    117            D1=D1+BB*(RT(I)**0.5)*DSINH(ANG)
>    118            E1=E1+BB*DCOSH(ANG)
>    119            H1=H1+CC*DCOSH(ANG)
>    120         20 CONTINUE
>    121            P=A3*C2-A2*C3
>    122            Q=B3*C2-B2*C3
>    123            R=D1*C2-A2*H1
>    124            S=E1*C2-B2*H1
>    125            COND=R*Q-P*S
>    126            RETURN
>    127            END
```

APPENDIX V

Graphs of $r/a \rightarrow \lambda/\pi$ and $K \rightarrow 2A/P$ for Griffith's graphical method.

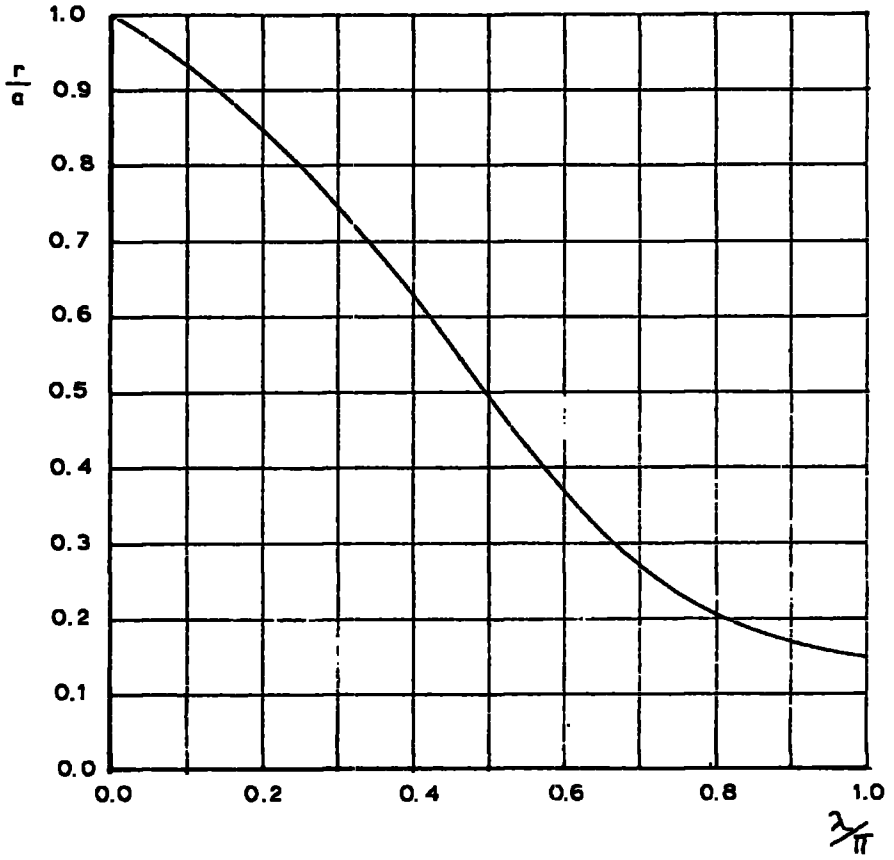

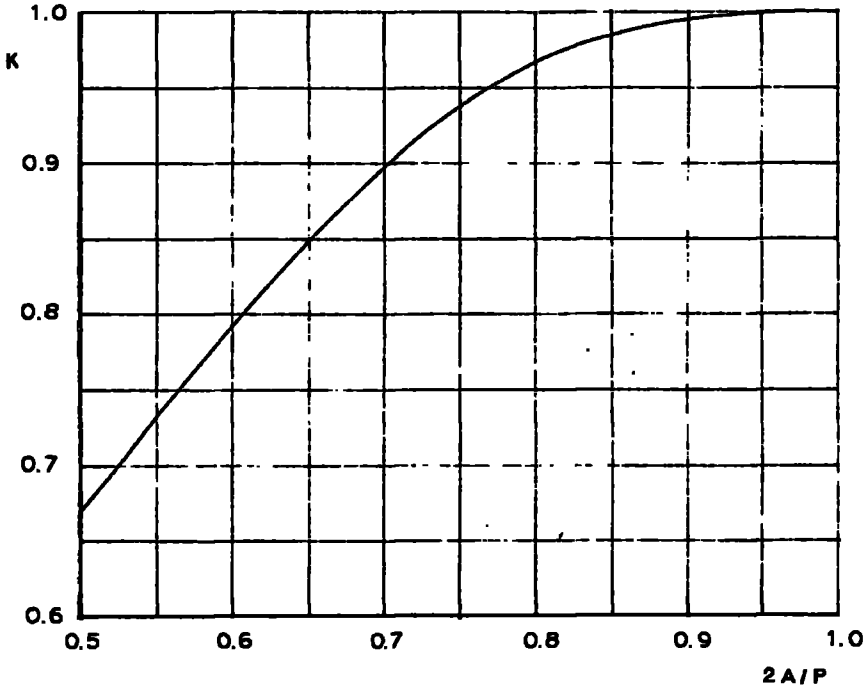

APPENDIX 6

Analysis of torsional oscillations

Consider for instance the beam for which $\alpha = 9.75^{\circ}$ at L = 0.4 m.

$$\frac{EIk^2}{4L^2} = \frac{2.09 \times 10^{11} \times 1.46 \times 10^{-4} \times 2.071 \times 10^{-6} \times \pi^2}{4 \times 0.16}$$

$$= 9.748 \times 10^{2}$$

$$\frac{C}{k_{\theta}^2} = \frac{83.57}{9.702 \times 10^{-5}} \qquad \text{assuming } k_{\theta}^2 = k_{cg}^2$$

$$= 8.61 \times 10^{5}$$

Assuming $r_y = 0.55 \times 10^{-2}$ for this beam

$$\epsilon = \frac{9.748 \times 10^{2}}{8.61 \times 10^{5} - 9.748 \times 10^{2}} \times 0.55 \times 10^{-2} \text{ m}$$

$$= 1.13 \times 10^{-3} \times 0.55 \times 10^{-2} \text{ m}$$

$$= \underline{\underline{6.23 \times 10^{-6} \text{ m}}}$$

APPENDIX 7

Beam Design

The following two figures show the variation with length of second and third XX bending modes and first torsional modes. These, of course take no account of coupling and are calculated on the basis of simple beam theory. It can be seen that the first torsion mode coicides with the second XX mode at lengths of less than 0.15 m, in which case effects of shear deflection and rotary inertia would not be negligible. Coincidence with the third XX mode is achieved between 0.3 and 0.4 m however, which is satisfactory.

A drawing of the beam mounting block is also included.

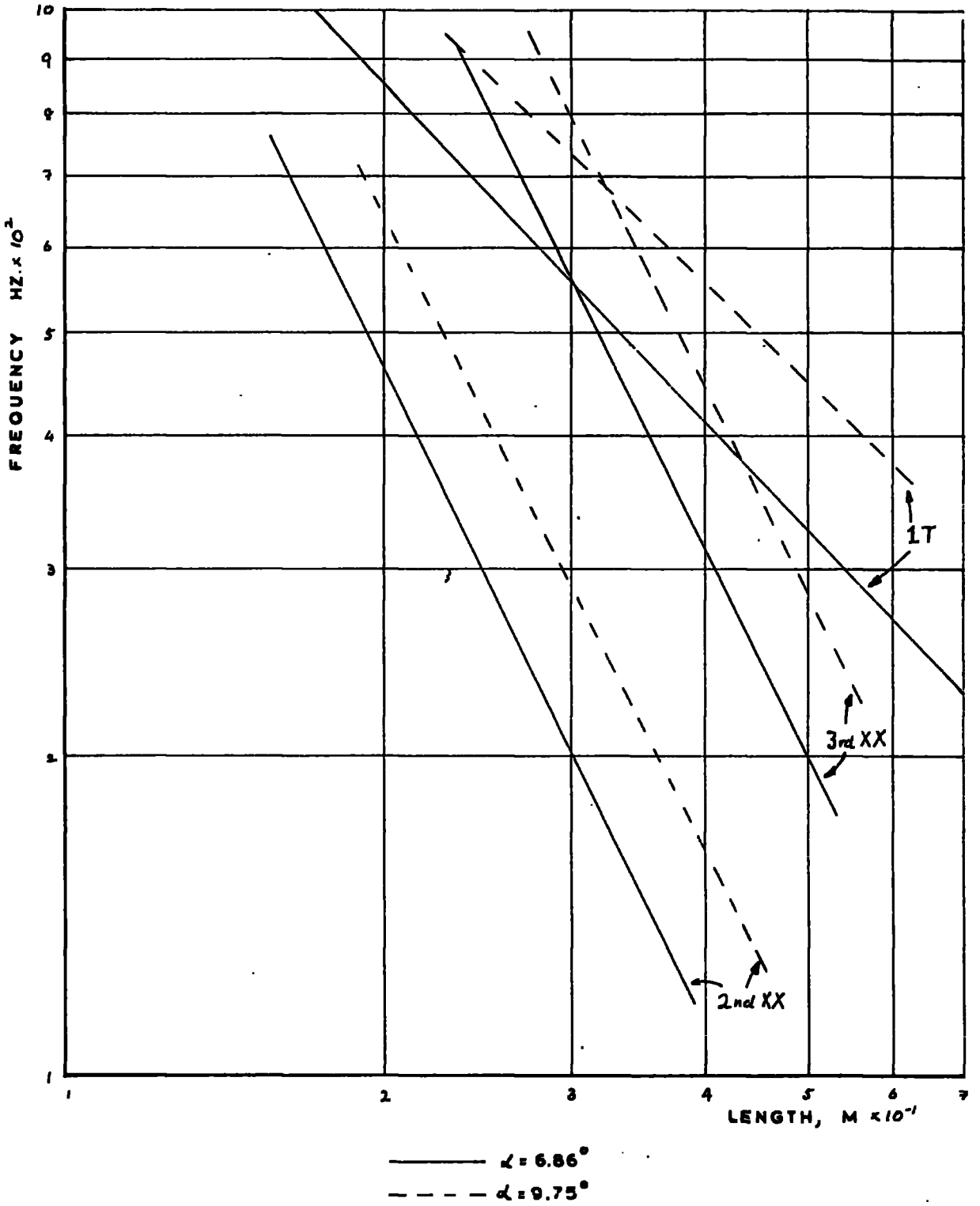

APPENDIX 7: BEAM DESIGN

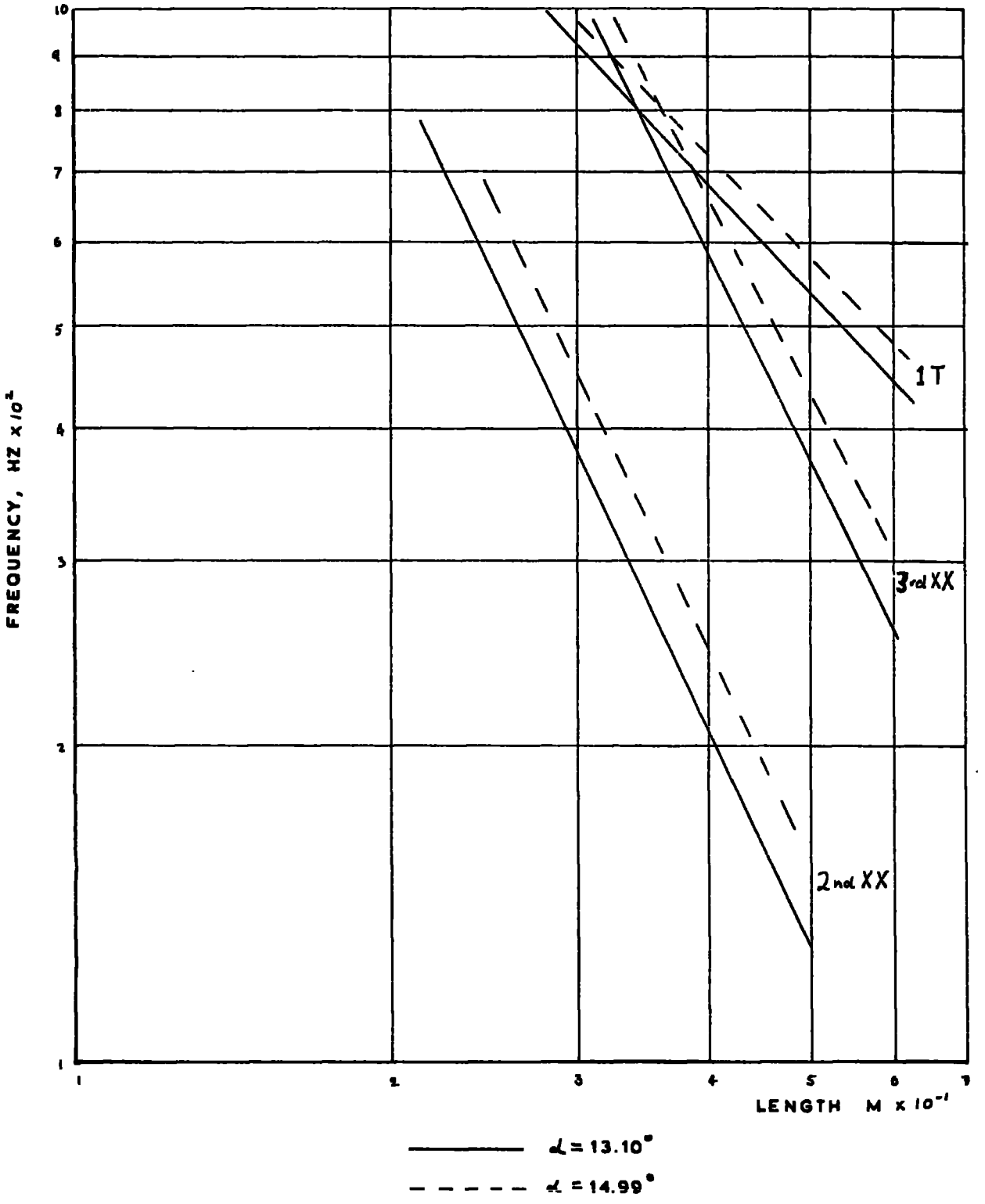

APPENDIX 7: BEAM DESIGN

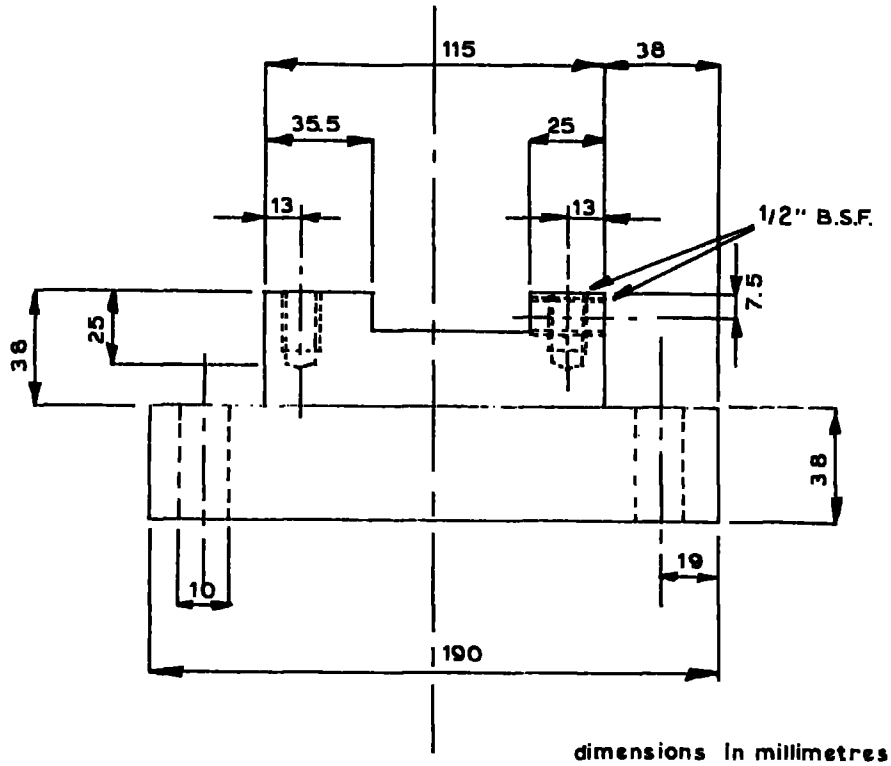

dimensions in millimetres.
scale: 1 : 2.5

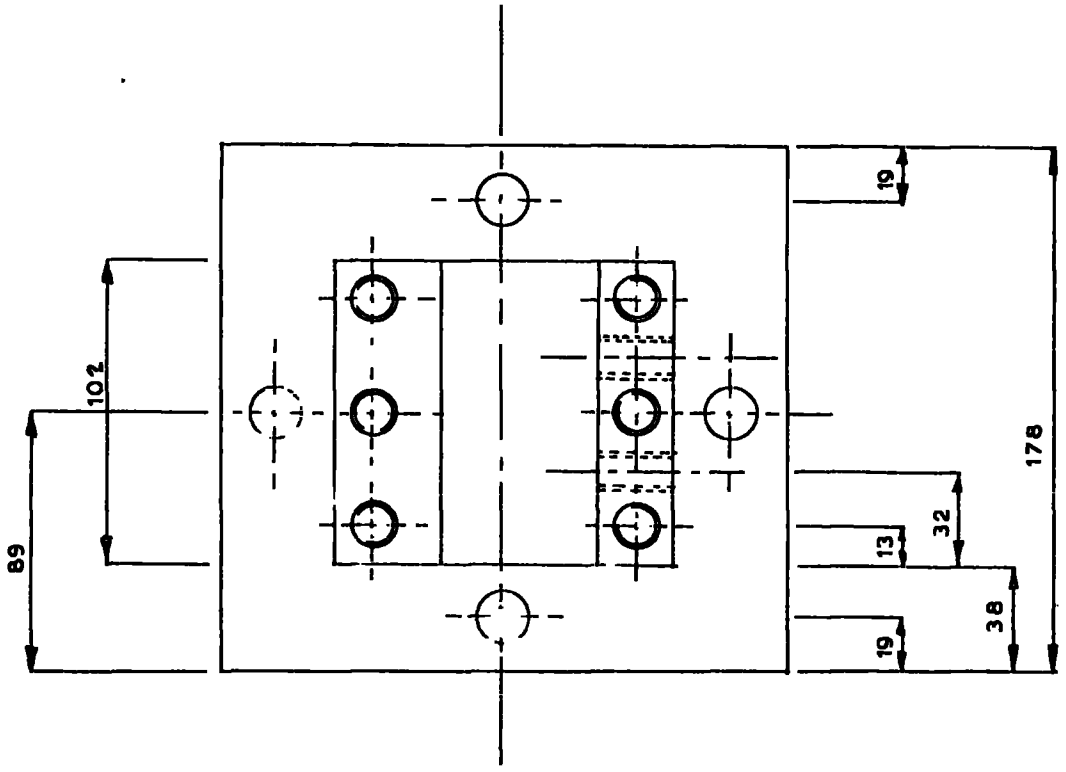

MOUNTING BLOCK: BASE.

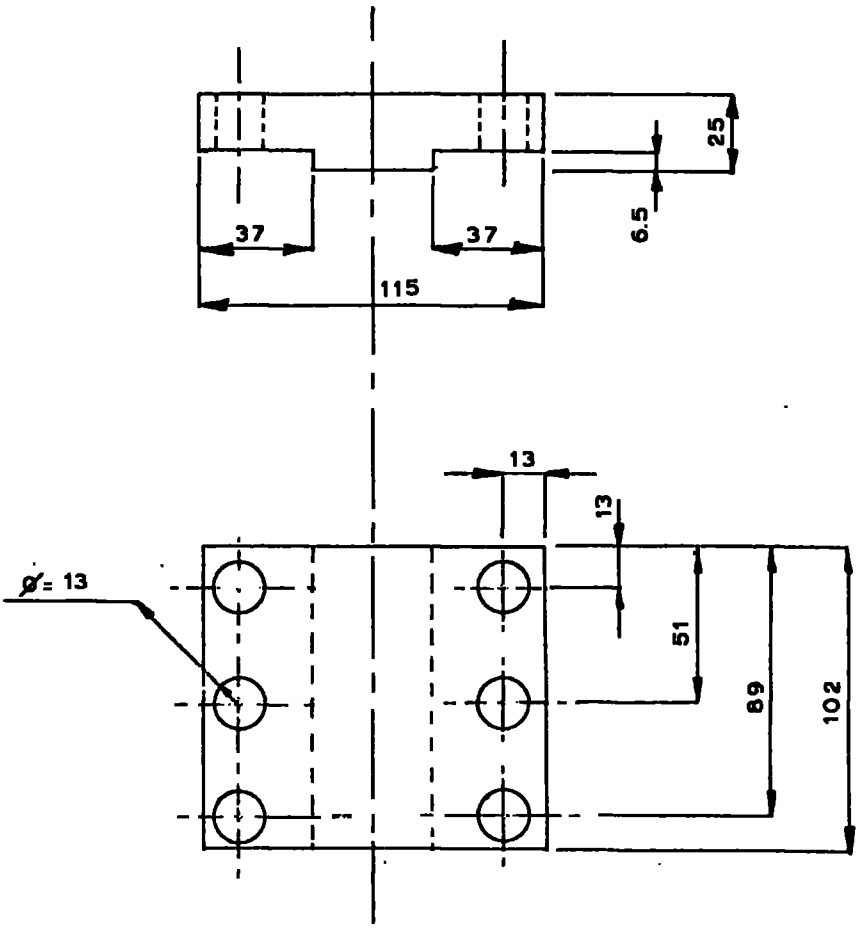

MOUNTING BLOCK: TOP PLATE.

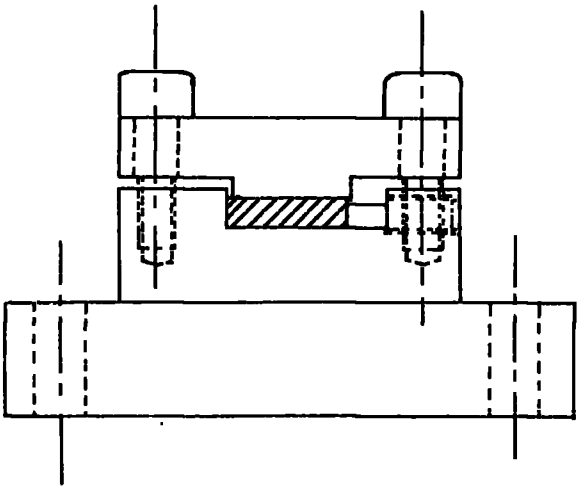

MOUNTING BLOCK: ASSEMBLED

APPENDIX 8

Preliminary Tests

Figure A V111 (1) shows the variation of beam deflection at right angles to the beam axis, and from the relative positions of the centroid and centre of flexure (by either formula) it is seen that the section is effectively oscillating about the centroid.

Figure A V111 (2) shows the variation in beam amplitude with piezo electric crystal response. This curve, which shows the tip amplitude in torsion at one edge for the beam where $\alpha = 130^{\circ}$, L = 0.36 m is not of course the absolute truth for all the beams as the precise values will vary with the beam, length of a given beam, mode number and position of the piezo electric crystal. The fact that the curve is smooth (not necessarily linear) shows that the piezo electric crystal is a satisfactory indicator of constant amplitude.

Figure A V111 (3) shows that for constant piezo electric crystal response the measured amplitude is invariant with coil position.

APPENDIX VIII (1)

Beam deflection — Probe position across section.

([illegible], Length 0.3 m)

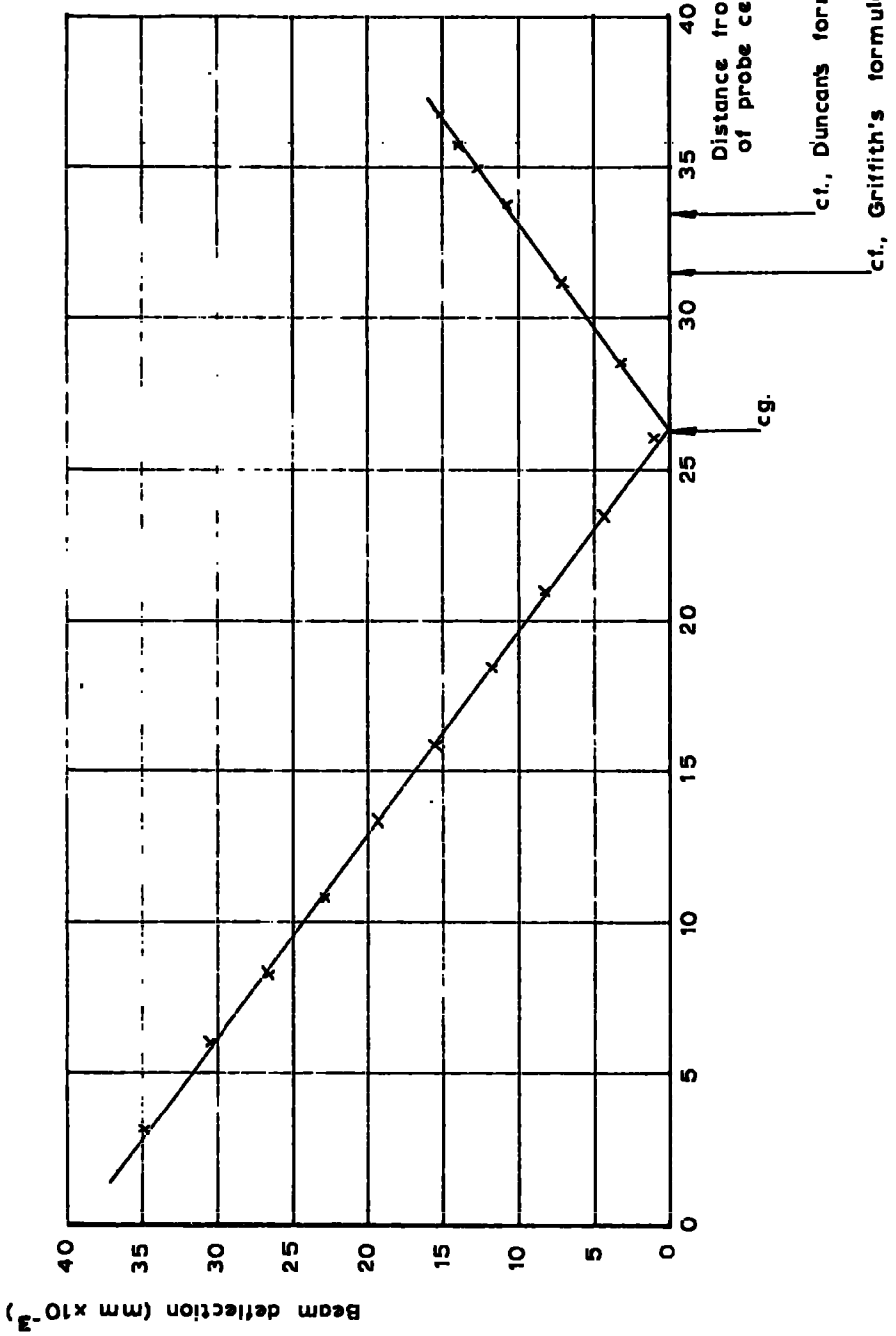

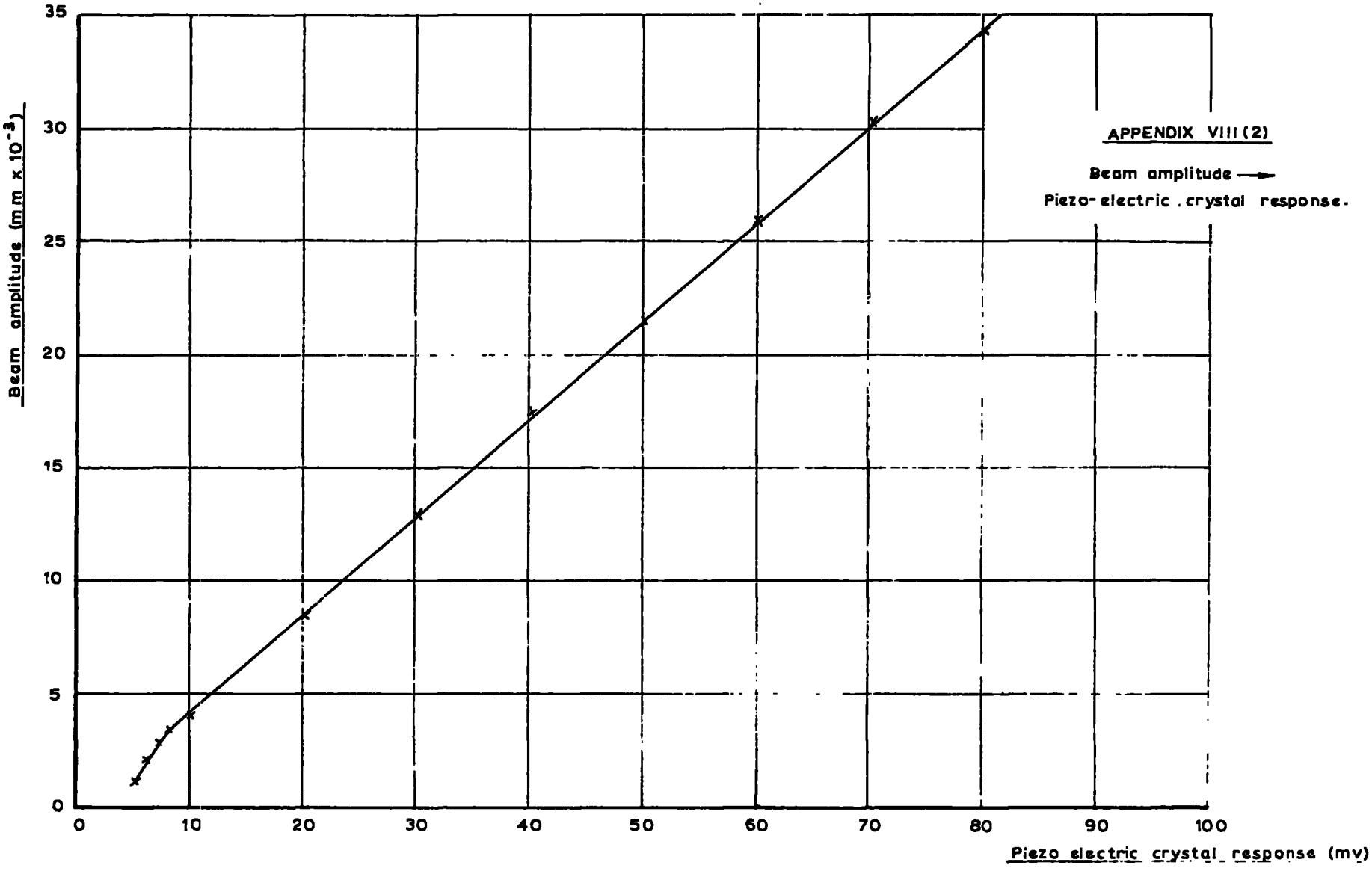
APPENDIX VIII (2)
Beam amplitude →
Piezo-electric . crystal response.
Beam amplitude (m.m x 10⁻³)
35
30
25
20
15
10
5
0
0
10
20
30
40
50
60
70
80
90
100
Piezo electric crystal response (mv)

COIL POSN		4TH MODE		5TH MODE	
DIST FROM ROOT (mm)	DIST FROM APEX (mm)	RELATIVE APEX DEFLECTION	RELATIVE BASE DEFLECTION	RELATIVE APEX DEFLECTION	RELATIVE BASE DEFLECTION
110	20	2·35	2·15	3·0	1·4
110	5	2·35	2·15	3·0	1·4
250	20	2·35	2·15	2·95	1·4
250	5	2·35	2·15	3·0	1·4
32	20	2·35	2·15	2·95	1·4
32	5	2·35	2·15	3·0	1·4

BEAM : $\Lambda = 13.10^{\circ}$
L = 0.40 m
Probes 0.395m from root

FIG A VIII(3) INVARIANCE OF RESPONSE WITH COIL POSITION

APPENDIX 9

1. Determination of the material properties.

Density ρ

Rectangular block shaped and ground:

Length = 0.04194 m

Width = 0.01993 m

Height = 0.01174 m

Mass = 0.076724 Kg.

Hence density ρ = 7.82×10^{3} Kg m^{-3}

Young's Modulus E

A test pice of suitable size for tension testing using an extensometer and ' Denison ' tension testing machine was manufactured from the same material as the beams.

The tension test shown in Graph A 9.1 was performed and the results analysed by linear regression.

From the formula

$$\frac{P}{A} = E \cdot \frac{\delta l}{L}$$

Where P = applied force

A = cross sectional area of test specimen

= 2.398×10^{-4} m^{2}

δl = extension due to P.

L = test length = 5.08×10^{-2} m

hence $E = \frac{P}{\delta l} \cdot \frac{L}{A}$

$\frac{\delta l}{P}$ from the regression analysis = $\frac{1.0149 \times 10^{-6}}{10^{3}}$

$$E = \frac{10^{9}}{1.0149} \cdot \frac{5.08 \times 10^{-2}}{2.398 \times 10^{-4}} = 2.09 \times 10^{11}\ N/m^{2}$$

Shear Modulus G

Torque measurement : B.P.A. force transducer on 5 in. torque arm.

Angular deflection measurement: torsiometer measuring linear deflection at a radius of 1" over test length of specimen.

Accuracy of torsiometer gauge.

The torsiometer is calibrated directly in radians, but its accuracy may be determined using slip gauges as the radius of 1" is known.

Gauge set to zero on 1.00" slip gauge.

ie. 1.00 ≡ 0.00 rads.

tests =

$0.95 + 0.120 = 1.070" \longrightarrow 70.5 \times 10^{-3}$ rads.

$0.95 + 0.140 = 1.090" \longrightarrow 90.5 \times 10^{-3}$ rads.

$0.95 + 0.130 = 1.080" \longrightarrow 80.5 \times 10^{-3}$ rads.

$0.85 + 0.30 = 1.050" \longrightarrow 50.0 \times 10^{-3}$ rads.

The gauge is therefore accurate to approximately 0.8%.

Using the formula $\frac{T}{J} = G\frac{\theta}{L}$ $\therefore G = \frac{L}{J} \cdot \frac{1}{\theta/T}$

where T = applied torque

J = polar moment of inertia = $\frac{\pi D^4}{32}$

D = specimen diameter = 6.37×10^{-3} m

L = test length (by travelling microscope)

= 4.972×10^{-2} m

$\frac{\theta}{T}$ from regression results = $\frac{4.56 \times 10^{-4}}{5 \times 2.54 \times 10^{-2}}$

hence G = $\frac{32 \times 4.972 \times 10^{-2}}{\pi (6.37)^4 \times 10^{-12}} \cdot \frac{5 \times 2.54 \times 10^{-2}}{4.56 \times 10^{-4}}$

= 8.83×10^{10} N/m²

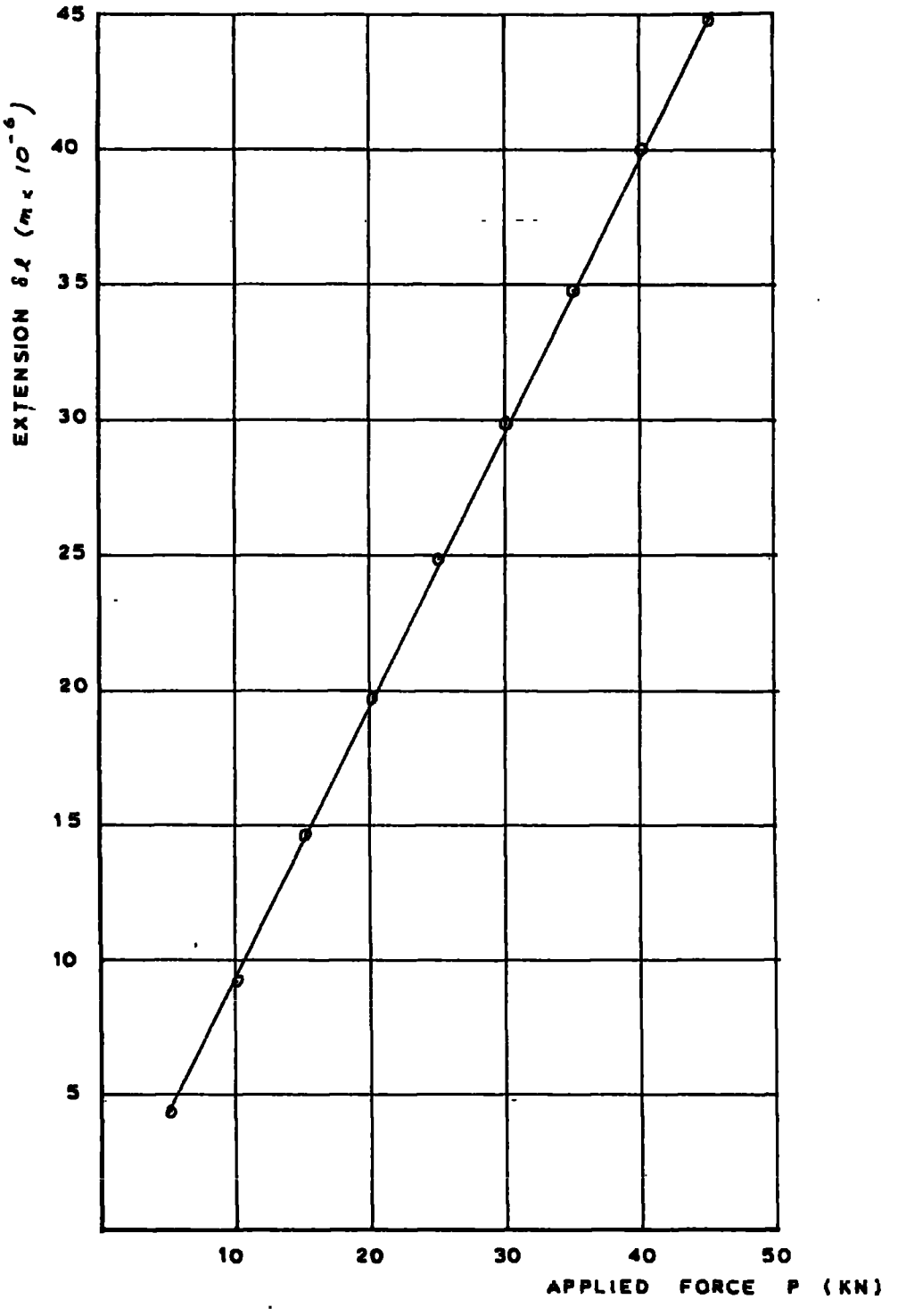

FIG A9.1 : TENSION TEST
EXTENSION → APPLIED FORCE

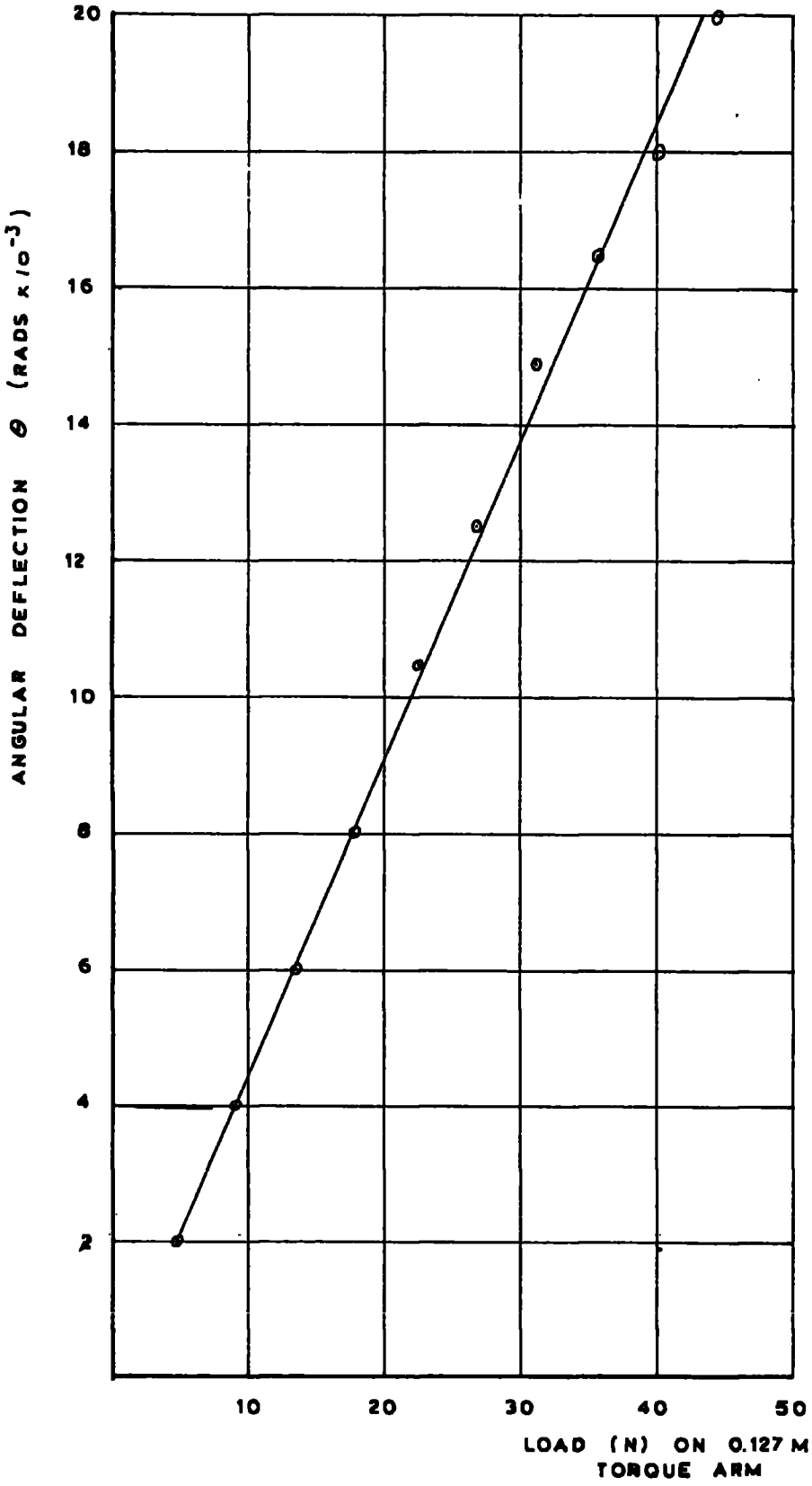

FIG A9.2 : TORSION TEST
ANGULAR DEFLECTION TORQUE ARM LOAD

Measurement of G by torsional oscillation of a rectangular sectioned beam

For a rectangular sectioned beam of width 2b and depth 2a Timoshenko and Goodier [23] give the formula

$$C = \frac{1}{3} G(2a)^3(2b)\left[1 - \frac{192}{\pi^5}\frac{a}{b}\sum_{n=1,3,5}^{\infty}\frac{1}{n^5}\tanh\frac{n\pi b}{2a}\right] \quad \text{— A9.1}$$

for the torsional stiffness per unit length.

Carnegie [12] gives the formula for the first torsional frequency (Hz) for a rectangular sectioned beam as

$$\omega = \frac{1}{4L}\sqrt{\frac{C}{\rho 4k^2_{cg}}}\sqrt{1 + \frac{\pi^2 E(2a)^3(2b)^3}{576\, CL^2}} \quad \text{— A9.2}$$

where the effect of fibre bending in torsion is included.

Constants

$E = 2.09 \times 10^{11}$ N / m^2

$\rho = 7.82 \times 10^3$ Kg /m^3

$L = 0.302$ m

Experiment 1

$2a = 0.01275$ m

$2b = 0.04334$ m

Summation $\Sigma = 1.0045$

Hence from A 9.1

$C = G \times 2.44 \times 10^{-8}$

first torsional mode measured at 1378 Hz

Hence from A 9.2

$C = 2.003 \times 10^3$

$G = 8.210 \times 10^{10}\ N/m^2$

Experiment 2

$2a = 0.00948$ m

$2b = 0.04334$ m

$\mathcal{E} = 1.0045$

hence $C = G \times 1.0613 \times 10^{-8}$

first torsional mode measured at 1075.5 Hz

hence $G = 8.33 \times 10^{10}\ N/m^2$

Experiment 3

$2a = 0.00640$ m

$2b = 0.04334$

$\mathcal{E} = 1.0045$

hence $C = G \times 3.435 \times 10^{-9}$

first torsional mode measured at 757.7 Hz

hence $G = 8.44 \times 10^{10}\ N/m^2$

APPENDIX 10

Relationship of computer program (finite element solution) to deflections measured by capacitive probes.

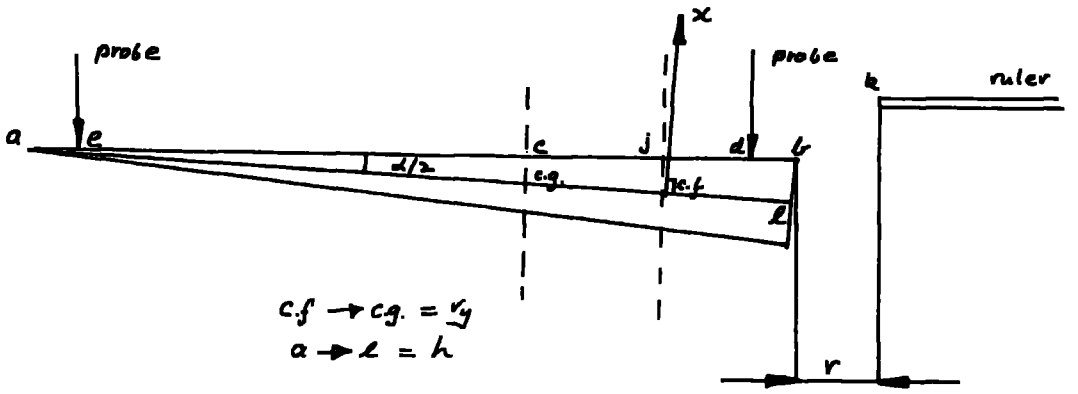

The output of the program is in terms of the deflection (x) of the centre of flexure (cf) and the rotation (θ) of the section, and it is desired to relate this to the deflection measured at the probes e and d in the above diagram in the form

$$\delta_e = x \cos d/2 + ej \cdot \theta$$

$$\delta_d = x \cos d/2 - jd \cdot \theta$$

Where δ_e, δ_d are deflections measured at the probes and the signs of the rotation term on the right hand side are known from the formulation of the program theory. It is therefore required to find the position of the probes in relation to the section, which is to determine ej and jd.

A travelling microscope was used to determine the horizontal distances:

1). ruler edge to beam edge = bk = r, and was set up to be acceptably constant over the beam length.

2). The distance between the probes = ed which was constant and = 0.0316 m.

3). The distance between the probe d and the edge of the block against the ruler = dk and was constant at 0.00722 m.

Hence the distance from the probe d to the edge of the beam (db) = (0.00722 - r) metres.

Now ac = $\frac{2}{3} h \cos \alpha/2$

and cd = ab - ac - db

cd = $\frac{h}{\cos \alpha/2} - \frac{2}{3} h \cos \alpha/2 - (0.722 - r)$

and ec = 0.0316 - cd

jd = cd - $r_y \cos \alpha/2$

and je = ec + $r_y \cos \alpha/2$

Hence the relative deflections δ_e and δ_α can be determined theoretically.

APEX ANGLE α°	14.99°	13.10°	9.75°	6.86°	130°
HEIGHT (m)	0.03972	0.03977	0.04134	0.03980	0.01003
WIDTH (m)	0.01045	0.00913	0.00705	0.00477	0.04229
AREA (m^2)	0.208×10^{-3}	0.182×10^{-3}	0.146×10^{-3}	0.949×10^{-4}	2.12×10^{-4}
C (Nm^2) ellipses	209.43	141.40	69.29	20.77	
C - Duncan, Ellis & Scruton	234.74	163.42	83.57	26.48	
C - Griffith formula	307.99	207.9	102.9	30.41	
C - " graphical	236.13	158.65	85.0	27.2	
C - Nuttall ($\alpha < 60°$)	183.78	124.1	60.72	18.23	
C - Sector 1	233.59	163.12	83.41	26.46	
C - " 2	241.75	167.5	84.63	26.65	
C - Scholes & Slater	258.34	175.42	86.99	27.02	

(Values of r_y are given in fig. 5.3.1)

APPENDIX II
SUMMARY OF SECTION PROPERTIES